DOE-ET-53088-251 IFSR#251

STOCHASTIC ELECTRON DYNAMICS DUE TO DRIFT WAVES IN A SHEARED MAGNETIC FIELD AND OTHER DRIFT MOTION PROBLEMS

James A. Robertson
Institute for Fusion Studies
The University of Texas at Austin
Austin, Texas 78712-1060

September 1986

STOCHASTIC ELECTRON DYNAMICS DUE TO DRIFT WAVES IN A SHEARED MAGNETIC FIELD AND OTHER DRIFT MOTION PROBLEMS

APPROVED BY

SUPERVISORY COMMITTEE:

Wendell Horton, Jr.

Wendell M Roberts

R D Hazeltine

William O Sellers

David N. Ross

STOCHASTIC ELECTRON DYNAMICS DUE TO DRIFT WAVES IN A SHEARED MAGNETIC FIELD AND OTHER DRIFT MOTION PROBLEMS

Publication No. _____

James Alexander Robertson, Ph.D.
The University of Texas at Austin, 1986

Supervising Professor: Wendell Horton

Electron motion in a single electrostatic wave in a sheared magnetic field is shown to become stochastic in the presence of a second wave at an amplitude well below that obtained from the overlapping pendulum resonance approximation. The enhanced stochasticity occurs for low parallel velocity electrons for which the parallel trapping motion from $eE_{\|}/m$ interacts strongly with the $\mathbf{E} \times \mathbf{B}$ trapping motion due to the presence of magnetic shear. The guiding-center equations for single particle electron orbits in given fields are investigated using both analytical and numerical techniques. The model assumes a slab magnetic field geometry with shear and two electrostatic plane waves propagating at an angle with respect to each other. Collisions and the self-consistent effect of the electron motion upon the fields are ignored. The guiding-center motion in an inertial reference frame moving in phase with the two waves is given by a two degree-of-freedom, autonomous Hamiltonian system. The single wave particle motion may be reduced to a two parameter family of one degree-of-freedom

Hamiltonians which bifurcate from a pendulum phase space to a topology with three chains of elliptic and hyperbolic fixed points separated in radius about the mode-rational surface. In the presence of a perturbing wave with a different helicity, electrons in the small parallel velocity regime become stochastic at an amplitude scaling as the fourth root of the wave potential. The results obtained for stochastic motion apply directly to the problem of electron diffusion in drift waves occuring in toroidal fusion confinement devices. The effect of an adiabatically changing radial electric field upon guiding-center orbits in tokamaks is also investigated. This perturbation causes a radial polarization drift of trapped particle tokamak orbits.

STOCHASTIC ELECTRON DYNAMICS DUE TO DRIFT WAVES IN A SHEARED MAGNETIC FIELD AND OTHER DRIFT MOTION PROBLEMS

by

JAMES ALEXANDER ROBERTSON, B.S.

DISSERTATION

Presented to the Faculty of the Graduate School of

The University of Texas at Austin

in Partial Fulfillment

of the Requirements

for the Degree of

DOCTOR OF PHILOSOPHY

THE UNIVERSITY OF TEXAS AT AUSTIN

December, 1986

Acknowledgments

During the course of this research, it has been a great privilege to have worked with two excellent advisors. I would like to express my deep gratitude toward Dr. F.L. Hinton for his many contributions both to the progress of this work and to my education in plasma physics. I am indebted to him for his advice, encouragement and patience. I would like to thank Professor Wendell Horton for his guidance during the later stages of this research project. He has provided me with invaluable insights into the important issues of this study, helping me to make sense of it all. I am particularly grateful to Dr. Horton for his enthusiasm for this project.

This work was carried out in part at the Institute for Fusion Studies at the University of Texas, and in part at G.A. Technologies, Inc. in La Jolla, California. I would like to express my appreciation to both of these research institutions for providing stimulating environments in which to carry out this research. I owe special thanks to Dr. C.S. Liu for hosting my stay at G.A.

I have benefited from discussions with many people, including Dr. D.I. Choi, Dr. T. Jensen, Dr. H. Ikesi, Dr. William Schieve, Dr. C.S. Liu, and Dr. G.S. Lee. Particular thanks are owed Dr. John Greene for his discussions concerning the finer points of dynamics, and the measure-preserving property of maps.

I would also like to convey my appreciation to the technical staff at G.A. Technologies and the Institute for Fusion Studies, in particular to Saralyn Stewart and to Suzy Crumley and Laura Patterson for assistance in technical typesetting with TEX.

Table of Contents

List of Figures

List of Tables

I. Introduction

The motion of electrons across the confining magnetic field due to the $\mathbf{E} \times \mathbf{B}$ motion associated with low frequency drift modes is well recognized as an important mechanism for the anomalous transport in plasmas.[1] In addition to producing anomalous transport, the nonlinear motions of the electrons changes the stability of the drift modes by modifying the electron charge density response function at finite wave amplitudes.[2,3,4] Recent studies[5,6] of the nonlinear $\mathbf{E} \times \mathbf{B}$ motion of the particles in drift wave fields obtain results for the diffusion and resonance broadening when the perpendicular $\mathbf{E} \times \mathbf{B}$ motion decouples from the parallel motion. This decoupling approximation is adequate for describing the nonlinear motion of ions[5,6], but fails for the electron motion considered here.

The electron motion in drift waves is influenced both by the parallel acceleration, $eE_{||}/m_e$, produced by the wave's electric field and the nonlinear $\mathbf{E} \times \mathbf{B}$ motion. In the presence of magnetic shear, Hirshman and Molvig[4] recognize that even the linear free-streaming electron motion directly couples to the nonlinear $\mathbf{E} \times \mathbf{B}$ motion. They show that with the approximation of constant parallel velocity, the nonlinear $\mathbf{E} \times \mathbf{B}$ motion reduces to the time-dependent pendulum Hamiltonian, with the canonical momentum equal to the radial coordinate and the canonical coordinate equal to the wave-particle phase variable. In this constant $v_{||}$ approximation, the onset of stochasticity and the diffusion approximation are well known from the results of $1\frac{1}{2}$D Hamiltonian (pendula) theory.[7,8] The constant $v_{||}$ approximation is good for electrons whose parallel kinetic energy in the wave frame is large compared with the electrostatic potential. For low parallel velocity electrons, where the difference between the parallel electron velocity $v_{||}$ and the parallel phase velocity is of the order of the trapping veloc-

ity $v_0 = (e\phi/m_e)^{1/2}$, the approximation fails qualitatively, due to the strong coupling between the parallel and cross-field nonlinear motions.

Non-collisional mechanisms of particle transport in high-temperature confined plasmas are of great interest in fusion research, for diffusion rates are observed to substantially exceed those predicted from the collisional transport calculations of classical and neoclassical transport theory. Both electrostatic and magnetic field fluctuations produce anomalous particle transport.[25,26] Not surprisingly, in a turbulent plasma, the particles display a random, diffusive response in the presence of random fields. Less intuitively obvious is the "intrinsic stochasticity"[27] which particle motion can display in a collisionless plasma in the presence of well-behaved, non-random fields. Highly chaotic, diffusive-like behavior can result from the interaction or overlap of resonances[7], even though the differential equations of motion are strictly deterministic (in contrast with stochastic differential equations, which contain random coefficients). In this work we examine a model system displaying the phenomenon of intrinsic stochasticity.

In the present study, we analyze the drift motion of electrons in two sinusoidal electrostatic plane waves in the presence of magnetic shear. Collisions are ignored, and we assume given fields without attempting a self-consistent treatment. The cyclotron frequency is assumed to be much larger than the wave frequencies, and the Larmor radius much smaller than the wave-lengths and shear scale length. Hence, we study the guiding-center equations of motion.

The problem of particle response to several drift modes associated with nearby rational surfaces of a tokamak provides the principle motivation for undertaking the study of this model. Our model is, however, quite self-contained

and does not rely especially upon the origin of the modes. The model could equally well apply to electrostatic modes other than gradient-driven ones and parameter regimes vastly different from those relevent to tokamak physics. The only requirement is that the scales be such that the guiding-center description is valid.

The magnetic field chosen for study in our model is a uniform slab with shear. The direction of $\mathbf{B}$ is independent of the y and z coordinates. The magnitude of the B-field is taken to be everywhere uniform, but the direction of the field twists as the coordinate x is varied. In an idealized tokamak, the magnetic field lines wrap helically about nested toroidal surfaces, referred to as flux surfaces. As one moves in the minor radial direction of the torus, from one flux surface to another, the pitch of the field lines changes. Viewed locally, the field twists as r is changed. Our slab model captures this local feature of the tokamak B-field, with the slab coordinate x corresponding to the minor radial coordinate of the tokamak. However, our model neglects other important global features of the full toroidal geometry, such as the magnetic particle trapping due to the major-radial dependence of the field's magnitude.

In a magnetically confined plasma, temperature and density gradients may give rise to the drift mode or universal mode, propagating approximately in a direction mutually perpendicular to the B-field and the gradients. In the tokamak, normal modes are centered about those flux surfaces having rational winding number, where the equipotential surfaces running parallel to the field lines are able to close upon themselves. It is probably reasonable to assume that those drift modes associated with flux surfaces of low order rationality are the most important. In a real experimental device, infinitely many modes may be

simultaneously present. In our model, we make the idealization that only two modes, associated with nearby rational surfaces are present. One wave is viewed as the primary wave. The second wave is considered to be a perturbation. In our idealized slab model, the two modes are taken to be plane waves with non-parallel wave vectors in the (y, z)-plane. We ignore the radial structure of the modes (i.e. the x-dependence). The presence of the second perturbing wave is observed in numerical experiments to destroy an isolating invariant of the motion. This results in diffusive behavior in the radial direction. In the realistic case where many modes associated with rational surfaces at various radii are present, the stochastic instability can open up a coridor for radial transport from one mode to the next. We view the study of the two-wave system as a first step in the understanding of the many-wave problem.

In Sec. II, we show that the motion in the two-wave system is governed by a 2 D autonomous Hamiltonian system. The guiding-center equations of motion are presented in both non-canonical and canonical coordinates. We determine relevent scales for the coordinates and recast the equations of motion in terms of dimensionless variables. This simplifies the problem by greatly reducing the number of free parameters.

If only one wave is present, the system is integrable. In Sec. V, we discuss the features of the single wave orbits. We make a complete classification of all the orbit types which occur in the single wave problem. The use of similarity methods is indispensible for this comprehensive orbit classification. A bifurcation pattern of the single wave phase-space is derived as a function of two dimensionless parameters. We find that the single wave electron orbits are generally too complex to be expressed in terms of elliptic functions. However,

motion on homoclinic orbits is found to be expressible in terms of well-known analytic functions.

Electrons in the low parallel kinetic energy regime display anomalous radial excursions over a scale determined by the geometric mean of the shear length L_s and the electron gyroradius calculated with the parallel trapping velocity, $\rho_0 = v_0/\omega_{ce}$, with v_0 given above. This radial scale-length thus displays $\phi^{1/4}$ dependence, as compared with the $\phi^{1/2}$ dependence of the pendulum regime considered by Hirshman and Molvig. We should point out that one must draw a distinction between the notion of Landau resonant electrons and electrons in the low kinetic energy regime. A Landau resonant particle remains in phase with the wave by virtue of satisfying the condition $v_\parallel \hat{\mathbf{b}} \cdot \mathbf{k} = \omega$. The parallel velocity in the wave frame for such resonant particles is therefore $v'_\parallel = \omega/\hat{\mathbf{b}}\cdot\mathbf{k} - \hat{\mathbf{b}}\cdot\mathbf{k}\omega/k^2 = [1-(\hat{\mathbf{b}}\cdot\hat{\mathbf{k}})^2]\omega/(k\hat{\mathbf{b}}\cdot\hat{\mathbf{k}})$. The Landau resonant particles thus do not necessarily have small parallel kinetic energy in the wave-frame. Close to the rational surface, where $\hat{\mathbf{b}}$ and $\hat{\mathbf{k}}$ are orthogonal, the parallel velocity of the resonant particles becomes very large.

In the one-wave problem particles located at the null-points of the electric field (i.e. $\mathbf{k}\cdot\mathbf{x} - \omega t = n\pi$) experience no parallel acceleration or cross-field drifts. If furthermore, the radial coordinate and parallel velocity are such that the Landau resonance condition $\omega = v_\parallel \hat{\mathbf{b}}(x)\cdot\mathbf{k} = v_\parallel k_y x/L_s$ is satisfied, then such particles will remain at the null-points of the electric field. These orbits are the stable and unstable fixed points of the phase space. The values of x and $v_\parallel$ at the fixed points stand in an inverse relationship to one another. The constant $v_\parallel$ approximation of earlier work focuses on the pendulum-like islands associated with the fixed points that occur for $v_\parallel$ large and x small. Little attention has

been paid to the opposite case of islands occuring for small $v_{\|}$ and large x.

We find that for canonical momenta exceeding a certain value, the chain of elliptic and hyperbolic fixed points occuring in the pendulum approximation bifurcates into three chains of fixed points separated in radius about the rational surface. Depending on parameter values, these chains of fixed points may be interconnected in a variety of ways. We have paid particular attention to a lattice-like homoclinic orbit with energy equal to $e\phi$ which ties all three chains together. This orbit displays the maximum radial excursion for the single wave problem.

In the presence of a perturbing second wave, the complex pattern of homoclinic orbits joining the fixed points of the single wave problem becomes a stochastic web for small values of the perturbing wave amplitude. We use the technique of Poincaré surfaces of section to observe, in numerical experiments, the destruction of an isolating integral of the motion and the resulting transition to stochastic motion. In Sec. III, we define our choice for the Poincaré map. In Sec. IV, we derive the invariant measure for the Poincaré map. The Poincaré surface of section for a 2 degree-of-freedom Hamiltonian system is known to produce a measure-preserving map. We prove that the measure-preserving property of the Poincaré map follows under weaker assumptions; i.e., the system needn't necessarily be Hamiltonian.

Applying the overlapping resonance ideas[7,8,9] to our 2 degree-of-freedom system, in Sec. VI, we estimate the value of the wave amplitudes for global stochasticity from two neighboring drift waves. For amplitudes exceeding this critical value, computer experiments show radial diffusion of the electrons. From the dimensionless variables appropriate for this system, we are able to establish

the scaling of the diffusion coefficient $D_\perp$. In the small parallel velocity regime, the computer experiments show that the orbits are particularly susceptible to the stochastic instability. In particular, orbits with energy equal to $e\phi$ are observed to be extremely fragile to the onset of chaos. This constant energy surface is highly singular. A continuous class of orbits with this energy are infinite-period homoclinic orbits. For even extremely small perturbations, we observe a diffusive wandering of the particle along the locus of homoclinic orbits of the unperturbed problem. We identify this behavior as a non-universal type of phenomenology, not generally present in two degree-of-freedom autonomous systems. The behavior of perturbed orbits in the vicinity of this singular energy surface appears to be akin to Arnold diffusion[12] which is generally present in systems possessing $2\frac{1}{2}$ or more degrees-of-freedom.

The simple model which we investigate in this work displays a rich variety of features and complications. The extension of the present work to the full toroidal geometry of the tokamak goes beyond the scope of this dissertation. However, in Sec. VII, we briefly point out some of the issues relating to the toroidal problem. In the toroidal geometry, the magnetic potential well has an effect similar to that of a stationary $m = 1$, $n = 0$ wave. The one-wave problem in toroidal geometry is then generically similar to the two-wave problem which we have studied in the slab geometry. In Sec. VII, we also do an analytic treatment of a somewhat simpler drift orbit problem in toroidal geometry. We consider the effect of an adiabatically increasing radial electric field upon the tokamak particle orbits. Due to the adiabatic nature of the perturbation, the particle motion is non-stochastic, and an analytic treatment is practical.

In our initial study of the drift orbit problem in slab geometry, we considered

the simple guiding-center equations of motion presented in Northrop's volume.[18] Littlejohn demonstrated that these equations of motion are non-Hamiltonian and small correction terms are required to restore the Hamiltonian structure of the original Newton-Lorentz equations to the reduced set of drift equations. In the course of investigating our model, we discovered that the simple non-Hamiltonian version of the drift system belongs to a class of generalized Hamiltonian systems studied by Y. Nambu.[22] We discuss, in an appendix, some of the features of this less widely known dynamical formalism. In Sec. VIII, we give a summary and conclusions.

II. The Equations of Motion

We investigate the motion of an electron in a magnetic field with shear in the presence of two electrostatic plane waves. We assume magnetic and electric fields of the form

$$\mathbf{B} = B_0 \left[\hat{\mathbf{e}}_y \sin\frac{x}{L_s} + \hat{\mathbf{e}}_z \cos\frac{x}{L_s} \right], \tag{2.1}$$

$$\mathbf{E} = -\nabla\Phi, \tag{2.2}$$

$$\text{where} \quad \Phi = \phi_1 \cos(\mathbf{k}_1 \cdot \mathbf{r} - \omega_1 t) + \phi_2 \cos(\mathbf{k}_2 \cdot \mathbf{r} - \omega_2 t). \tag{2.3}$$

The wave-vectors $\mathbf{k}_1$ and $\mathbf{k}_2$ are taken to be non-parallel and to both lie in the y-z plane. The above choice of electrostatic potential neglects mode-coupling effects[10] and the radial structure (i.e. the x-dependence) of the modes[5,6]. The field of Eq. (2.1) is produced by a current $\mathbf{j} = \frac{cB_0}{4\pi L_s} [\hat{e}_z \cos(x/L_s) + \hat{e}_y \sin(x/L_s)]$. Our choice of B-field for the present model was motivated by the fact that it has the nice feature of a constant magnitude. The detailed form of the sheared B-field is, however, not especially important, since we are interested in values of x small compared with the shear length L_s.

We make a Galilean transformation to a reference frame moving with velocity $\mathbf{w}$ with respect to the lab frame. Denoting the transformed coordinates with primes, $\mathbf{r}' \equiv \mathbf{r} - \mathbf{w}t$. $\mathbf{w}$ is chosen so as to simultaneously solve $\omega_1 = \mathbf{k}_1 \cdot \mathbf{w}$ and $\omega_2 = \mathbf{k}_2 \cdot \mathbf{w}$. In matrix notation, $\mathbf{w}$ must satisfy

$$\begin{pmatrix} \omega_1 \\ \omega_2 \end{pmatrix} = \begin{pmatrix} k_{1_y} & k_{1_z} \\ k_{2_y} & k_{2_z} \end{pmatrix} \begin{pmatrix} w_y \\ w_z \end{pmatrix}.$$

The value of w_x is arbitrary. Inverting this, one finds $w_y = (k_{2_z}\omega_1 - k_{1_z}\omega_2)/d$, and $w_z = (k_{1_y}\omega_2 - k_{2_y}\omega_1)/d$, where $d \equiv k_{1_y}k_{2_z} - k_{1_z}k_{2_y}$. We take $w_x = 0$. With this choice for $\mathbf{w}$, one finds that $\mathbf{k}_i \cdot \mathbf{r} - \omega_i t = \mathbf{k}_i \cdot \mathbf{r}'$ for $i = 1, 2$. Hence,

the fields are time-independent in the transformed reference frame. Note that the transformation is not possible when $\mathbf{k}_1$ and $\mathbf{k}_2$ are parallel, since, in this case, $d = 0$. For non-relativistic $\mathbf{w}$, the fields in the wave-frame are given by $\mathbf{E}' = \mathbf{E} + c^{-1}\mathbf{w} \times \mathbf{B}$ and $\mathbf{B}' = \mathbf{B} - c^{-1}\mathbf{w} \times \mathbf{E}$. We ignore the induced magnetic field, taking $\mathbf{B}' = \mathbf{B}$, since $| \mathbf{E} | \ll B_0$.

The guiding-center equations of motion for electron orbits are then given, in terms of the wave frame coordinates, by

$$\frac{dv'_{\|}}{dt} = -\frac{e}{m_e}\hat{\mathbf{b}} \cdot \mathbf{E}, \tag{2.4}$$

$$\frac{d\mathbf{r}'}{dt} = v'_{\|}\hat{\mathbf{b}} + \frac{c}{B_0^2}\left[\mathbf{E} + \frac{\mathbf{w} \times \mathbf{B}}{c}\right] \times \mathbf{B}, \tag{2.5}$$

where e is the magnitude of the electron charge, m_e is the electron mass, $\hat{\mathbf{b}}$ is the unit vector in the direction of the magnetic field, and $v'_{\|} = \hat{\mathbf{b}} \cdot d\mathbf{r}'/dt$ is the parallel velocity.

The guiding-center equations thus constitute a two-degree-of-freedom, autonomous, dynamical system with phase space coordinates $(v'_{\|}, x', y', z')$. We note that adding a third wave having wave-vector $\mathbf{k}_3$ in the y-z plane would, in general, preclude the possibility of finding a wave-frame where the fields are time-independent, since the additional condition $\omega_3 = \mathbf{k}_3 \cdot \mathbf{w}$ results in an overdetermined set of equations. Only in the special case where $\omega_3 = \alpha\omega_1 + \beta\omega_2$ and $\mathbf{k}_3 = \alpha\mathbf{k}_1 + \beta\mathbf{k}_2$ can one still boost to a time-independent wave-frame. Hence, the extension of the present problem to three or more co-planer waves is, in general, fundamentally different in character from the two-wave problem investigated in this work. The additional "half degree" of freedom, not removable through coordinate transformation, opens up the possibility of Arnold diffusion[11,12], not generally present in two-degree-of-freedom, autonomous systems.

Upon substituting the expressions for the fields, given by Eqs. (2.1)–(2.3), into Eqs. (2.4) and (2.5), one obtains the following equations of motion for the guiding-center orbits:

$$\frac{dv_\parallel}{dt} = -\frac{e}{m_e}\sum_{i=1,2}\phi_i k_{i_\parallel}(x)\sin(\mathbf{k}_i\cdot\mathbf{r}) \tag{2.6}$$

$$\frac{dx}{dt} = \frac{c}{B_0}\sum_{i=1,2}\phi_i k_{i_\perp}(x)\sin(\mathbf{k}_i\cdot\mathbf{r}) \tag{2.7}$$

$$\frac{dy}{dt} = v_\parallel \sin\frac{x}{L_s} - w_\perp(x)\cos\frac{x}{L_s} \tag{2.8}$$

$$\frac{dz}{dt} = v_\parallel \cos\frac{x}{L_s} + w_\perp(x)\sin\frac{x}{L_s}, \tag{2.9}$$

where

$$w_\perp(x) \equiv w_y\cos\frac{x}{L_s} - w_z\sin\frac{x}{L_s}$$
$$k_{i_\perp}(x) \equiv k_{i_y}\cos\frac{x}{L_s} - k_{i_z}\sin\frac{x}{L_s}$$
$$k_{i_\parallel}(x) \equiv k_{i_y}\sin\frac{x}{L_s} + k_{i_z}\cos\frac{x}{L_s}.$$

For notational convenience, we have dropped the primes denoting wave-frame quantities. Here, and in the remainder of the discussion, the phase space coordinates are understood to refer to wave-frame quantities. In comparing these equations with earlier investigations of motion in one wave, one should bear in mind that other authors[13] have expressed the motion in terms of a parallel velocity relative to the *lab* frame and a phase coordinate, $\theta = \mathbf{k}\cdot\mathbf{r} - \omega t$, relative to the *wave* frame; a sort of mixed representation. Our coordinates are the particle's physical position and velocity as seen by an observer in an inertial frame moving with the waves.

The helical symmetry of the **B** field specified in Eq. (2.1) permits one, without loss of generality, to take $k_{1_z} = 0$. One may choose the y-axis of the

coordinate system to be parallel to $\mathbf{k}_1$. Then one specifies the origin of the x-axis as the point at which $\mathbf{B}$ is orthogonal to $\mathbf{k}_1$ to recover the expression for $\mathbf{B}$ given in Eq. (2.1).

One may verify, by differentiation, that the energy function,

$$H \equiv \frac{1}{2} m_e v_{\parallel}^2 - e\Phi'(x,y,z), \tag{2.10}$$

is conserved under the motion specified by Eqs. (2.6)–(2.9). Here, Φ', the electrostatic potential in the wave-frame, is given by

$$\Phi' \equiv \sum_{i=1.2} \phi_i \cos \mathbf{k}_i \cdot \mathbf{r} - \frac{1}{c} \mathbf{w} \cdot \mathbf{A}(\mathbf{x}), \tag{2.11}$$

where $\mathbf{A}$ is a vector potential consistent with $\mathbf{B} = \nabla \times \mathbf{A}$. For the magnetic field of Eq. (2.1), $\mathbf{A}$ may be taken as

$$\mathbf{A} \equiv B_0 L_s \left[\hat{\mathbf{e}}_y \sin \frac{x}{L_s} + \hat{\mathbf{e}}_z \cos \frac{x}{L_s} \right]. \tag{2.12}$$

If, furthermore, one assumes that $\phi_2 = 0$, then Eqs. (2.6)–(2.7) may be combined and integrated to give a second conserved quantity

$$F \equiv \cos\left(\frac{x}{L_s}\right) \exp\left[-\frac{v_{\parallel}}{\omega_{ce} L_s}\right] = \text{const.}$$

Here, ω_{ce} is the electron cyclotron frequency, $eB_0/m_e c$.

A. The Hamiltonian Equations

The equations of motion (2.4)–(2.5) have the virtue of clearly displaying the principle physics of the present problem: namely, that the electric field produces acceleration along the field lines and $\mathbf{E} \times \mathbf{B}$ drifts across the field lines. This reduced set of equations, however, suffers the drawback of not retaining the underlying Hamiltonian structure of the complete Newton-Lorentz equations of motion. Littlejohn[14] corrects this deficiency of the simple drift equations by systematically constructing the guiding-center equations, to arbitrary order in the magnetic moment. Following his phase space Lagrangian formulation of guiding-center motion[14], the equations of motion, to lowest order in the magnetic moment, may be obtained by applying Hamilton's principal to the Lagrangian

$$L(v_\parallel, x, y, z) = \frac{d\mathbf{r}}{dt} \cdot \left[m_e v_\parallel \hat{\mathbf{b}} - \frac{e}{c}\mathbf{A} \right] - H, \tag{2.13}$$

where the Hamiltonian function, H, and the vector-potential, $\mathbf{A}$, are defined by Eqs. (2.10)–(2.12). One is to regard the four phase space coordinates, $v_\parallel$, x, y, and z, as the generalized coordinates.

Defining the 4-component vectors $\mathbf{z} \equiv (v_\parallel, \mathbf{r})$ and $\mathbf{P}(\mathbf{z}) \equiv (0, m_e v_\parallel \hat{\mathbf{b}} - (e/c)\mathbf{A})$, and using the Einstein summation convention, the Lagrangian (2.13) may be rewritten as

$$L(\mathbf{z}, \dot{\mathbf{z}}) = \dot{z}^i P_i(\mathbf{z}) - H(\mathbf{z}). \tag{2.14}$$

The only non-vanishing components of $\mathbf{P}$ are

$$P_y(v_\parallel, x) \equiv m_e(v_\parallel - \omega_{ce} L_s) \sin\frac{x}{L_s} \tag{2.15}$$

$$P_z(v_\parallel, x) \equiv m_e(v_\parallel - \omega_{ce} L_s) \cos\frac{x}{L_s}. \tag{2.16}$$

Independent variation of the z^i leads to the Euler-Lagrange equations $\omega_{ij}\dot{z}^j = \partial H/\partial z^i$, where the symplectic tensor $\boldsymbol{\omega}$ is defined as $\omega_{ij} \equiv \partial P_j/\partial z^i - \partial P_i/\partial z^j$. The equations of motion, for the non-canonical coordinates z^i, are then given by

$$\frac{dz^i}{dt} = J^{ij}\frac{\partial H}{\partial z^j}, \tag{2.17}$$

where the cosymplectic tensor $\mathbf{J}$ is defined to be the inverse of $\boldsymbol{\omega}$. $\mathbf{J}$ may be written in terms of the block matrix $\mathbf{M}$ and its transpose $\mathbf{M}^T$ as

$$\mathbf{J} \equiv \begin{pmatrix} 0 & \mathbf{M} \\ -\mathbf{M}^T & 0 \end{pmatrix},$$

where

$$\mathbf{M} \equiv \frac{1}{m_e}\begin{pmatrix} -\sin\frac{x}{L_s} & -\cos\frac{x}{L_s} \\ \frac{1}{\omega_{ce}\beta}\cos\frac{x}{L_s} & -\frac{1}{\omega_{ce}\beta}\sin\frac{x}{L_s} \end{pmatrix}.$$

Here, the function β, derived by Littlejohn, is defined as

$$\beta \equiv 1 + \frac{v_\parallel}{\omega_{ce}}\hat{\mathbf{b}}\cdot\nabla\times\hat{\mathbf{b}} = 1 - \frac{m_e c v_\parallel}{eB_0 L_s},$$

and arises from the twisting of the magnetic field lines due to the sheared $\mathbf{B}(x)$. The term $\frac{m_e c v_\parallel}{eB_0 L_s}$ in β equals $\frac{\rho_L v_\parallel}{L_s v_\perp}$, where ρ_L is the Larmor radius. Assuming $v_\perp \simeq v_\parallel$ and $\rho_L \ll L_s$, this term is small, and $\beta \simeq 1$. With β approximated by unity, Eq. (2.17) becomes identical to Eqs. (2.6)–(2.9).

The conservation of energy is readily apparent in the Hamiltonian formulation. The total time-derivative of H may be written

$$dH/dt = (\partial H/\partial z^i)J^{ij}(\partial H/\partial z^j).$$

From the antisymmetry of $\mathbf{J}$, one immediately sees that H is a constant of the motion. If, additionally, ϕ_2 is taken to be zero, the Lagrangian (2.14) becomes

cyclic in the coordinate z. Thus, with only one wave, P_z, the z-component of the gyro-phase-averaged canonical momentum defined in Eq. (2.16), is a conserved quantity. We note that $-P_z/(m_e\omega_{ce}L_s)$ differs from the quantity F defined above only by terms which are of second order in the small factor $\rho_L v_\parallel/(L_s v_\perp)$.

From the definition of ω_{ij}, one finds that the Jacobi tensor, $\mathbf{S}$, whose covariant components are defined by

$$S_{lmn} \equiv \frac{\partial \omega_{lm}}{\partial z^n} + \frac{\partial \omega_{mn}}{\partial z^l} + \frac{\partial \omega_{nl}}{\partial z^m},$$

is identically zero. According to Darboux's theorem, any antisymmetric, nonsingular $\mathbf{J}$ with vanishing Jacobi tensor, may be brought into canonical form by a suitable coordinate transformation. (We note that setting $\beta = 1$ in $\mathbf{J}$ yields a Jacobi tensor, $\mathbf{S}$, which ceases to vanish, thus demonstrating that Eqs. (2.6)–(2.9) are non-Hamiltonian.) Darboux's theorem offers no clue for finding such a transformation. However, an appropriate transformation for the present system is obvious from the form of the Lagrangian:

$$L = \dot{y}P_y(v_\parallel, x) + \dot{z}P_z(v_\parallel, x) - H(v_\parallel, x, y, z).$$

Using P_y and P_z as generalized coordinates, in lieu of $v_\parallel$ and x, the Lagrangian becomes $L = \dot{y}P_y + \dot{z}P_z - H(P_y, P_z, y, z)$. The Euler-Lagrange equations which result by considering P_y, P_z, y and z as independent coordinates have the form of Hamilton's equations[15]:

$$\begin{aligned} \dot{y} &= \frac{\partial H}{\partial P_y} \qquad & \dot{P}_y &= -\frac{\partial H}{\partial y} \\ \dot{z} &= \frac{\partial H}{\partial P_z} \qquad & \dot{P}_z &= -\frac{\partial H}{\partial z}. \end{aligned} \tag{2.18}$$

The Hamiltonian (2.10) must be rewritten in terms of P_y, P_z, y and z by inverting Eqs. (2.15)–(2.16) to express $v_\parallel$ and x in terms of P_y and P_z. One obtains

$$H =$$

$$\frac{1}{2m_e}\left[\frac{eB_0L_s}{c}+\sigma\sqrt{P_y^2+P_z^2}\right]^2+\sigma\frac{eB_0L_s[w_yP_y+w_zP_z]}{c\sqrt{P_y^2+P_z^2}}-e\sum_{i=1.2}\phi_i\cos(\mathbf{k}_i\cdot\mathbf{r}), \tag{2.19}$$

where $\sigma \equiv \pm 1$. The Hamiltonian has two branches, specified by σ, since $v_\parallel$ and x are multi-valued functions of P_y and P_z. Darboux's theorem is local. It doesn't guarantee a global set of canonical coordinates. It is, however, likely that orbits of interest will not cross from one branch to the other. To do so requires that $P_y^2 + P_z^2$ go to zero. From Eqs. (2.15) and (2.16), one finds that this, in turn, requires $v_\parallel$ to go through $L_s v_\perp/\rho_L$, which is a large number.

B. Dimensionless Units

The particle motion, given by either Eqs. (2.6)–(2.9), Eq. (2.17), or Eqs. (2.18), depends upon a fairly large set of dimensioned parameters:

$$\{e, m_e, c, \phi_1, \phi_2, k_{1_y}, k_{2_y}, k_{2_z}, B_0, L_s, \omega_1, \omega_2\}.$$

By exploiting dynamical similarity, one can reduce the number of free parameters from 12 to 5. This is accomplished by expressing the equations of motion in terms of a set of dimensionless variables. We now outline the approach we have taken in arriving at a suitable parametrization.

We first establish a relevent scale-length for the x-coordinate. Consider the simplified problem of motion in one wave, in the limit $\mathbf{w} \longrightarrow 0$ (i.e., the wave is stationary in the lab frame). Furthermore, assume that excursions in x away from the rational surface ($x = 0$) remain small compared with the shear length, L_s. The two conserved quantities,

$$P_z \approx m_e v_\parallel + \frac{\omega_{ce} m_e}{L_s} \frac{x^2}{2}$$

and

$$H \equiv \frac{1}{2} m_e v_\parallel^2 - e\phi_1 \cos(k_{1_y} y),$$

may be combined to express the projection of the orbits upon the x-y plane. We discuss the form of these orbits in more detail in Sec. V. For the present, we use the result that the motion remains bounded in the x-direction, and that the maximum excursion in the x-direction is attained by a homoclinic orbit parametrized by $H = e\phi_1$, $P_z = 2m_e v_0$, where

$$v_0 \equiv \sqrt{e\phi_1/m_e}$$

is the familiar trapping velocity. This orbit, which is pictured in Fig. 5.1a, has turning points at $x = \pm\sqrt{8L_s v_0/\omega_{ce}}$. This maximal excursion distance suggests defining the dimensionless coordinate

$$\tilde{x} \equiv \frac{x}{\epsilon L_s},$$

where

$$\epsilon \equiv \sqrt{\frac{v_0}{\omega_{ce} L_s}} \ .$$

Substituting this into the expression for the canonical momentum, one obtains

$$\frac{P_z}{m_e v_0} = v_\parallel/v_0 + \tilde{x}^2/2 \equiv \tilde{P}_z.$$

We therefore define the rescaled parallel velocity

$$u \equiv \frac{v_\parallel}{v_0} \ .$$

For $x \ll L_s$ and $\phi_2 = 0$, Eq. (2.7) becomes $d\tilde{x}/dt = k_{1_y} v_0 \epsilon \sin(\mathbf{k}_1 \cdot \mathbf{r})$. We therefore define the dimensionless time

$$\tilde{t} \equiv k_{1_y} v_0 \epsilon \, t.$$

It is convenient to replace the coordinates y and z with the two phase coodinates

$$\psi_i \equiv \mathbf{k}_i \cdot \mathbf{r}, \qquad i = 1, 2.$$

Using the $\beta = 1$ approximation, Eqs. (2.6)–(2.9), we obtain the following equations of motion:

$$\frac{du}{d\tilde{t}} = -\frac{1}{\epsilon}\{\sin(\epsilon\tilde{x}) \ \sin\psi_1 + \phi k \ \sin(\epsilon\tilde{x} + \theta) \ \sin\psi_2\} \tag{2.20}$$

$$\frac{d\tilde{x}}{d\tilde{t}} = \cos(\epsilon\tilde{x}) \ \sin\psi_1 + \phi k \ \cos(\epsilon\tilde{x} + \theta) \ \sin\psi_2 \tag{2.21}$$

$$\frac{d\psi_1}{d\tilde{t}} = \frac{1}{\epsilon}\{u \ \sin(\epsilon\tilde{x}) - [\tilde{w}_y \cos(\epsilon\tilde{x}) - \tilde{w}_z \sin(\epsilon\tilde{x})] \cos(\epsilon\tilde{x})\} \tag{2.22}$$

$$\frac{d\psi_2}{d\tilde{t}} = \frac{k}{\epsilon}\{u \ \sin(\epsilon\tilde{x} + \theta) - [\tilde{w}_y \cos(\epsilon\tilde{x}) - \tilde{w}_z \sin(\epsilon\tilde{x})] \cos(\epsilon\tilde{x} + \theta)\}, \tag{2.23}$$

where $k \equiv \mid \mathbf{k}_2 \mid / \mid \mathbf{k}_1 \mid$, $\phi \equiv \phi_2/\phi_1$, $\tilde{\mathbf{w}} \equiv \mathbf{w}/v_0$, and θ is the angle between the wave-vectors. The conserved energy for these equations is given by

$$H \equiv \frac{u^2}{2} - \cos\psi_1 - \phi\cos\psi_2 + \frac{1}{\epsilon^2}\left[\tilde{w}_y \sin\epsilon\tilde{x} + \tilde{w}_z \cos\epsilon\tilde{x}\right].$$

The equations of motion (2.20)–(2.23) retain the helically symmetric B-field of Eq. (2.1). These equations are general enough to describe a variety of different special cases. For example, one may choose θ, the angle between the wave vectors, to be any value. The wave vector of the first wave was fixed to be in the y-direction. Near $\tilde{x} = 0$, this wave is nearly perpendicular to the B-field. Motion for small $\tilde{x}$ is thus the relevent case for the drift wave problem. However, since the B-field twists helically, by examining the the orbits in the vicinity of $\tilde{x} = \pi/(2\epsilon)$, one can investigate the case of an electrostatic wave whose direction of propagation is approximately parallel to the B-field. We now specialize the equations of motion to the case which is appropriate for modeling the motion in drift waves in a tokamak. By assuming that the orbits remain close to the rational surface associated with the first wave (weakly sheared field) and that the angle θ is small (the waves correspond to nearby rational surfaces), an additional parameter drops out of the problem, reducing the number of free parameters from 6 to 5.

We assume that the separation, $\Delta x \equiv \theta L_s$, between the mode-rational surfaces associated with the two waves is small compared with the shear length L_s. We also assume that the radial excursion, $x \equiv \epsilon L_s \tilde{x}$, of the particle away from the first wave's rational surface remains small compared with the shear length. We therefore make the approximations $\epsilon\tilde{x} \ll 1$ and $\theta \ll 1$ and Eqs.

(2.20)–(2.23) become

$$\frac{du}{d\tilde{t}} = -\left[\tilde{x}\ \sin\psi_1 + \phi k(\tilde{x} + \theta/\epsilon)\sin\psi_2\right] \tag{2.24}$$

$$\frac{d\tilde{x}}{d\tilde{t}} = \sin\psi_1 + \phi k\ \sin\psi_2 \tag{2.25}$$

$$\frac{d\psi_1}{d\tilde{t}} = u\tilde{x} + \tilde{w}_z\tilde{x} - \frac{\tilde{w}_y}{\epsilon} \tag{2.26}$$

$$\frac{d\psi_2}{d\tilde{t}} = k\left[u\left(\tilde{x} + \frac{\theta}{\epsilon}\right) + \tilde{w}_z\tilde{x} - \frac{\tilde{w}_y}{\epsilon}\right]. \tag{2.27}$$

Thus, a set of 5 parameters, $\{\tilde{w}_y/\epsilon, \phi, k, \theta/\epsilon, \tilde{w}_z\}$, is required to specify the two-wave system. θ/ϵ equals the distance, $\Delta\tilde{x}$, between the rational surfaces of the two waves (i.e. the difference between the values of $\tilde{x}$ where each of the waves' k-vector is perpendicular to the B-field).

The dimensionless conserved energy for these equations is given by

$$H \equiv \frac{u^2}{2} - \cos\psi_1 - \phi\ \cos\psi_2 + \frac{\tilde{w}_y\tilde{x}}{\epsilon} - \frac{\tilde{w}_z\tilde{x}^2}{2},$$

and the dimensionless canonical momentum, conserved in the one-wave problem, is given by

$$\tilde{P}_z \equiv u + \frac{\tilde{x}^2}{2}.$$

We note that the system of equations (2.24)–(2.27) is Hamiltonian. We have found that they can be written in the form $\dot{z}^i = J^{ij}\partial H/\partial z^j$, where J is an antisymmetric, non-singular tensor, with vanishing Jacobi tensor S. The Hamiltonian structure which was lost in making the $\beta = 1$ approximation was apparently regained fortuitously upon making the further approximations $\epsilon\tilde{x} \ll 1$, $\theta \ll 1$.

C. The Constant Parallel Velocity Approximation

If the magnitude of $v_{\|}$ is large, one sees, from the invariance of the Hamiltonian, Eq. (2.10), that the relative variation in $v_{\|}$ becomes small. Thus, in the limit of large energy, u may be treated as a constant. Eqs. (2.26) and (2.27) may then be combined to give

$$\frac{d}{d\tilde{t}}(k\psi_1 - \psi_2) = -uk\theta/\epsilon.$$

Solving for ψ_2, one finds $\psi_2 = k\psi_1 + uk\theta(\tilde{t} - \tilde{t}_0)/\epsilon$, where $\tilde{t}_0$ is determined by initial conditions. Substituting this into Eq. (2.25), one finds that Eqs. (2.25)–(2.26) assume the form of a non-autonomous, canonical system, generated by the Hamiltonian

$$\eta(\psi_1, \tilde{x}, \tilde{t}) = \frac{1}{2}(u + \tilde{w}_z)\left[\tilde{x} - \frac{\tilde{w}_y}{\epsilon(u + \tilde{w}_z)}\right]^2 + \cos\psi_1 + \phi\,\cos[k\psi_1 + uk\theta(\tilde{t} - \tilde{t}_0)/\epsilon] \tag{2.28}$$

in which ψ_1 and $\tilde{x}$ fill the role of canonical coordinate and momentum, respectively. We emphasize that the Hamiltonian $\eta(\psi_1, \tilde{x}, \tilde{t})$, valid only for large $v_{\|}$, is distinct from the generally applicable Hamiltonian treatment presented in Sec. IIA of this work. Combining Eqs. (2.25) and (2.26), one obtains the following second order equation for ψ_1 :

$$\frac{d^2\psi_1}{d\tilde{t}^2} = (u + \tilde{w}_z)\left[\sin\psi_1 + \phi k\,\sin\left(k\psi_1 + uk\theta(\tilde{t} - \tilde{t}_0)/\epsilon\right)\right]. \tag{2.29}$$

In the limit of large parallel velocity ($u \gg 1$), the problem thus reduces to the familiar perturbed pendulum, which has been studied extensively in the literature.[7,8,16]

To motivate our consideration of the regime where the constant $v_{\|}$ approximation ceases to be valid, consider a particle with $u = 0$. The parallel velocity

in the lab-frame is then $v_{\|_{lab}} = \mathbf{w} \cdot \hat{b}$. If the particle is located at a value of x where $\hat{b}$ is parallel to $\mathbf{w}$, then $\mathbf{k}_i \cdot \hat{b} v_{\|_{lab}} = \mathbf{k}_i \cdot \hat{b}\, w\, \hat{b} \cdot \hat{b} = \mathbf{k}_i \cdot \mathbf{w} \equiv \omega_i$, for $i = 1, 2$. Hence, such a particle is simultaneously Landau resonant with both waves. The simultaneous resonance of electrons with two plane waves leads to the anomalously large nonlinear Vlasov-Poisson mode-coupling matrix elements, analyzed by Choi and Horton[17] from third order perturbation theory. Here, these orbits are calculated exactly.

III. Poincaré Surfaces of Section and the Transition to Chaos

The conservation of H confines a given orbit to a 3-dimensional manifold in phase space. When only one wave is present, a second conserved integral, P_z, exists and the motion is constrained to lie on a 2-dimensional manifold. We treat ϕ, the ratio of wave amplitudes, as a perturbation parameter. For $\phi \neq 0$, a second isolating integral of motion may cease to exist in some regions of phase space, leading to the stochastic instability.

Each constant-H surface is of the same generic variety as the magnetic field line problem in fusion confinement devices with toroidal geometry. It may therefore be of some help in visualizing the nature of this system to recast it in the language of tokamak physics. To make the correspondence concrete, consider Eqs. (2.24)–(2.27). The conserved integral for these equations is

$$H = u^2/2 - \cos\psi_1 - \phi\cos\psi_2 + \tilde{w}_y\tilde{x}/\epsilon - \tilde{w}_z\tilde{x}^2/2. \tag{3.1}$$

Let us define the strictly positive quantity $\rho \equiv \exp(u + \tilde{x}^2/2)$. The time-derivative of ρ is $\dot{\rho} = -\phi k\theta\epsilon^{-1}\rho\sin\psi_2$. One can invert ρ and H to express $\dot{\psi}_1$ and $\dot{\psi}_2$ as functions of H, ρ, ψ_1 and ψ_2 (and branch parameters). Thus adopting the coordinates (ρ, ψ_1, ψ_2), with H fixed, one sees that ρ is analogous to the minor radius of the tokamak, and ψ_1 and ψ_2 correspond to the poloidal and toroidal angles, as illustrated in Fig. 3.1. When $\phi = 0$, $\dot{\rho} = 0$ and the orbits are confined to nested toroidal surfaces of circular cross-section. For $\phi \neq 0$, one sees the emergence of islands, as shown in the figure. (The island separatrices of Fig. 3.1 were actually traced from numerically integrated trajectories, rather than merely being a schematic rendering.) For large enough perturbations, one sees the destruction of "good" two-dimensional surfaces and the emergence of

FIG. 3.1 The toroidal structure of the constant-energy surface. The poloidal and toroidal directions corespond to $\mathbf{k}_1 \cdot \mathbf{x}$ and $\mathbf{k}_2 \cdot \mathbf{x}$, respectively. The minor radius corresponds with $\exp(u + \tilde{x}^2/2)$.

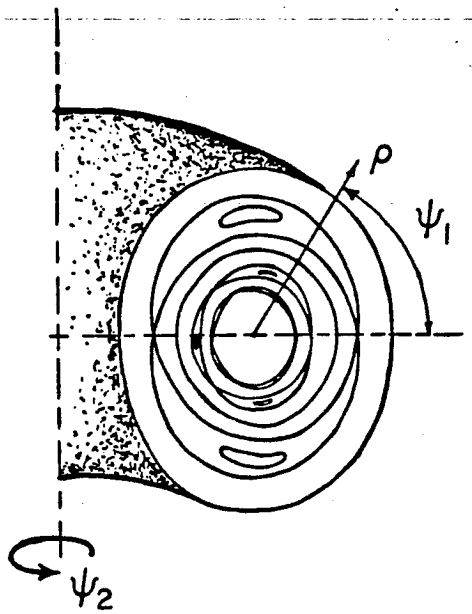

stochastic regions. Unlike the tokamak field problem, we must contend with a continuous class of such toroidal systems; one "tokamak" for each value of H.

We use the method of Poincaré surfaces of section to observe, in numerical experiments, the destruction of the second isolating integral. For a given value of H, we integrate a number of orbits, plotting a point in the $(\psi_1 \bmod 2\pi, \tilde{x})$-plane each time the trajectory passes through the surface $\psi_2 = 0 \mod 2\pi$. (Since u is a double-valued function of H, $\tilde{x}$, ψ_1 and ψ_2, only those orbits crossing the surface of section with a given sign of u should be plotted, so as to avoid a "double-exposure" effect.) Orbits for which a second isolating integral is preserved produce points in the Poincaré map which fall on one-dimensional curves. Orbits for which the second integral is destroyed yield a haphazard scatter of points, filling an area. Examples of Poincaré surfaces of section are given in Figs. 6.1–6.3 which we discuss in Section VI.

The Poincaré map defined above is a measure-preserving map of the $(\psi_1, \tilde{x})$-plane onto itself. We show in the next section that the quantity

$$\delta A \frac{\dot{\psi}_2}{\frac{\partial H}{\partial u}} \exp\left[-\int^{\tilde{t}} d\tilde{t}\, \frac{\partial \dot{z}_i}{\partial z_i}\right]$$

remains invariant under the above defined Poincaré map, where δA is an infinitesimal area element in the surface of section, and $\partial \dot{z}_i / \partial z_i$ is the divergence of the flow velocity. For Eqs. (2.20)–(2.23), the divergence of the flow velocity is $\partial \dot{\tilde{x}} / \partial \tilde{x} = \epsilon^2 du/d\tilde{t}$, hence $\delta A \dot{\psi}_2 e^{-\epsilon^2 u}/u$ is invariant under the Poincaré map. For Eqs. (2.24)–(2.27), the flow in the 4-dimensional phase space is incompressible, and $\delta A \dot{\psi}_2 / u$ is invariant under the Poincaré map.

The destruction of the second invariant integral of the motion in two degree-of-freedom systems, such as the present one, is accompanied by a transition to

chaotic behavior. Despite the fact that the equations of motion for such systems are strictly deterministic, the resulting motion appears as if the particle were being subjected to a random force.[7] Motion in the stochastic regime, corresponding to the orbits which fill a two-dimensional region of the Poincaré map, appears as if it were non-deterministic and statistical in character. The details of the long-time behavior of the orbits is highly sensitive to the initial conditions, with nearby orbits tending to diverge exponentially.

In Figs. 3.2a – 3.2d, we plot the behavior of the radial coordinate $\tilde{x}$ as a function of $\tilde{t}$. We make the following choices for the parameters: $\tilde{\mathbf{w}} = 0$, $k = 1$, $\theta/\epsilon = 3.33$, $\tilde{H} = 2$. These are the same parameter values as in the Poincaré surfaces of section of Figs. 6.1 which are discussed below. In Fig. 3.2a, ϕ is set to 0 and the motion in $\tilde{x}$ is periodic. In Figs. 3.2b and 3.2c, ϕ is set to .16, the same as its value in Fig. 6.1b. Fig. 3.2b shows the behavior of a regular (non-stochastic) orbit occuring within the 5-fold chain of islands within the trapping region of Fig. 6.1b. In the $\tilde{x}$ *vs.* $\tilde{t}$ plot of Fig. 3.2b, the motion is nearly periodic, with the amplitude of oscillation appearing to be modulated in a regular way. In Fig. 3.2c, the parameters are the same as in Fig. 3.2b, but the initial conditions $\tilde{x} = \psi_1 = 0$ place the orbit in the stochastic layer seen in Fig. 6.1b. The motion in $\tilde{x}$ is again oscillatory. However, the $\tilde{x}$-extrema seem to vary in a more haphazard way than the smoothly modulated $\tilde{x}$-extrema of Fig. 3.2b.[24] In Fig. 3.2d, the stochastic orbit is again plotted, but with ϕ increased to 1.0. The motion becomes very erratic, as if the particle were being subjected to noisy fields rather than the nicely-behaved fields which are actually present.

FIG. 3.2 The behavior of the radial coordinate as a function of time, for parameter values $\mathbf{w} = 0$, $k = 1$, $\theta/\epsilon = 3.33$, $\tilde{H} = 2$. $\phi = 0$ in (a), .16 in (b) and (c), and 1.0 in (d). (a) and (b) represent regular regions and (c) and (d) stochastic regions.

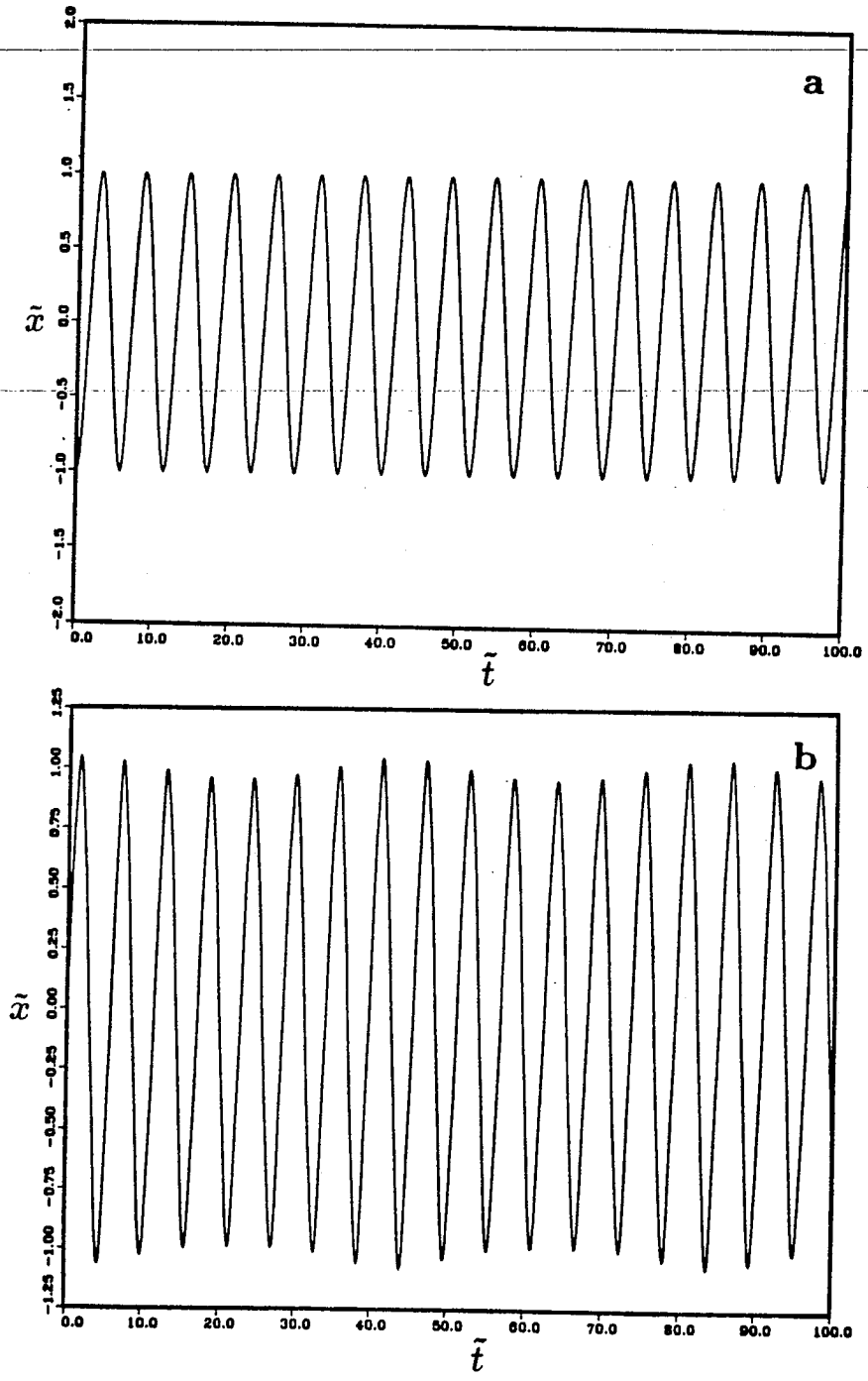

FIG. 3.2 (continued)

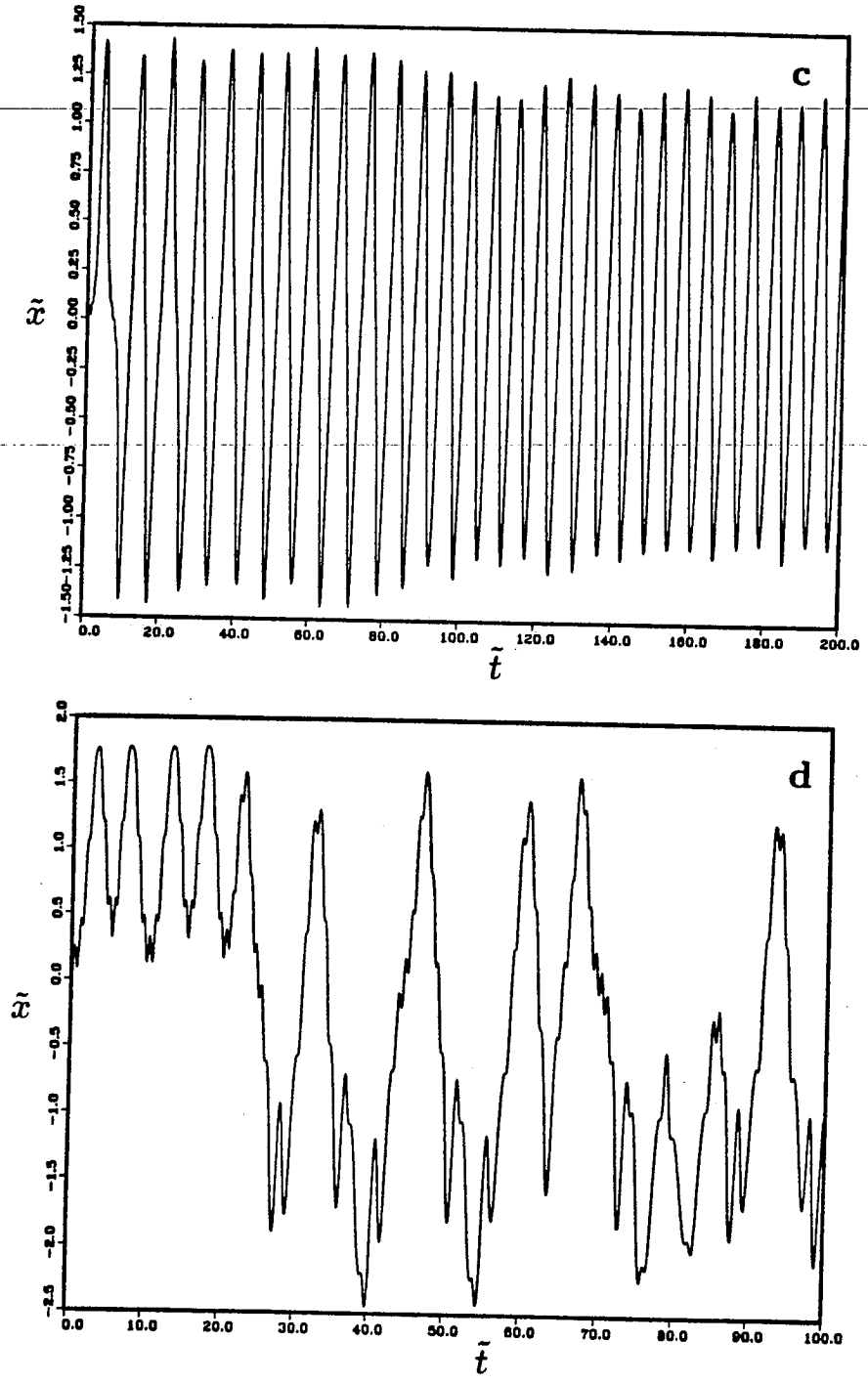

IV. Measure-Preserving Properties

Dynamical systems obeying Hamilton's equations produce a volume-preserving flow in phase space. Let us imagine a large ensemble of N (non-interacting) particles, each obeying the canonical Hamiltonian equations of motion, $\dot{q}^i = \partial H/\partial p^i$, $\dot{p}^i = -\partial H/\partial q^i$. They are initially distributed in phase space with density $\rho(z^i)$, where z^i represents the q's and p's. The evolution of the density of this ensemble of systems with time then obeys the continuity equation

$$\frac{\partial \rho}{\partial t} + \frac{\partial}{\partial z^i}\left(\rho \dot{z}^i\right) = \frac{d\rho}{dt} + \rho \frac{\partial \dot{z}^i}{\partial z^i} = 0. \tag{4.1}$$

From Hamilton's equations, one finds that the divergence of the flow velocity, $\partial \dot{z}^i/\partial z^i$, is 0, leading to the Liouville theorem, $d\rho/dt = 0$. The ensemble of phase points therefore behaves as an incompressible fluid. If the initial ensemble density is chosen to be constant within a small closed volume and zero outside that region, then such a cluster will change shape as it evolves in time, while retaining a constant volume and density. The flow is thus said to be volume-preserving.

For a Hamiltonian system in non-canonical coordinates, the flow is not incompressible. It is, however, measure-preserving. There always exists a time-independent coordinate transformation which carries the system into canonical form. Therefore, the volume of an infinitesimal phase element depends, as it evolves in time, only upon its location in phase space and not upon the history of its motion. If the small phase element returns to its initial position, then its volume returns to its original value.

In Sec. III, we discussed the Poincaré map for a two degree-of-freedom system possessing a conserved energy. Orbits lying on a constant-energy surface,

S_H, are followed, and a point is plotted each time the orbit passes through some specified surface, S_P. In our case, the surface S_H was defined by

$$H(u, x, \psi_1, \psi_2) = \text{const.},$$

and the surface S_P was defined by $\psi_2 = 0 \bmod 2\pi$. The Poincaré map is thus a mapping defined on the two-dimensional manifold $S_H \cap S_P$. For two degree-of-freedom, autonomous Hamiltonian systems, the existence of the integral invariants of Poincaré ensures that this mapping is measure-preserving. Under each iteration of the Poincaré map, a small area in the surface-of-section maps to a region whose area depends only upon its position in the surface-of-section, and not upon its history.

The equations of motion (2.17) or (2.18), being Hamiltonian, thus result in a measure-preserving flow in phase space and a measure-preserving Poincaré map. As discussed in Sec. IIA, the simple-minded guiding center equations (2.6)–(2.9), which result by applying the $\beta = 1$ approximation to equations (2.17), are non-Hamiltonian. One has no *a priori* reason to believe that the equations of motion retain the measure-preserving properties discussed above upon making the $\beta = 1$ approximation. It does turn out, however, that the equations of motion (2.6)–(2.9) produce a flow in phase space and a Poincaré map which are measure-preserving, despite the fact that these equations are non-Hamiltonian.

In subsections A and B below, we discuss conditions for the flow and the Poincaré map to be measure-preserving. The system needn't be Hamiltonian. The measure-preserving properties follow under weaker assumptions. In subsection A, we review the well-known result that the phase space flow is measure-preserving if the divergence of the flow velocity is a perfect time-derivative of

some function of the phase space coordinates. In subsection B, we prove that the Poincaré map is also measure-preserving, so long as the flow in the phase space as a whole is measure-preserving and there exists a conserved integral of the motion. These conditons are not equivalent to the conditions for a system to be Hamiltonian. Eqs. (2.6)–(2.9) provide a counter-example of a system possessing a conserved energy, H, and whose flow in phase space is measure-preserving, but whose structure is non-Hamiltonian.

We address the above issues in such detail in order to point out that the lack of the Hamiltonian structure in the traditional guiding-center equations of motion may not be such a serious defect as previously thought. The inclusion of Littlejohn's corrections in the equations of motion has been considered to be important in order that the nice properties associated with Hamiltonian systems will remain intact in the guiding-center system. One such property associated with Hamiltonian systems is a measure-preserving Poincaré map. For an arbitrary non-Hamiltonian system, it seems conceivable that the Poincaré map might display dissipative behavior while the flow in phase space remained measure-preserving. The proof in subsection B that the Poincaré map is in fact measure-preserving under weak assumptions thus appears to make the question of whether the equations are Hamiltonian a less crucial issue.

A. The Phase Space Flow

Consider a two degree-of-freedom autonomous system with phase-space coordinates

$$(z^1, z^2, z^3, z^4).$$

For the system of Sec. II, these may be identified with (u, x, ψ_1, ψ_2). The equations of motion are given by $\dot{z}^i = f^i(\mathbf{z})$. Linearizing the equations of motion about a given orbit, the displacement $\delta\mathbf{z}$ between nearby orbits is given to lowest order by the linear system

$$\delta\dot{z}^i = M^i{}_j \delta z^j, \tag{4.2}$$

where

$$M^i{}_j(t) \equiv \frac{\partial f^i}{\partial z^j}.$$

One obtains the matrix M by integrating the equations of motion $\dot{z}^i = f^i(\mathbf{z})$ for a given set of initial conditions and then substituting the solution $z^k = z^k(t)$ into the expressions for $\partial f^i/\partial z^j$. The coefficients of M are therefore functions only of the time. One may think of $\delta\mathbf{z}$ as a free vector whose tail stays attached to given particle's trajectory, which we will refer to as the central orbit. The vector's head remains attached to a particle which is infinitesimally close to the central particle.

Eq. (4.2) possesses four linearly independent solutions. We introduce the so-called *integral* matrix U, the columns of which represent 4 independent solutions to Eq. (4.2):

$$U(t) = \begin{pmatrix} U^1_1 & U^1_2 & U^1_3 & U^1_4 \\ U^2_1 & U^2_2 & U^2_3 & U^2_4 \\ U^3_1 & U^3_2 & U^3_3 & U^3_4 \\ U^4_1 & U^4_2 & U^4_3 & U^4_4 \end{pmatrix}. \tag{4.3}$$

The matrix U evolves according to

$$\dot{U}^i{}_j = M^i{}_k U^k{}_j. \tag{4.4}$$

The four columns of U define a parallelepiped in the four-dimensional phase space. The volume of this parallelepiped is given by the absolute value of the determinant of U. Therefore, in order to learn the behavior of the volume of an infinitesimal phase element with time, we calculate the value of $\det(U)$ as a function of t. The determinant of U may be written in terms of the Levi-Civita tensor as

$$\det(U) = U^1{}_i U^2{}_j ... U^{N-1}{}_n U^N{}_p \epsilon^{ij...np} \tag{4.5}$$

Here, N is the row or column dimension of U. For the present case, N is equal to 4. Differentiating with respect to time and substituting in Eq. (4.4), one obtains

$$\frac{d}{dt}\det(U) = \sum_{q=1}^{N} U^1{}_i U^2{}_j ... U^{q-1}{}_k M^q{}_r U^r{}_l U^{q+1}{}_m ... U^{N-1}{}_n U^N{}_p \epsilon^{ij...klm...np} \tag{4.7}$$

The antisymmetry of ϵ collapses the sum over r to the term $r = q$ yielding

$$\begin{aligned}\frac{d}{dt}\det(U) &= \sum_{q=1}^{N} M^q{}_q U^1{}_i U^2{}_j ... U^{N-1}{}_n U^N{}_p \epsilon^{ij...np} \\ &= \mathrm{Tr}(M)\ \det(U),\end{aligned} \tag{4.8}$$

where $\mathrm{Tr}(M)$ is the trace of M. The solution for $\det(U)$ as a function of time may then be written

$$\det\left(U(t)\right) = \det\left(U(t_0)\right) \cdot \exp \int_{t_0}^{t} dt'\ \mathrm{Tr}\left(M(t')\right). \tag{4.9}$$

This is a well-known result due to Jacobi. The trace of M is just the divergence of the flow velocity, $\partial f^i/\partial z^i = \partial \dot{z}^i/\partial z^i$.

Another approach may be used to obtain the above result with less work. Consider an ensemble of systems occupying an infinitesimal volume of phase space. The volume $\delta \mathrm{V}$ of the ensemble, as it evolves, is inversely proportional to the ensemble density. Substituting this inverse relationship into the continuity equation (4.1), we obtain

$$\begin{aligned} 0 &= \frac{d}{dt}\delta \mathrm{V}^{-1} + \delta \mathrm{V}^{-1}\frac{\partial \dot{z}^i}{\partial z^i} \\ &= -\frac{1}{\delta \mathrm{V}^2}\frac{d\delta \mathrm{V}}{dt} + \frac{1}{\delta \mathrm{V}}\frac{\partial \dot{z}^i}{\partial z^i} \end{aligned}$$

or

$$\frac{d\delta \mathrm{V}}{dt} = \delta \mathrm{V}\frac{\partial \dot{z}^i}{\partial z^i}$$

Again, we arrive at the same result as Eq. (4.8).

If the divergence of the flow velocity is the perfect time-derivative of some function of the phase space coordinates (with no explicit time-dependence), i.e.,

$$\frac{\partial \dot{z}^i}{\partial z^i} = \frac{d}{dt}\lambda(\mathbf{z}), \tag{4.10}$$

then the infinitesimal volume δV is given by

$$\delta V(t) = \delta V(t_0) \cdot e^{\lambda(\mathbf{z}(t)) - \lambda(\mathbf{z}(t_0))}. \tag{4.11}$$

No explicit time-dependence appears in the expression for the volume δV, and the flow in phase space is thus measure-preserving.

For each of the formulations of the equations of motion presented in Sec. II, the divergence of the flow velocity is a perfect time-derivative of a function of the phase space coordinates. For example, in Eqs. (2.6)–(2.9),

$$\frac{\partial \dot{z}^i}{\partial z^i} = \frac{\partial \dot{x}}{\partial x} = \frac{m_e c}{eB_0 L_s}\frac{dv_\parallel}{dt}.$$

Therefore, for this system,

$$\delta V \exp\left\{-\frac{m_e c v_{\|}}{e B_0 L_s}\right\}$$

remains invariant as the ensemble evolves.

B. The Poincaré Map

In subsection A, we placed no constraints upon the coefficients of the matrix U other than requiring that the columns be linearly independent. (Linearly dependent columns would yield a parallelepiped of zero volume.) In order to determine the behavior of the area of an element in the surface-of-section under iterations of the Poincaré map, we make some particular choices for the columns of U. First, observe that $\delta z^i = \text{const.} \cdot f^i(t)$ represents one possible solution of Eq. (4.2), since

$$\dot{f}^i = \dot{z}^j \frac{\partial f^i}{\partial z^j} = f^j \frac{\partial f^i}{\partial z^j}.$$

This solution simply corresponds to a displacement along the central trajectory. In other words, the vector $\mathbf{f}(t)$ is tangent to the central trajectory, and a displacement of $\delta\mathbf{z} = \mathbf{f}$ from the central orbit amounts to a time-shift of the central orbit. With this choice for the first column of U, we write

$$U(t) = \begin{pmatrix} f^1 & U^1_2 & U^1_3 & U^1_4 \\ f^2 & U^2_2 & U^2_3 & U^2_4 \\ f^3 & U^3_2 & U^3_3 & U^3_4 \\ f^4 & U^4_2 & U^4_3 & U^4_4 \end{pmatrix}. \tag{4.12}$$

(Strictly speaking, one should multiply the matrix U by an infinitesimal scaler, in order that the volume be infinitesimal. We suppress this scaler without any danger.) Note that the vector $\mathbf{f}(t)$ is tangent to the constant energy surface, since $f^i H_i = \dot{z}^i H_i = \dot{H} = 0$, where we have adopted the notation

$$H_i \equiv \partial H / \partial z^i. \tag{4.13}$$

At time $t = 0$, we assume that the central orbit is in the surface-of-section. In Sec. III, we made a specific choice for the surface-of-section, namely $\psi_2 = 0 \bmod 2\pi$. We shall adhere to this specific choice in the following argument.

Identifying z^4 with the coordinate ψ_2, we therefore assume that at $t = 0$, $z^4 = 0$. We also assume that at $t = 0$, the second and third columns of U are vectors lying in the surface-of-section. We therefore assume that at $t = 0$, $U^4_2 = U^4_3 = 0$. Furthermore, we assume that initially

$$U^1_2 \equiv -(H_2 U^2_2 + H_3 U^3_2)/H_1 \tag{4.14}$$

$$U^1_3 \equiv -(H_2 U^2_3 + H_3 U^3_3)/H_1. \tag{4.15}$$

The initial values of U^2_2, U^3_2, U^2_3, and U^3_3 are arbitrary, so long as the 2-component column vectors

$$\mathbf{a} \equiv \begin{pmatrix} U^2_2 \\ U^3_2 \end{pmatrix} \quad \text{and} \quad \mathbf{b} \equiv \begin{pmatrix} U^2_3 \\ U^3_3 \end{pmatrix}$$

are linearly independent. The constraints of Eqs. (4.14)–(4.15) ensure that the second and third columns of U are initially tangent to the energy surface. This can be seen by observing that the normal to the energy surface, $H_i = \partial H/\partial z^i$, is orthogonal to U^i_2 and U^i_3, i.e. $H_i U^i_2 = H_i U^i_3 = 0$. Thus, at $t = 0$, the vectors $\mathbf{a}$ and $\mathbf{b}$ define a parallelogram-shaped region in the surface-of-section having an area

$$\begin{vmatrix} U^2_2 & U^2_3 \\ U^3_2 & U^3_3 \end{vmatrix}.$$

In order that the 4 columns of U be independent, one must assume that the fourth column contains a component normal to the energy surface. We thus assume that initially, $H_i U^i_4 = \gamma \neq 0$. Observe that for any of the solutions $\delta\mathbf{z}$,

$$\begin{aligned} \frac{d}{dt}\left(\delta z^i H_i\right) &= \delta \dot{z}^i \frac{\partial H}{\partial z^i} + \delta z^i \dot{z}^j \frac{\partial^2 H}{\partial z^j \partial z^i} \\ &= \delta z^i \left[\frac{\partial f^j}{\partial z^i}\frac{\partial H}{\partial z^j} + \dot{z}^j \frac{\partial^2 H}{\partial z^j \partial z^i}\right] \\ &= \delta z^i \frac{\partial}{\partial z^i}\left(\frac{dH}{dt}\right) \\ &= 0. \end{aligned}$$

The last line holds by the conservation of H. Therefore, the expressions $\delta z^i H_i$ are invariants of the system given by Eqs. (4.2). Hence, the relations

$$H_i U^i{}_2 = 0 \tag{4.16}$$

$$H_i U^i{}_3 = 0 \tag{4.17}$$

$$H_i f^i = 0 \tag{4.18}$$

and

$$H_i U^i{}_4 = \gamma = \text{const.} \tag{4.19}$$

which we assumed to hold initially, hold identically for all time.

Assuming the initial conditions specified above, let us now imagine the system to evolve in time, and that after a time T, z^4 has returned to the surface-of-section. In the case of the two drift wave problem, we assume $z^4(T) \equiv \psi_2(T) = 0 \bmod 2\pi$. The second and third columns of $U(T)$ no longer represent displacements which are in the surface-of-section, since $U^4{}_2(T)$ and $U^4{}_3(T)$ are not necessarily 0. In other words, all points in the Poincaré surface-of-section do not return to the section after a period T. However, since the column vectors of U represent infinitesimal displacements away from the central trajectory, they can be restored to the surface-of-section by adding a small time-shift to T. The displacements represented by the second and third columns of U return to the surface-of-section after periods of $T - U^4{}_2(T)/f^4(T)$ and $T - U^4{}_3(T)/f^4(T)$, respectively. By subtracting appropriate multiples of $\mathbf{f}$ from the second and third columns of U, one can, in effect, introduce the necessary time-shifts to restore these two displacement vectors to the surface-of-section We thus define

the new tensor

$$V(T) = \begin{pmatrix} f^1 & U^1_{\ 2} - f^1 U^4_{\ 2}/f^4 & U^1_{\ 3} - f^1 U^4_{\ 3}/f^4 & U^1_{\ 4} \\ f^2 & U^2_{\ 2} - f^2 U^4_{\ 2}/f^4 & U^2_{\ 3} - f^2 U^4_{\ 3}/f^4 & U^2_{\ 4} \\ f^3 & U^3_{\ 2} - f^3 U^4_{\ 2}/f^4 & U^3_{\ 3} - f^3 U^4_{\ 3}/f^4 & U^3_{\ 4} \\ f^4 & 0 & 0 & U^4_{\ 4} \end{pmatrix}$$

Note that by the elementary properties of determinants,

$$\det(U) = \det(V). \tag{4.20}$$

The submatrix

$$D(T) \equiv \begin{pmatrix} (U^2_{\ 2} - f^2 U^4_{\ 2}/f^4) & (U^2_{\ 3} - f^2 U^4_{\ 3}/f^4) \\ (U^3_{\ 2} - f^3 U^4_{\ 2}/f^4) & (U^3_{\ 3} - f^3 U^4_{\ 3}/f^4) \end{pmatrix}$$

then defines a parallelogram of area $\det(D)$ in the (z^2, z^3)-plane which represents the image, under application of the Poincaré map, of the initial parallelogram defined by $\left(U^2_{\ 2}(0), U^3_{\ 2}(0)\right)$ and $\left(U^2_{\ 3}(0), U^3_{\ 3}(0)\right)$. By calculating the value of $\det\left(D(T)\right)$, we discover the behavior of a small element of the surface-of-section under iteration of the Poincaré map. In the following, we demonstrate that a measure-preserving flow in the phase space as a whole implies a measure-preserving Poincaré map by deriving a simple relationship between $\det\left(D(T)\right)$ and $\det\left(U(T)\right)$.

Evaluating the determinants of D and V, one finds

$$\det(D) =$$

$$\frac{1}{f^4}\left[f^2(U^3_{\ 2}U^4_{\ 3} - U^4_{\ 2}U^3_{\ 3}) + f^3(U^4_{\ 2}U^2_{\ 3} - U^2_{\ 2}U^4_{\ 3}) + f^4(U^2_{\ 2}U^3_{\ 3} - U^3_{\ 2}U^2_{\ 3})\right] \tag{4.21}$$

and

$$\det(V) = U^4_{\ 4}d_1 - f^4\left[U^1_{\ 4}\det(D) - U^2_{\ 4}d_2 + U^3_{\ 4}d_3\right], \tag{4.22}$$

where

$$d_1 \equiv \begin{vmatrix} f^1 & U^1_{\ 2} & U^1_{\ 3} \\ f^2 & U^2_{\ 2} & U^2_{\ 3} \\ f^3 & U^3_{\ 2} & U^3_{\ 3} \end{vmatrix},$$

$$d_2 \equiv \frac{1}{(f^4)^2} \begin{vmatrix} (f^4U^1_{\ 2} - f^1U^4_{\ 2}) & (f^4U^1_{\ 3} - f^1U^4_{\ 3}) \\ (f^4U^3_{\ 2} - f^3U^4_{\ 2}) & (f^4U^3_{\ 3} - f^3U^4_{\ 3}) \end{vmatrix},$$

and

$$d_3 \equiv \frac{1}{(f^4)^2} \begin{vmatrix} (f^4U^1_{\ 2} - f^1U^4_{\ 2}) & (f^4U^1_{\ 3} - f^1U^4_{\ 3}) \\ (f^4U^2_{\ 2} - f^2U^4_{\ 2}) & (f^4U^2_{\ 3} - f^2U^4_{\ 3}) \end{vmatrix}.$$

Using Eqs. (4.16) and (4.17) to eliminate $U^1_{\ 2}$ and $U^1_{\ 3}$ from the expressions for d_1, d_2 and d_3, straightforward evaluation of these determinants yields, after some algebraic simplification,

$$d_1 = \frac{1}{H_1}\{[H_1f^1 + H_2f^2 + H_3f^3][U^2_{\ 2}U^3_{\ 3} - U^3_{\ 2}U^2_{\ 3}]$$

$$+H_4[f^2(U^3_{\ 3}U^4_{\ 2} - U^3_{\ 2}U^4_{\ 3}) + f^3(U^2_{\ 2}U^4_{\ 3} - U^2_{\ 3}U^4_{\ 2})]\},$$

$$d_2 = \frac{1}{H_1f^4}\{[H_1f^1 + H_3f^3 + H_4f^4][U^3_{\ 2}U^4_{\ 3} - U^3_{\ 3}U^4_{\ 2}]$$

$$+H_2[f^3(U^4_{\ 3}U^2_{\ 2} - U^2_{\ 3}U^4_{\ 2}) + f^4(U^2_{\ 3}U^3_{\ 2} - U^2_{\ 2}U^3_{\ 3})]\},$$

$$d_3 = \frac{1}{H_1f^4}\{[H_1f^1 + H_2f^2 + H_4f^4][U^2_{\ 2}U^4_{\ 3} - U^2_{\ 3}U^4_{\ 2}]$$

$$+H_3[f^4(U^2_{\ 2}U^3_{\ 3} - U^2_{\ 3}U^3_{\ 2}) + f^2(U^4_{\ 3}U^3_{\ 2} - U^4_{\ 2}U^3_{\ 3})]\}.$$

Using Eq. (4.18), one finds, upon comparison with Eq. (4.21),

$$d_1 = -\frac{f^4H_4}{H_1}\det(D)$$

$$d_2 = -\frac{H_2}{H_1}\det(D)$$

$$d_3 = \frac{H_3}{H_1}\det(D).$$

From Eq. (4.22), we therefore find

$$\det(V) = -\frac{f^4}{H_1}\left[H_4 U^4{}_4 + H_1 U^1{}_4 + H_2 U^2{}_4 + H_3 U^3{}_4\right].$$

Using Eqs. (4.19)–(4.20), one obtains

$$\det(D) = -\frac{H_1}{\gamma f^4}\det(U). \tag{4.23}$$

γ, given by Eq. (4.19), is simply a constant determined by the initial value of the vector $U^i{}_4$ which is chosen to be non-tangential to the energy surface, but whose choice is otherwise arbitrary. Therefore,

$$\frac{\det(U)}{\det(D)}\frac{f^4}{H_1}$$

remains a constant under each iteration of the Poincaré map. In subsection A above, we found that if the divergence of the flow velocity is given by

$$\frac{\partial \dot{z}^i}{\partial z^i} = \frac{d}{dt}\lambda(\mathbf{z}),$$

the perfect time-derivative of a function of the phase space coordinates, then the quantity

$$\det(U)e^{-\lambda(\mathbf{z})}$$

remains constant under the phase space flow. Combining these results, one finds that

$$\det(D)\frac{f^4}{H_1}e^{-\lambda(\mathbf{z})}$$

remains invariant under iteration of the Poincaré map, assuming the flow in phase space is measure-preserving.

$\det(D)$ is the area of the infinitesimal parallelogram-shaped region in the Poincaré surface of section. One can build up an arbitrarily shaped area from

infinitesimal parallelograms. Therefore, more generally, for an arbitrarily shaped infinitesimal element in the surface of section having area δA, the quantity

$$\delta A \frac{f^4}{H_1} e^{-\lambda(\mathbf{z})}$$

remains invariant under the Poincaré map. For example, for Eqs. (2.20)–(2.23),

$$\frac{\partial \dot{z}^i}{\partial z^i} = \frac{\partial \dot{\tilde{x}}}{\partial \tilde{x}} = \epsilon^2 \frac{du}{d\tilde{t}},$$

so, in this case, $\lambda = \epsilon^2 u$. For this system,

$$f^4 = \dot{\psi}_2 = \frac{k}{\epsilon}\{u \sin(\epsilon\tilde{x} + \theta) - [\tilde{w}_y \cos(\epsilon\tilde{x}) - \tilde{w}_z \sin(\epsilon\tilde{x})]\cos(\epsilon\tilde{x} + \theta)\}$$

and $H_1 = \partial H/\partial u = u$. Therefore,

$$\delta A e^{-\epsilon^2 u} \frac{k}{\epsilon}\left\{\sin(\epsilon\tilde{x} + \theta) - \frac{1}{u}[\tilde{w}_y \cos(\epsilon\tilde{x}) - \tilde{w}_z \sin(\epsilon\tilde{x})]\cos(\epsilon\tilde{x} + \theta)\right\}$$

is invariant under the Poincaré map. This provides an example of a non-Hamiltonian system with a measure-preserving Poincaré map.

V. Motion in One Wave — The Unperturbed Problem

Before discussing the two-wave problem, we give the properties of the unperturbed problem. With $\phi = 0$ (one wave), the equations of motion (2.24)–(2.26) reduce to the one parameter family of trajectories

$$\dot{\tilde{u}} = -\tilde{x} \sin \psi_1 \tag{5.1}$$

$$\dot{\tilde{x}} = \sin \psi_1 \tag{5.2}$$

$$\dot{\psi}_1 = \tilde{u}\tilde{x} - \lambda, \tag{5.3}$$

where $\lambda \equiv \tilde{w}_y/\epsilon$. The parameter $\tilde{w}_z$ has been absorbed into the parallel velocity by defining a "shifted" velocity $\tilde{u} \equiv u + \tilde{w}_z$.

The motion is completely specified, within a similarity transformation, by the initial coordinate values and the single parameter λ. That is to say, for two distinct choices of the dimensional parameters which yield the same value of λ, the resulting solutions to the equations of motion will differ only by a change of scales. The parameter λ is reminiscent of the Reynolds number of fluid dynamics. In the limiting case where the wave is stationary in the lab frame ($\tilde{w}_y = 0$), the problem contains *no* parameters, and we have the somewhat remarkable result that assigning arbitrary values to the 8 quantities $\{e, m_e, c, \phi_1, k_{1_y}, k_{1_z}, B_0, L_s\}$ results in motion which is identical, up to a similarity transformation.

One can verify that the quantities $\tilde{H} = \tilde{u}^2/2 - \cos \psi_1 + \lambda\tilde{x}$ and $\tilde{P}_z = \tilde{u} + \tilde{x}^2/2$ are invariants of the motion. $\tilde{H}$ and $\tilde{P}_z$ are related to the small x/L_s limit versions of Eqs. (2.10) and (2.16) by $\tilde{P}_z \equiv P_z/(m_e v_0)$ and $\tilde{H} \equiv (H + w_z P_z)/(m v_0^2)$, up to additive constants. The system of equations (5.1)–(5.3) is integrable, in the sense that expressions for the motion may be reduced to quadrature. However, the prospect of obtaining general solutions for the motion

in terms of well-known analytic functions seems doubtful. The two constants of the motion may be combined with Eq. (5.1) to give

$$d\tilde{t} = \frac{d\tilde{u}}{-\sigma_1\sigma_2\sqrt{2[\tilde{P}_z - \tilde{u}]}\sqrt{1 - \left\{\tilde{u}^2/2 - \tilde{H} + \lambda\sigma_1\sqrt{2[\tilde{P}_z - \tilde{u}]}\right\}^2}}, \tag{5.4}$$

where σ_1 and σ_2 are branch parameters equal to ± 1. Even for the case $\lambda = 0$, the expression under the radical is a quintic polynomial in $\tilde{u}$. This apparently precludes the possibility of integrating Eq. (5.4) in terms of elliptic integrals,[23] except for special values of $\tilde{H}$ and $\tilde{P}_z$ where singular points in the expression for $d\tilde{t}/d\tilde{u}$ degenerate into simple poles (i.e. homoclinic orbits). In Sec VB, below, we consider a few examples of separatrices for which analytic expressions may be obtained.

As was pointed out in Sec. IIC, for large values of $\tilde{u}$, the motion in the $(\psi_1, \tilde{x})$-plane becomes isomorphic to that of the pendulum. On the other hand, in the small-$\tilde{u}$ regime, this approximation ceases to be valid and a much richer variety of behavior is displayed. The correct second integral of motion is the z-component of the canonical momentum, not the parallel velocity. We now undertake a classification of the various orbits which are possible. Combining the two integrals of the motion, the projections of the orbits upon the $(\psi_1, \tilde{x})$-plane are given by

$$\tilde{H} = \frac{1}{2}\left[\tilde{P}_z - \frac{\tilde{x}^2}{2}\right]^2 - \cos\psi_1 + \lambda\tilde{x}. \tag{5.5}$$

Each orbit in the $(\psi_1, \tilde{x})$-plane is specified by the values of $\tilde{H}$ and $\tilde{P}_z$. For the purpose of graphically illustrating the various kinds of orbits which may occur, we fix the value of $\tilde{P}_z$ and plot a number of orbits in the $(\psi_1, \tilde{x})$-plane for several

values of $\tilde{H}$. One's first instinct might be to take the opposite tack and fix the value of $\tilde{H}$, constructing a plot of several orbits having various values of $\tilde{P}_z$. Plotting orbits on the constant-$\tilde{H}$ surface seems the preferable approach, since $\tilde{H}$ remains a good constant of the motion when we go to the two-wave problem; whereas $\tilde{P}_z$ does not. However, since $\tilde{u}$ is a double-valued function of $\tilde{H}$, it is possible for two distinct trajectories to cross in the constant-$\tilde{H}$ projection. This complication does not arise if we consider orbits plotted in the constant-$\tilde{P}_z$ projection; we have taken this approach in order to render a comprehensive orbit classification tractable. Eliminating $\tilde{u}$ in favor of $\tilde{P}_z$, Eqs. (5.2)–(5.3) become

$$\dot{\tilde{x}} = \sin\psi_1 \qquad\qquad \dot{\psi_1} = \left[\tilde{P}_z - \frac{\tilde{x}^2}{2}\right]\tilde{x} - \lambda. \tag{5.6}$$

Treating ψ_1 and $\tilde{x}$ as canonical coordinates, Eq. (5.5) is the Hamiltonian which generates the equations of motion (5.6).

The phase portraits in the $(\psi_1, \tilde{x})$-plane, produced by Eqs. (5.6), fall into twelve distinct categories, depending upon the values of $\tilde{P}_z$ and λ. Figs. 5.1a–5.1l are representative of the possible classes. Figs. 5.1b–5.1f are all topologically equivalent to the pendulum. Fig. 5.2 gives an atlas showing which of the classes *a* through *l* occurs for each value of the parameter pair $\tilde{P}_z$ and λ. For example, each pair of parameters $(\lambda, \tilde{P}_z)$ falling within the two-dimensional domain labeled *g* in Fig. 5.2 will give rise to a phase portrait which is topologically similar to the orbits of Fig. 5.1g. The classes *c, d, h, i* and *l* are one-dimensional sets in the $(\lambda, \tilde{P}_z)$-plane, while the classes *a, e* and *f* are zero-dimensional sets. In order to construct such an atlas, we carry out a singular point analysis of Eqs. (5.6).

FIG. 5.1 Orbit classes for the one-wave problem. Plots show projections of orbits upon $(\psi_1, \tilde{x})$-plane for constant value of P_z.

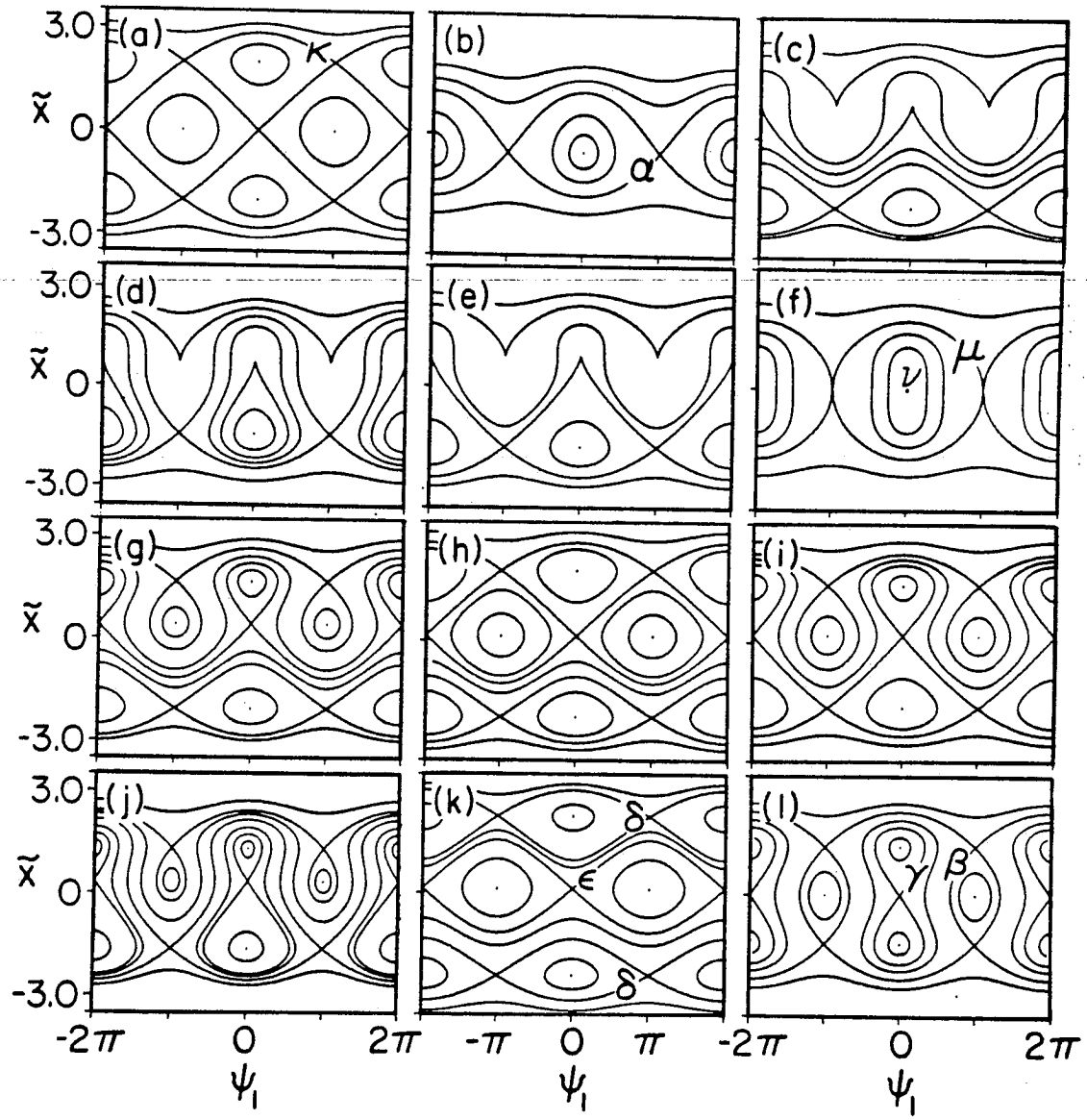

FIG. 5.2 Atlas of one-wave orbit classes. Letters a through l label the regions of the $(\lambda = \tilde{w}_y/\epsilon, \tilde{P}_z)$-plane which produce the corresponding orbit topologies of Figs. 5.1a – 5.1l.

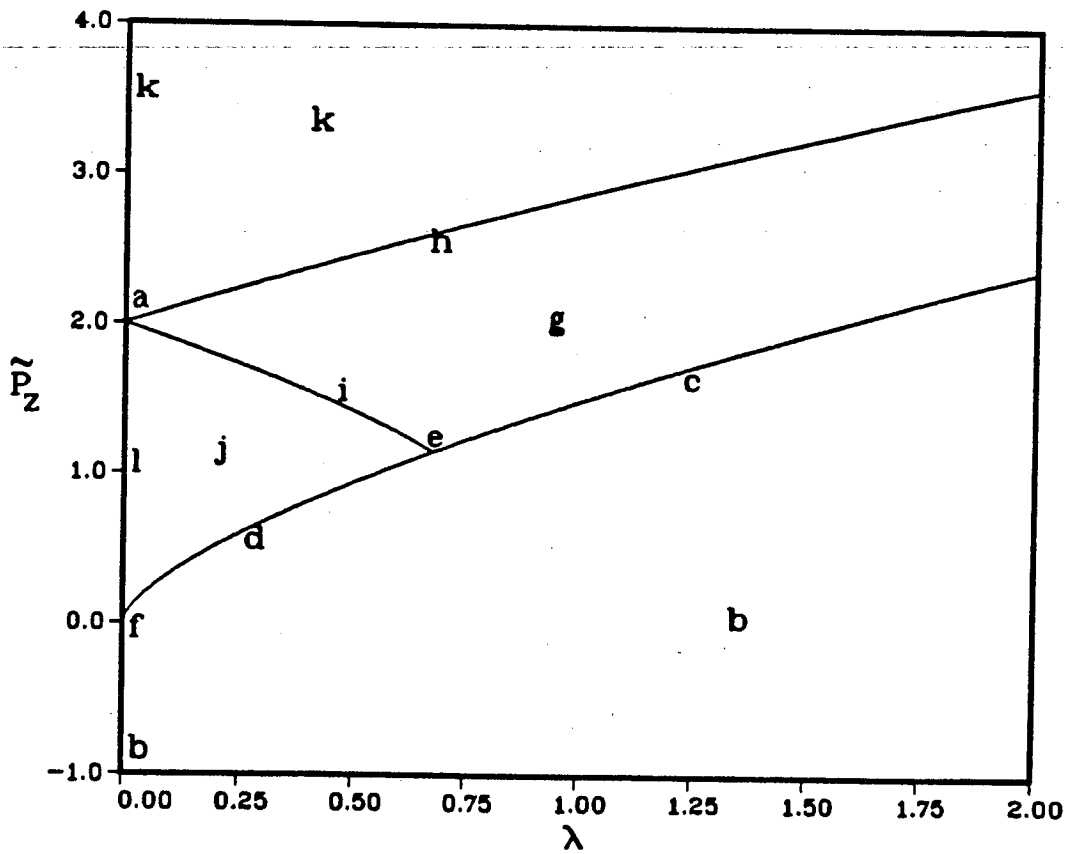

FIG. 5.3 Plot of the curve $b = (\zeta^2 + 2\zeta^{-1})/3$, where $b \equiv 2/3\lambda^{-2/3}\tilde{P}_z$ and $\zeta \equiv \lambda^{-1/3}\tilde{x}$. This curve yields, for each given value of $\tilde{P}_z$ the radial location of the fixed points.

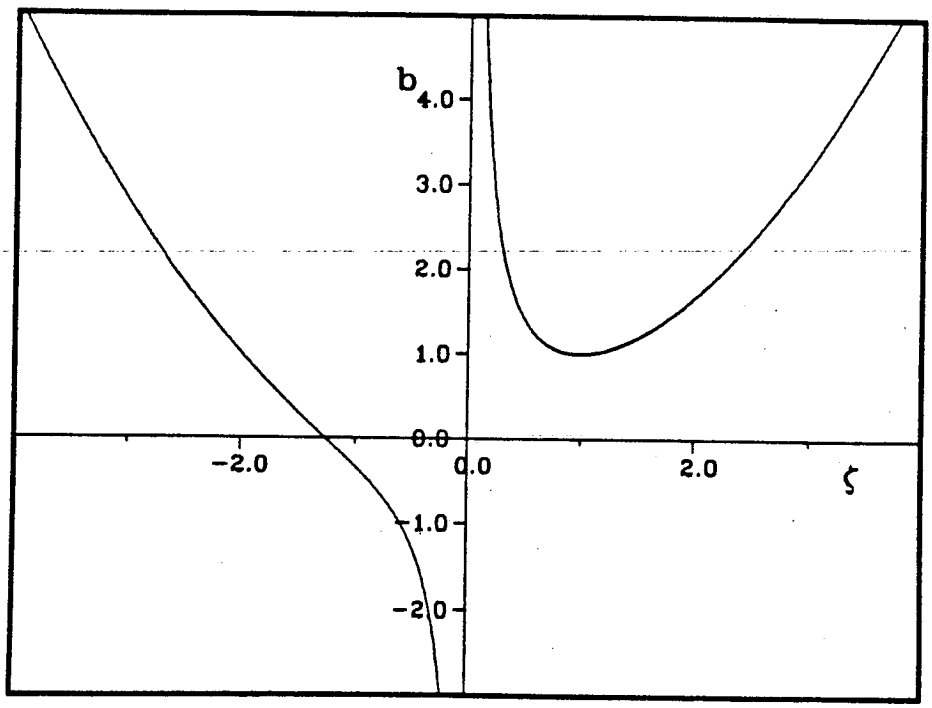

A. Orbit Classes for $\lambda \neq 0$

Let us first consider the case $\lambda \neq 0$. One may assume, without loss of generality, that λ is positive, since the one-wave equations of motion (5.1)–(5.3) remain invariant under the transformation $(\tilde{x}, \psi_1, \lambda) \longrightarrow (-\tilde{x}, -\psi_1, -\lambda)$. Looking for the fixed points of Eqs. (5.6), defined by $\dot{\psi}_1 = \dot{\tilde{x}} = 0$, one finds that the fixed points occur for $\psi_1 = n\pi$, n an integer, and $\tilde{x} = \lambda^{1/3}\zeta$, where ζ is a root of the cubic equation

$$b = (\zeta^2 + 2\zeta^{-1})/3 \tag{5.7}$$

and b is defined by the equation

$$\tilde{P}_z = \frac{3}{2}\lambda^{2/3} b. \tag{5.8}$$

Eq. (5.7) is plotted in Fig. 5.3, showing b as a function of ζ. Looking at this plot, one sees that, for $b < 1$, only one real root, which we call ζ_3, exists. It is always negative. For $b > 1$, three real roots to Eq. (5.7) exist. One can express these roots as

$$\zeta_1 = 2\sqrt{b}\,\cos\left[\frac{1}{3}\arccos\left(-b^{-3/2}\right)\right] \tag{5.9}$$

$$\zeta_2 = 2\sqrt{b}\,\cos\left[\frac{4\pi}{3} + \frac{1}{3}\arccos\left(-b^{-3/2}\right)\right] \tag{5.10}$$

$$\zeta_3 = 2\sqrt{b}\,\cos\left[\frac{2\pi}{3} + \frac{1}{3}\arccos\left(-b^{-3/2}\right)\right], \qquad (b > 1) \tag{5.11}$$

$$= -\sqrt[3]{1 - \sqrt{1 - b^3}} - \sqrt[3]{1 + \sqrt{1 - b^3}}, \quad (b \leq 1)$$

where $\zeta_1 > 1$, $0 < \zeta_2 < 1$, and $\zeta_3 < 0$.

A stability analysis of Eqs. (5.6) indicates that the point

$$(\psi_1, \tilde{x}) = (n\pi, \lambda^{1/3}\zeta)$$

is a stable fixed point if $(-1)^n[\zeta^{-1} - \zeta^2] < 0$, and unstable otherwise. From this relation, one can determine the stability of the fixed points corresponding to the three roots for ζ and even and odd values of n. These results are summarized in Table 5.1.

Table 5.1

Stability of the fixed points occuring at $\psi_1 = n\pi$ and $\tilde{x} = (\tilde{w}_y/\epsilon)^{1/3}\zeta$. The ζ_i are the 3 roots to the cubic equation Eq. (5.7).

	n Even	n Odd
$\zeta_1 > 1$	Stable	Unstable
$0 < \zeta_2 < 1$	Unstable	Stable
$\zeta_3 < 0$	Stable	Unstable

In Fig. 5.2, the bottom curve is the function $\tilde{P}_z = \frac{3}{2}\lambda^{2/3}$, which, according to Eq. (5.8), corresponds to $b = 1$. This curve thus divides the $(\lambda, \tilde{P}_z)$-plane into the 1-root and 3-root regions. Below this curve, the plots are all topologically similar to the pendulum, e.g. Fig. 5.1b.

When $b = 1$, the topology is also that of the pendulum. However, the coalescence of the two roots ζ_1 and ζ_2 results in the appearence of cusp singularities at $\tilde{x} = \lambda^{1/3}$. When $\lambda > (16/27)^{3/4}$, the cusps corresponding to both n odd and n even fall outside the separatrix, as illustrated in Fig. 5.1c. For $\lambda < (16/27)^{3/4}$, one set of cusps falls inside the separatrix, as illustrated in Fig. 5.1d. For $\lambda = (16/27)^{3/4}$, one set of cusps occur on the separatrix (Fig. 5.1e). (One arrives at this value by calculating the intersection of the $b = 2\tilde{P}_z\lambda^{-2/3}/3 = 1$ curve and the curve labeled i in Fig. 5.2, which we discuss below.)

For $b > 1$ and $\lambda \neq 0$, five classes are possible. These are illustrated in Figs. 5.1g–5.1k. Writing Eq. (5.5) in terms of b and ζ,

$$\tilde{H}\lambda^{-4/3} = \frac{1}{8}\left[3b - \zeta^2\right]^2 - \lambda^{-4/3}\cos\psi_1 + \zeta. \tag{5.12}$$

For the class of orbits illustrated in Fig. 5.1h, the X-points at $(\pi, \lambda^{1/3}\zeta_1)$ and $(0, \lambda^{1/3}\zeta_2)$ fall on the same trajectory. Hence, they share a common value of $\tilde{H}$. Using Eq. (5.12), one finds that the plots of class e must obey the relation

$$\lambda = 8\left[\zeta_2^4 - \zeta_1^4 - 6b(\zeta_2^2 - \zeta_1^2) + 8(\zeta_2 - \zeta_1)\right]^{-3/4}. \tag{5.13}$$

Eqs. (5.13) and (5.8), along with the definitions of ζ_1, ζ_2, and ζ_3 given in Eqs. (5.9)–(5.11), constitute a parametric representation of a curve in the $(\lambda, \tilde{P}_z)$-plane, where the parameter b is allowed to range from 1 to ∞. This yields the curve labeled h in Fig. 5.2.

Similarly, the class of orbits illustrated in Fig. 5.1i, where the **X**-points at $(0, \lambda^{1/3}\zeta_2)$ and $(\pi, \lambda^{1/3}\zeta_3)$ fall on the same trajectory, occur for values of $\tilde{P}_z$ and λ obeying the parametric relationship given by Eq. (5.8) and

$$\lambda = 8\left[\zeta_2^4 - \zeta_3^4 - 6b(\zeta_2^2 - \zeta_3^2) + 8(\zeta_2 - \zeta_3)\right]^{-3/4}. \tag{5.14}$$

This curve is labeled i in Fig. 5.2. After finding the above classes of zero measure in the $(\lambda, \tilde{P}_z)$-plane, as well as those discussed below in Sec. VB, it is a straightforward matter to assign the remaining classes of non-zero measure, g, j and k, to the appropriate regions of the atlas.

B. Orbit Classes for $\lambda = 0$

We now discuss the orbits for the case where the wave is stationary in the lab frame. This regime is represented by the $\tilde{P}_z$-axis in Fig. 5.2. For $\lambda = 0$, the fixed points are given by $\psi_1 = n\pi$ and $\tilde{x}$ equal to 0, as well as $\pm\sqrt{2\tilde{P}_z}$ when $\tilde{P}_z$ is positive. For $\tilde{P}_z < 0$, the plots are topologically similar to those of the pendulum, belonging to the class b discussed for the $\lambda \neq 0$ case. However, for $\lambda = 0$, the orbits are symmetric about the ψ_1 axis. When $\tilde{P}_z = 0$, the triply degenerate root for $\tilde{x}$ leads to a separatrix which is parabolic-shaped, rather than linear, at the unstable singularities, and motion near the stable fixed points which is anharmonic. This case is illustrated in Fig. 5.1f.

As $\tilde{P}_z$ becomes positive, the fixed points bifurcate into a triplet of fixed points. Since, for $\lambda = 0$, $\tilde{H}$ is an even function of $\tilde{x}$, the fixed points at $(\psi_1, \tilde{x}) = (n\pi, \pm\sqrt{2\tilde{P}_z})$, n odd, all have the same value of $\tilde{H}$; namely $\tilde{H} = 1$. For $0 < \tilde{P}_z \leq 2$, these X-points all fall on the same trajectory. This class of orbits is illustrated in Fig. 5.1l. As $\tilde{P}_z$ is increased to 2, one sees, from Eq. (5.5) that the figure-eight separatrix of Fig. 5.1l also attains a value of $\tilde{H}$ equal to 1. All of the separatrices merge into one web for $\tilde{P}_z = 2$, $\lambda = 0$, resulting in the orbits shown in Fig. 5.1a.

As $\tilde{P}_z$ is made greater than 2, a reconnection of the separatrices occurs, producing the topology of Fig. 5.1k. As with class b, the class k occurs for both $\lambda \neq 0$ and $\lambda = 0$. Again, in the latter case, the orbits differ from those of Fig. 5.1k in that they are symmetric about the ψ_1 axis. A set of 3 pendulum-like "islands" emerge. The upper and lower islands move off toward $\pm\infty$ as $\tilde{P}_z$ is made large. The stable fixed points at the centers of these islands simply represent particles with zero parallel velocity, sitting at the bottom of the electrostatic

potential well. Such particles feel a stable restoring force along the field lines for any value of $\tilde{x} \neq 0$.

Setting $\lambda = 0$ in Eq. (5.5) and using our knowledge of where the X-points occur, we can find a set of relatons between $\tilde{P}_z$ and $\tilde{H}$ which hold on the separatrices. For the separatrix labeled α in Fig. 5.1b, one finds $\tilde{H} = \tilde{P}_z^2/2 + 1$. For the separatrices labeled ε and γ in Figs. 5.1k and 5.1l, $\tilde{H} = \tilde{P}_z^2/2 - 1$. All of the separatrices μ, β, κ and δ have a constant value of $\tilde{H} = 1$. These relations are plotted in Fig. 5.4.

FIG. 5.4 Locus of the separatrices for the one wave system, taking $\mathbf{w} = 0$.

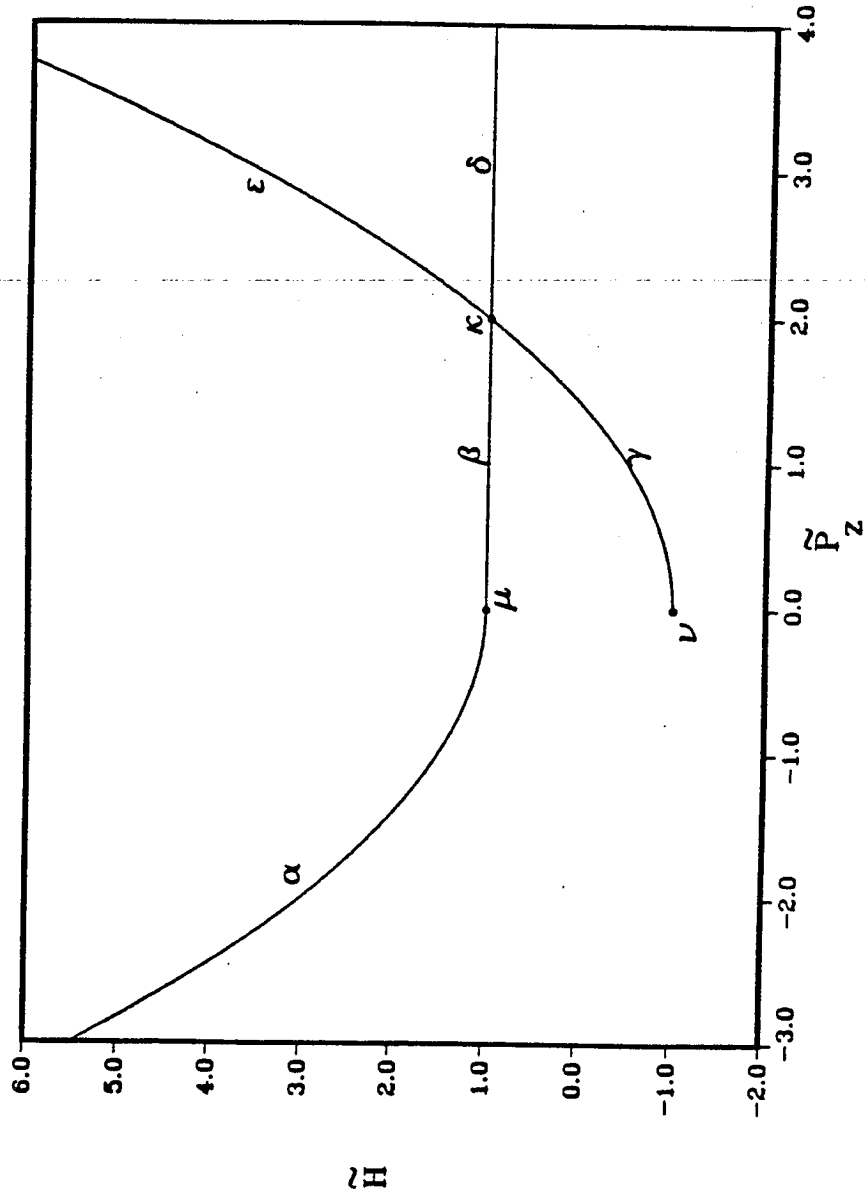

The curves in Fig. 5.4 thus constitute a locus of the separatrices for the $\lambda = 0$ case. Each point in the $(\tilde{P}_z, \tilde{H})$-plane of Fig. 5.4 represents an orbit, and due to the constancy of $\tilde{P}_z$ and $\tilde{H}$ for one wave, a point remains stationary with time in this projection. This plot suppresses the phase information. Those points falling on one of the plotted curves are orbits of infinite period.

As we mentioned previously, Eq. (5.4) can be integrated analytically for the separatrices in the $\lambda = 0$ case. For example, consider the separatrix labeled β in Fig. 5.1l. For this orbit, $\tilde{H} = 1$. Substituting values of $\tilde{H} = 1$ and $\lambda = 0$ into Eq. (5.4), one obtains

$$d\tilde{u}/d\tilde{t} = \pm\tilde{u}\sqrt{2(\tilde{P}_z - \tilde{u})(1 - \tilde{u}^2/4)}$$

This is integrable in terms of elliptic functions, since the expression under the radical is a cubic polynomial in $\tilde{u}$.[24] For the portion of this separatrix where $\tilde{u} > 0$, the solution may be written

$$t = \pm\frac{1}{\sqrt{2}}\left[\mathrm{F}(A,B) + \frac{2-\tilde{P}_z}{\tilde{P}_z}\,\Pi(A, -\frac{\tilde{P}_z+2}{2\tilde{P}_z}, B)\right],$$

where

$$A \equiv \arcsin\sqrt{\frac{\tilde{P}_z - \tilde{u}}{(2-\tilde{u})(\tilde{P}_z+2)}},$$

$$B \equiv \frac{\sqrt{\tilde{P}_z+2}}{2}.$$

Here, $F(\phi,k)$ and $\Pi(\phi,n,k)$ are the elliptic integrals of the first and third kinds, respectively.

Finding the analytic solutions for the remainder of the separatrices (in the $\lambda = 0$ problem) is straightforward, if tedious. We will not write down the solution for all of the separatrices, but only mention the special case of the orbit

labeled κ in Fig. 5.1a. For this case, $d\tilde{u}/d\tilde{t} = \pm 2\tilde{u}(1-\tilde{u}/2)\sqrt{1+\tilde{u}/2}$. The motion on this separatrix may be solved in terms of elementary functions as

$$t = \text{const.} \pm \frac{1}{2\sqrt{2}} \ln \left[\frac{\text{sgn}(\tilde{u})(1+D)(D-1/\sqrt{2})^{\sqrt{2}}}{(1-D)(D+1/\sqrt{2})^{\sqrt{2}}} \right],$$

where

$$D \equiv \sqrt{\frac{1+\tilde{u}/2}{2}}.$$

VI. Motion in Two Waves — The Perturbed Problem

We now consider the perturbed problem. For $\phi \neq 0$, one sees the emergence of resonance "islands," as shown in Fig. 3.1. These islands are located near the tori of the unperturbed problem having rational winding numbers. As the perturbation strength ϕ is increased, the islands grow in size. One begins to see a transition to stochastic behavior as islands associated with neighboring, low-order rational surfaces approach each other. In subsection A., we calculate island overlap criteria by approximating the locations and widths of the lowest order resonance islands, using perturbation theory. In subsection B., we obtain global stochasticity criteria by investigating the conditions for strong interaction of the primary trapping regions associated with each of the two waves.

In these analyses, we confine the discussion to the case $\mathbf{w} = 0$ (waves at rest in the lab frame). We have focused our attention upon this limiting case, in this first investigation, in an attempt to simplify the problem; we make no assertion that $\mathbf{w} = 0$ is a realistic approximation.

However, this limiting case may not be so unrepresentative as it might appear to be at first sight. The two-wave system considered in this work contrasts sharply with other two-wave systems considered by previous authors. In some other two-wave systems, the zero frequency limit is a rather uninteresting degenerate case. For example, consider the "canonical" stochastic problem of the perturbed pendulum with Hamiltonian

$$H = \frac{p^2}{2} - \phi_1 \cos(q) - \phi_2 \cos(kq - \omega t + \alpha).$$

This system may be used to describe, for example, the one-dimensional motion of a charged particle in two electrostatic plane waves propagating in the same

direction in an unmagnetized plasma. In the limit $\omega \longrightarrow 0$ (i.e., the waves have the same phase velocity in some inertial frame), the motion is integrable. For given values of ϕ_1 and ϕ_2, the level of stochasticity is dictated by the value of ω/k. For ω/k roughly equal to $2\left[\sqrt{\phi_1}+\sqrt{\phi_2}\right]$, and ϕ_1 roughly comparable to ϕ_2 in magnitude, one observes a high level of stochasticity.

Similarly, in the two-wave, magnetized plasma system considered by Kleva and Drake[5] and Horton[6], where the parallel motion decouples from the cross-field drifts, the motion produced by the Hamiltonian

$$H(x,y,t) = ux + \sin(x)\,\cos(y) + \phi\,\sin(kx+\alpha)\,\cos\left[q(y-vt)\right],$$

(x and y taken to be canonically conjugate), becomes integrable in the limit $v \longrightarrow 0$. In these $1\frac{1}{2}$ degree-of-freedom systems, the mismatch between phase velocities of the two waves is the crucial parameter (along with the wave amplitudes) in controlling the transition to chaos. In particular, if the phase velocities of both waves are zero, then the motion is integrable.

In contrast, stochasticity may be present in the magnetic shear problem for any values of the wave frequencies $\omega_i, i = 1,2$, even for $\omega_1 = \omega_2 = 0$. This is related to the fact that our system is of higher dimensionality than the $1\frac{1}{2}$ degree-of-freedom systems cited above. Our system is a two degree-of-freedom in which stochastic motion does not require the appearence of a time-dependent perturbation. For the system of equations (2.24)–(2.27), the parameter θ, the angle between the two waves (or θ/ϵ, the distance between the ratonal surfaces associated with the two waves), plays a role somewhat analogous to the phase velocity mismatch of the two-wave systems studied by other authors, which were mentioned above. The parameter θ controls the radial

separation $\Delta\tilde{x}$ between resonance trapping regions associated with each of the two waves considered in isolation. This is analogous to the role of the parameter ω/k in the perturbed pendulum, which controls the phase-space separation Δp between trapping regions of the two waves.

For non-zero values of $\mathbf{w}$ (i.e. a wave-frame moving at a finite velocity with respect to the lab frame), the particle sees an induced electric field in the wave-frame which points in the x-direction. This field produces some qualitative changes in the behavior of the system. This issue is discussed in Sec. VID.

A. Perturbation Treatment of Resonance Islands

We first establish the location of the resonance islands; that is to say, the values of $\tilde{H}$ and $\tilde{P}_z$ for which the perturbing wave couples resonantly with the unperturbed orbits. For $\phi = 0$, $\tilde{P}_z$ is a constant of the motion. For small values of $\phi \neq 0$, we attempt to construct a new constant of the motion, p, "close" to $\tilde{P}_z$, as an assymptotic series in ϕ. We define $p \equiv \tilde{P}_z + \phi p_1 + \phi^2 p_2 + ...$, and assume that $\dot{p}$ is identically 0. The first order correction p_1, the only term we shall consider, then obeys the equaton

$$0 = \dot{\tilde{P}}_z(\psi_2) + \phi \left[\frac{\partial p_1}{\partial \psi_1} \dot{\psi}_1(H_0, \tilde{P}_z, \psi_1) + \frac{\partial p_1}{\partial \psi_2} \dot{\psi}_2(H_0, \tilde{P}_z, \psi_1) \right]. \qquad (6.1)$$

The terms $\dot{\psi}_i$, given by Eqs. (2.26) and (2.27), are to be expressed as functions of ψ_1, $\tilde{P}_z$ and the unperturbed energy $H_0 \equiv u^2/2 + \tilde{x}[\tilde{w}_y/\epsilon - \tilde{w}_z\tilde{x}/2] - \cos\psi_1$. This is accomplished by inverting the expressions for $\tilde{P}_z$ and H_0 to express $\tilde{x}$ and u as functions of $\tilde{P}_z$ and H_0. To simplify the discussion, we consider the case $\tilde{\mathbf{w}} = 0$. Adopting the notation $\Omega_i \equiv \dot{\psi}_i(H_0, \tilde{P}_z, \psi_1)$, we have $\Omega_1 = u\tilde{x}$ and $\Omega_2 = ku(\tilde{x} + \theta/\epsilon)$, where $u = \sigma_1\sqrt{2(H_0 + \cos\psi_1)}$ and $\tilde{x} = \sigma_2\sqrt{2(\tilde{P}_z - u)}$, $\sigma_i = \pm 1$. We replace the coordinates ψ_1 and ψ_2 with the new coordinates $\zeta_1 \equiv \frac{1}{q(H_0,\tilde{P}_z)} \int^{\psi_1} d\psi_1 \Omega_2/\Omega_1$ and $\zeta_2 \equiv \psi_2$, where the winding number q is given by $q(H_0, \tilde{P}_z) \equiv \frac{1}{2\pi} \oint d\psi_1 \Omega_2/\Omega_1$. The integrals are taken along the unperturbed orbits, and $\oint$ denotes the integral over a complete period of the unperturbed motion. Eq. (6.1) then becomes

$$\frac{1}{q(H_0, \tilde{P}_z)} \frac{\partial p_1}{\partial \zeta_1} + \frac{\partial p_1}{\partial \zeta_2} = Q(H_0, \tilde{P}_z, \zeta_1, \zeta_2),$$

where $Q \equiv -\dot{\tilde{P}}_z/(\phi\Omega_2) = k\theta\epsilon^{-1}\Omega_2^{-1} \sin\zeta_2$. Defining ζ_1 to be 0 when $\psi_1 = 0$, Q may be written as the Fourier series $Q = \sum_{m=0}^{\infty} Q_m(H_0, \tilde{P}_z)[\sin(m\zeta_1 + \zeta_2) -$

$\sin(m\zeta_1 - \zeta_2)]$, whence the solution for p_1 may be written

$$p_1 = -\sum_{m=0}^{\infty} Q_m(H_0, \tilde{P}_z)\left[\frac{\cos(m\zeta_1 + \zeta_2)}{1 + m/q} + \frac{\cos(m\zeta_1 - \zeta_2)}{1 - m/q}\right].$$

For $m \geq 1$, $Q_m(H_0, \tilde{P}_z) = \frac{1}{2\pi}\frac{k\theta}{\epsilon}\int_0^{2\pi} d\zeta_1 \cos(m\zeta_1)/\Omega_2(H_0, \tilde{P}_z, \zeta_1)$. The perturbation treatment breaks down in the vicinity of the resonances, where $m + qn = 0$, $n = \pm 1$.

To approximate the island widths, we make the usual assumption that each island is well isolated from all other islands and, in the vicinity of a particular (m, n) resonance, we can replace the expression $\dot{\tilde{P}}_z = -\phi\Omega_2 Q$ with the single-harmonic approximation $\Delta\dot{\tilde{P}}_z = -\phi n \Omega_2 Q_m|_R \sin(m\zeta_1 + n\zeta_2)$, where $m = 0, 1, 2, ...$ and $n = \pm 1$. $Q_m|_R$ denotes the value of $Q_m(H_0, \tilde{P}_z)$ at the resonant values of $\tilde{P}_z$ and H_0, and $\Delta\tilde{P}_z$ is the deviation of $\tilde{P}_z$ away from resonance. Terms which can be demonstrated to be of order $\phi^{3/2}$ have been dropped. Defining $\xi \equiv m\zeta_1 + n\zeta_2$, the time-derivative of ξ is given, to lowest order in ϕ, by $\dot{\xi} = -\Delta\tilde{P}_z[\partial q/\partial\tilde{P}_z]_R\Omega_2/m$. Combining this with the expression for $\Delta\dot{\tilde{P}}_z$, one obtains $(d\Delta\tilde{P}_z)n\Delta\tilde{P}_z = d\xi\ \phi m \sin\xi\ [Q_m/(\partial q/\partial\tilde{P}_z)]_R$, which may be integrated to give the familiar pendulum description of the islands:

$$\frac{\Delta\tilde{P}_z^2}{2} + A_{m,n}\cos\xi = \text{const.},$$

where

$$A_{m,n} \equiv \frac{\phi m}{n}\left[\frac{Q_m}{\frac{\partial q}{\partial\tilde{P}_z}}\right]_R.$$

Taking the separatrix, whose half-width is given by $\Delta\tilde{P}_z = 2\sqrt{|A_{m,n}|}$, as an indication of the extent of an island, we define the overlap criterion for a pair of resonances (m, n) and (m', n') as

$$S \equiv \frac{2\left[\sqrt{|A_{m,n}|} + \sqrt{|A_{m',n'}|}\right]}{\left|\tilde{P}_{z_{m,n}} - \tilde{P}_{z_{m',n'}}\right|}.$$

Here, $\tilde{P}_{z_{m,n}}$ is the value of $\tilde{P}_z$ at the (m,n) resonance.

We have worked out a numerical example of the S parameter for comparison with the numerical integration of the equations of motion. We consider the case where $\theta = .1$, $\epsilon = .03$, $k = 1$, and $\tilde{\mathbf{w}} = 0$. The Poincaré surfaces of section of Figs. 6.1a and 6.1b were calculated with these parameters and show points in the $(\psi_1, \tilde{x})$-plane as the orbits cross the surface $\psi_2 = 0 \bmod 2\pi$, with positive value of u. The energy is fixed at $\tilde{H} = 2$. With this choice of parameters, the separatrix of the corresponding unperturbed problem belongs to the class of separatrices labeled ε in Figs. 5.1k and 5.4. The total energy is small enough in comparison with the wave potential that the constant $v_\parallel$ approximation of Sec. IIC fails quantitatively, despite the qualitative similarity in the appearence of the orbits to those of the pendulum. We examine the islands with mode numbers $(m,n) = (1,1)$, $(2,1)$, $(3,1)$, and $(4,1)$ which occur in the lower portion of Figs. 6.1a and 6.1b, among the passing orbits. From the definition of q, we calculate that the $m = 1$ resonance occurs at $\tilde{P}_z = 3.42$, the $m = 2$ resonance at $\tilde{P}_z = 2.73$, the $m = 3$ resonance at $\tilde{P}_z = 2.53$, and the $m = 4$ resonance at 2.48. The "potential well" strengths A for these islands are calculated from the above formulae to be $A_{1,1} = -.30\phi$, $A_{2,1} = .049\phi$, $A_{3,1} = -.013\phi$, $A_{4,1} = .0036\phi$. Using the values of the amplitudes, we calculate the overlap parameters $S_{m,m+1}$ between adjacent pairs of islands, obtaining $S_{1,2} = 2.2\sqrt{\phi}$, $S_{2,3} = 3.5\sqrt{\phi}$, and $S_{3,4} = 5.9\sqrt{\phi}$. These results are summarized in Table 6.1.

Table 6.1

Numerical parameters relating to resonance islands calculated from a first order perturbation analysis. Parameter values for this example are $\theta/\epsilon = 3.33$, $k = 1$, $\mathbf{w} = 0$, $\tilde{H} = 2$.

m	$\tilde{P}_x$	$Q_m\|_R$	$\frac{\partial q}{\partial \tilde{P}_x}\|_R$	$\|A_{m,n}\|$	$S_{m,m+1}$
1	3.423895	-.2243779	.7550856	$.2971556\phi$	$2.198096\sqrt{\phi}$
2	2.725704	.07422671	3.00608	$.04938439\phi$	$3.47621\sqrt{\phi}$
3	2.533485	-.04187644	10.03838	$.0125149\phi$	$5.886017\sqrt{\phi}$
4	2.475062	.02957350	32.78498	$.003608177\phi$	

FIG. 6.1 Poincaré surfaces of section for $\tilde{H} = 2$, $\theta = .1$, $\epsilon = .03$, $k = 1$, and $\mathbf{w} = 0$. $\phi = .1$ in (a), and $\phi = .16$ in (b).

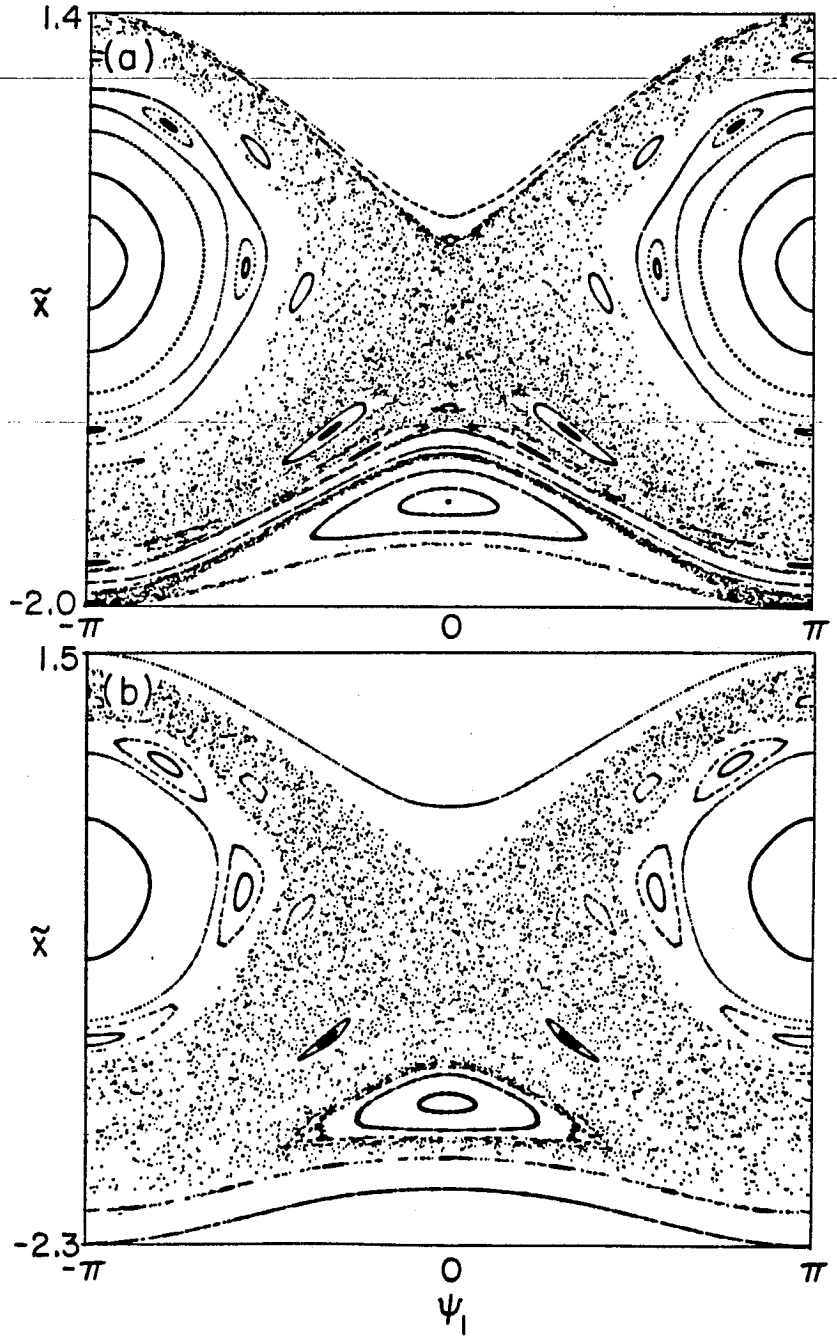

FIG. 6.2 Poincaré surfaces of section for $\tilde{H} = 0$, $\theta/\epsilon = 4.06$, $k = 1$, and $w = 0$. $\phi = .5$ in (a), and $\phi = .01$ in (b).

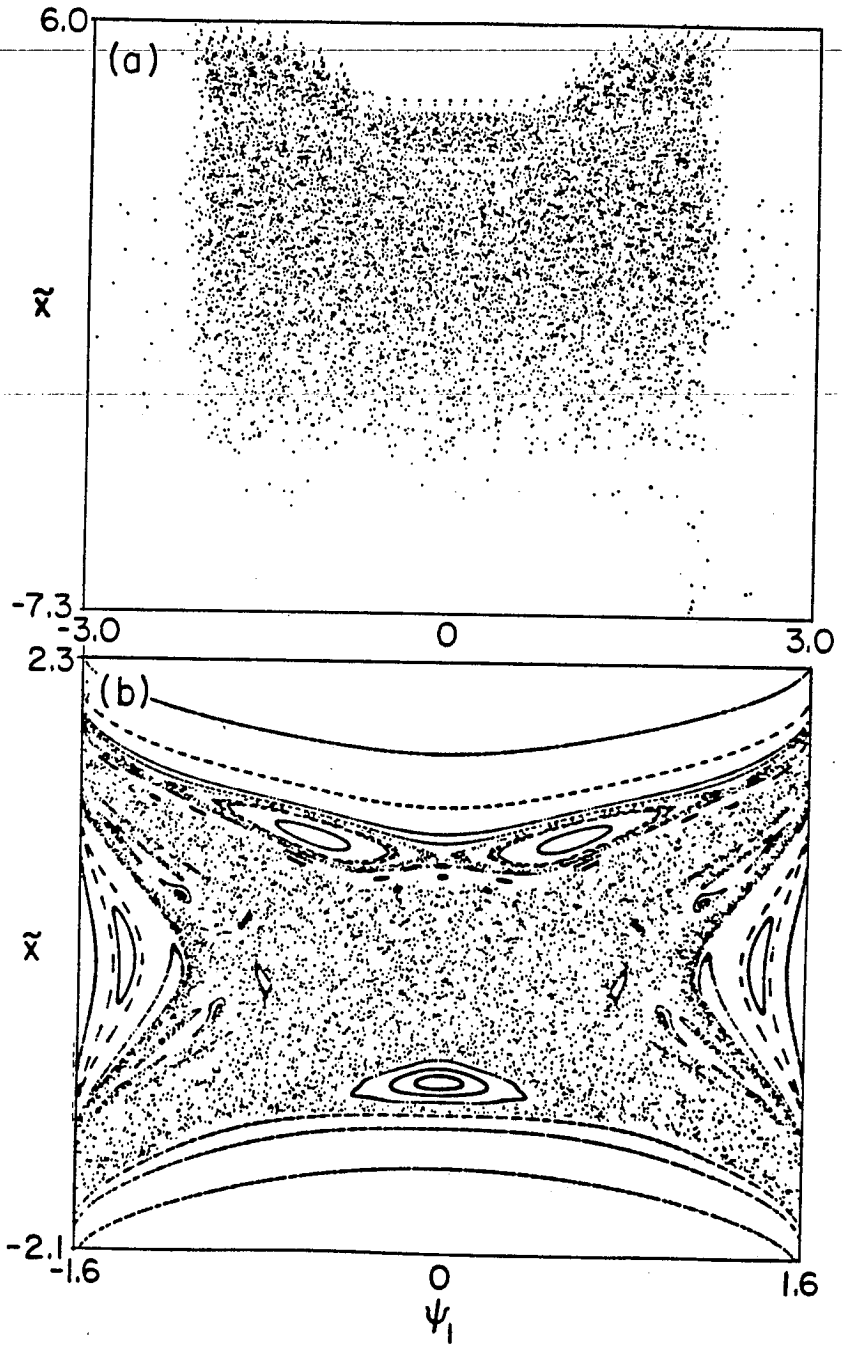

As the resonances approach the separatrix (increasing value of m), the overlap parameters are found to steadily increase. This is consistent with the familiar notion that the resonances "pile up" at the separatrices, making the separatrix sensitive to the stochastic instability.

Figs. 6.1a and 6.1b have values of ϕ equal to .1 and .16, respectively, yielding overlap parameters between the $m = 1$ and $m = 2$ islands of roughly $S = .70$ and $S = .88$. For the case of $\phi = .1$, some stochasticity appears between the $m = 1$ and $m = 2$ islands, but there appear to remain preserved K.A.M. tori which impose a barrier between these two resonance regions. For $\phi = .16$, the $m = 2$ island has been all but lost in the stochastic sea, and no preserved tori remain separating the two regions. These results are consistent with numerical results for other dynamical systems where a transition to stochastic behavior is typically observed to occur as the island overlap parameter is increased through the range of roughly .7 to 1.0.

For values of the overlap parameter in the range of roughly .5 to 1.0, as in the above examples, the island separatrices are not well-defined, having broadened into stochastic regions. On the other hand, for small values of ϕ and hence $S_{m,m+1}$, the island separatrices in the Poincaré surfaces of section become fairly well-defined curves. In the limit of small ϕ, the results of the first order perturbation analysis should converge to the results of the numerically integrated trajectories. In order to check the validity of the above perturbation results, we look at a small perturbation of $\phi = .01$. The other parameters are chosen to be identical to those considered in the previous example.

In the pendulum approximation of an isolated resonance island, which was

derived above, the island separatrices are given by

$$\Delta\tilde{P}_z = \pm 2\sqrt{|A_{m,n}|}\,\cos\frac{\xi}{2}$$

for m odd, and

$$\Delta\tilde{P}_z = \pm 2\sqrt{|A_{m,n}|}\,\sin\frac{\xi}{2}$$

for m even. Since ξ is defined to be $m\zeta_1 + n\zeta_2$, and we wish to compare the analytic results for the island separatrices with Poincaré surfaces of section defined at $\psi_2 = \zeta_2 = 0 \bmod 2\pi$, we set ξ equal to $m\zeta_1$ in the above formulae. Using the above definitions of $\Delta\tilde{P}_z$ and ζ_1, one may transform these separatrices into the coordinates $\tilde{x}$ and ψ_1. In Fig. 6.4a, we plot the perturbation results for the separatrices corresponding to the islands with mode numbers $m = 1$, $m = 2$, and $m = 3$. These islands occur among the passing orbits of the unperturbed problem. Fig. 6.4b gives the corresponding surfaces of section for numerically integrated orbits. In Fig. 6.4c, these two sets of results are plotted on the same graph for comparison. The agreement between theory and numerical experiment is quite good.

FIG. 6.4 Resonance island separatrices for $m = 1$, $m = 2$ and $m = 3$ islands occuring in untrapped region of $\tilde{H} = 2$ torus. Results of first order perturbation analysis given in (a). Poincaré surfaces of section with initial conditions chosen for orbits to lie on island separatrices given in (b). Plot (c) gives the results of plots (a) and (b) superimposed for direct comparison of theory and numerical experiment.

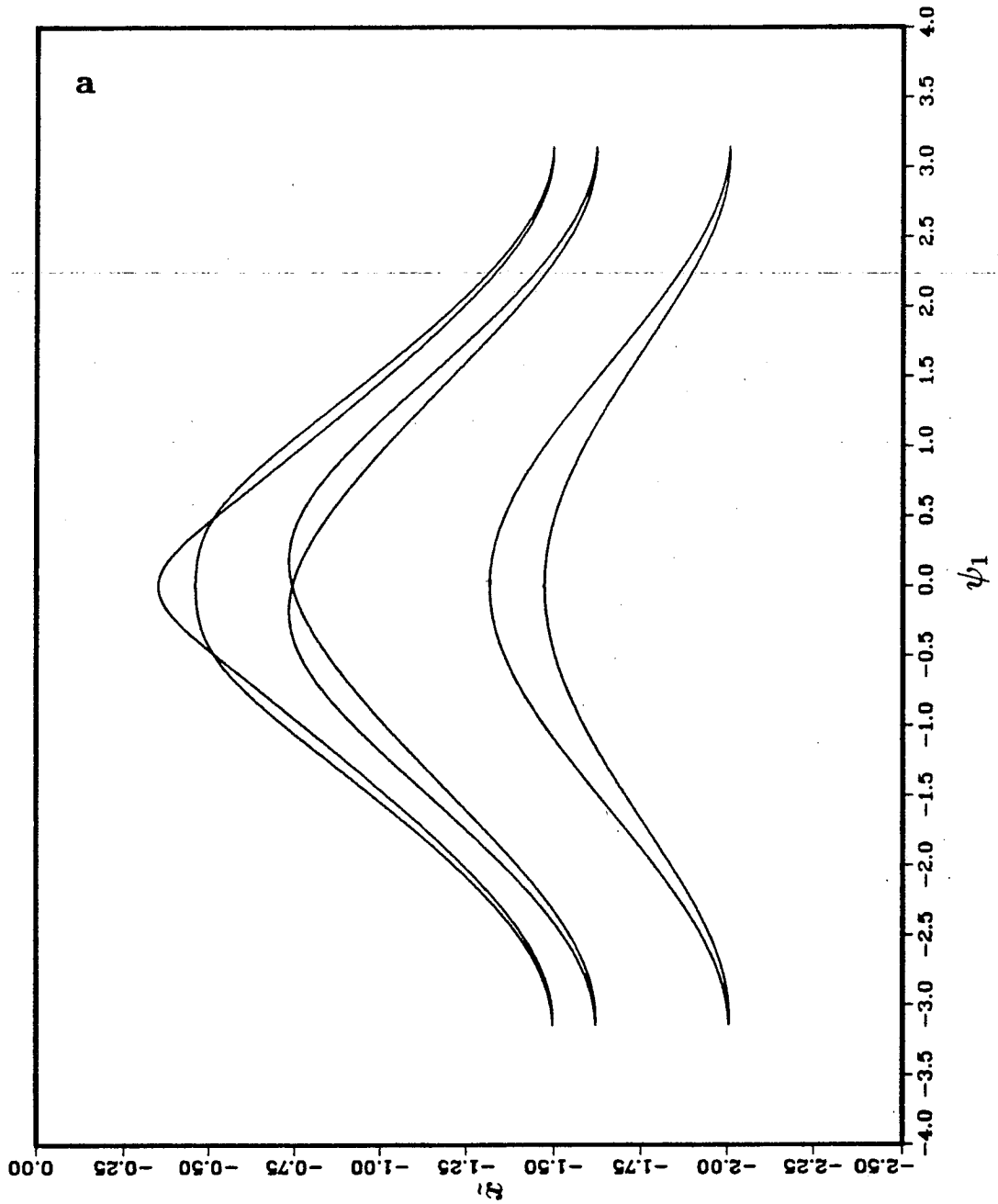

FIG. 6.4 (continued)

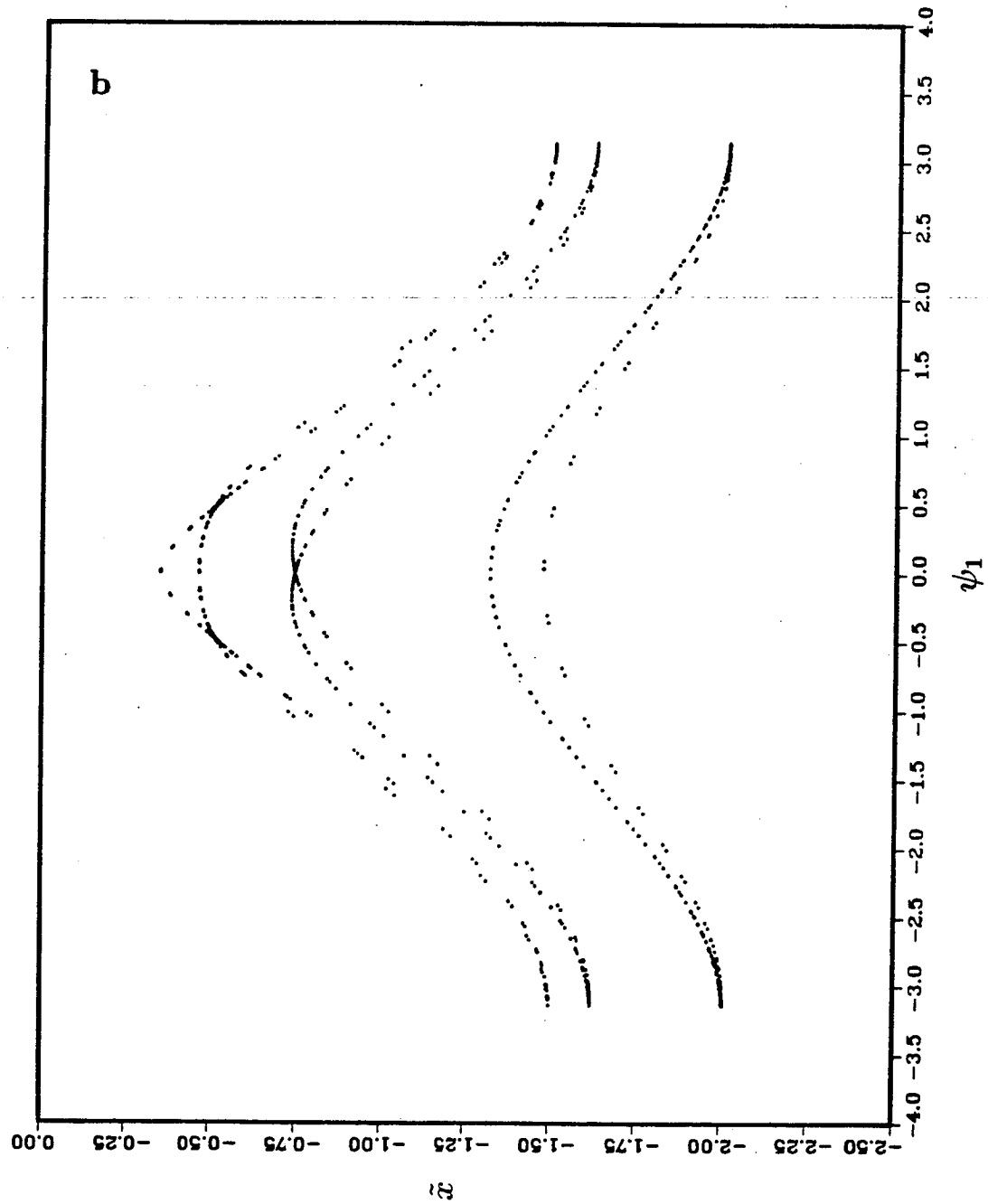

FIG. 6.4 (continued)

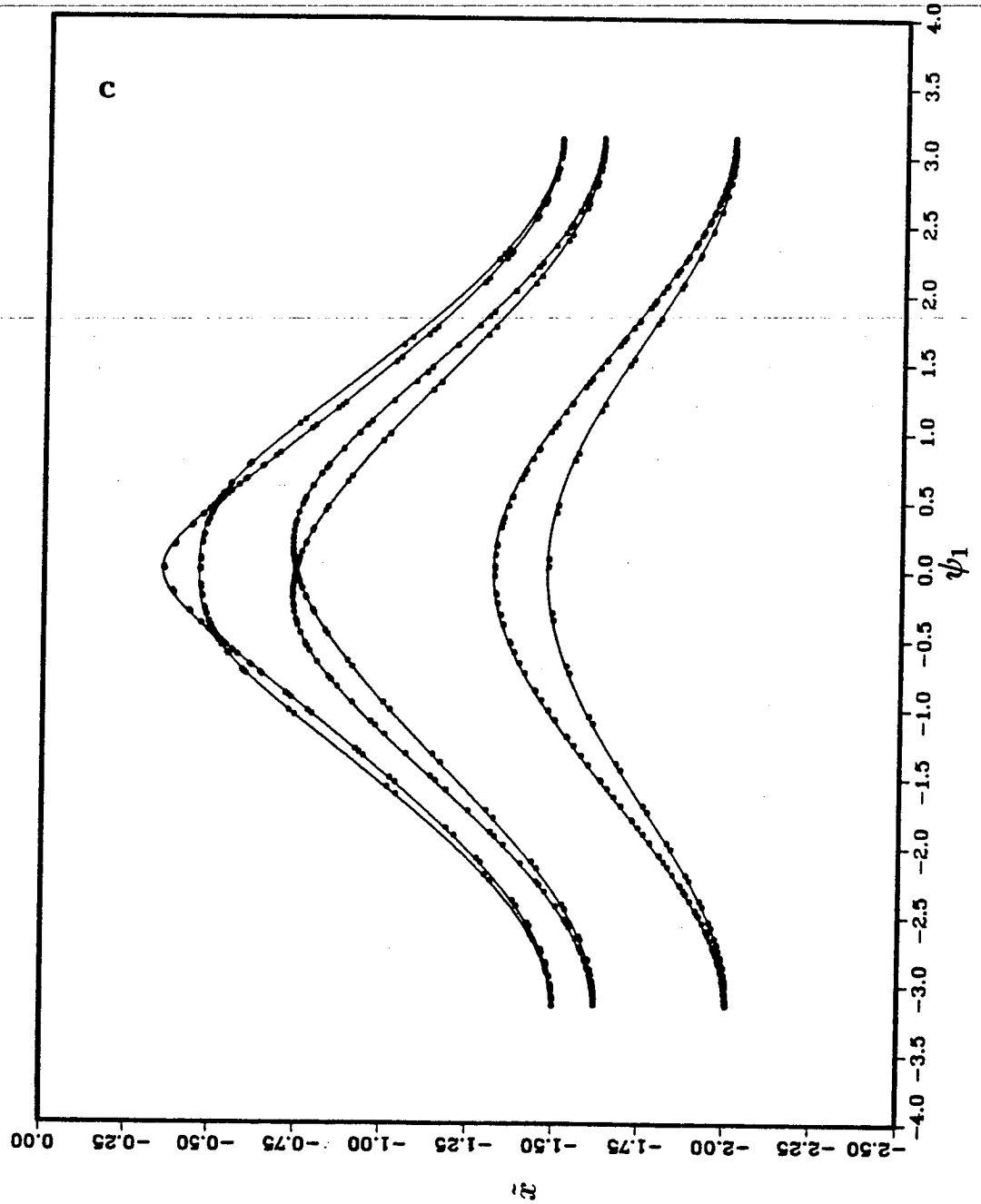

B. Global Stochasticity Estimates

The above calculation of the overlap parameter S provides reasonably detailed information concerning the transition to stochasticity. However, the calculation is unwieldy, especially since the unperturbed orbits apparently can not be described by well-known analytic functions. We would like to have at our disposal a simpler means of predicting the appearence of global stochasticity. In this section, we provide a more rough-and-ready estimate of the conditions under which global stochasticity can be expected to occur. We adopt the view that strong stochasticity can be expected when the primary separatrices associated with each of the two waves begin to touch. We expect that if the separatrices due to the first wave considered in isolation are well removed from the separatrices of the second wave considered in isolation, then minimal stochasticity will be present. We wish to find an overlap criterion which is defined to be equal to 1 when two separatrices are just touching (or rather would be just touching if each separatrix were constructed ignoring the effect of the other wave). Since there is a whole host of separatrices (a continuous one-parameter family corresponding to the curve of Fig. 5.4), we must make the notion of overlap more precise. Consider a particle which has initial conditions such that if ϕ_2 were set equal to 0, it would be at the maximal x-value of a separatrix due to the first wave. We consider this separatrix to "just touch" a separatrix of the second wave if a particle started with identical initial phase space coordinates would fall on the minimal x-value of a separatrix of the second wave, if only that wave were present. Under such conditions, we anticipate strong interaction between the resonances of the two waves and the presence of a significant degree of global stochasticity.

To simplify the problem, we again restrict our attention to the case $\mathbf{w} = 0$. From the discussion of Sec. IIC, we know that in the large parallel kinetic energy regime, where the behavior is that of the pendulum, the separatrix widths should scale as $\phi^{1/2}$. But as shown in Sec. IIB, the full width of the separatrix κ of Fig. 5.1a is given by $\sqrt{32L_s v_0/\omega_{ce}}$. This width, which, except for a factor of $\sqrt{32}$, equals ϵL_s, was the characteristic distance used in defining our dimensionless coordinates and scales as $\phi^{1/4}$. This fourth-root scaling suggests that for small wave potential, the resonance overlap criteria should display stronger ϕ-dependence in the low kinetic energy regime than one would glean from the standard pendulum approximation. This transition from $\phi^{1/2}$ scaling to $\phi^{1/4}$ scaling is illustrated vividly by the separatrix of type α in Fig. 5.1b. One easily calculates it's full width to be

$$\Delta x = \left[8L_s\omega_{ce}^{-1}\sqrt{2/m_e}\left(\sqrt{H+e\phi}-\sqrt{H-e\phi}\right)\right]^{1/2}.$$

For $H \gg e\phi$, the assymptotic behavior of the width is given by

$$\Delta x = 4\left[-L_s e\phi/(\omega_{ce}m_e v_{\|})\right]^{1/2}.$$

At the minimum value of H for which this type of separatrix occurs, namely $H = e\phi$, the full width is given by

$$\Delta x = 4\left[\frac{L_s}{\omega_{ce}}\sqrt{e\phi/m_e}\right]^{1/2}.$$

In Table 6.2 we have compiled the values of the x-extrema for the various separatrices of the $\lambda = 0$ problem, along with the values of $v_{\|}$ attained at the x-extrema.

Table 6.2

Properties of separatrices for $\mathbf{w} = 0$, one-wave system. Letters $\alpha - \kappa$ correspond to curve labels of Figs. 5.1 and 5.4. Listed are allowed ranges of $\tilde{P}_z$, radial extrema, and values of parallel velocity at radial extrema for respective separatrix classes.

Orbit Type	Parameter Range	x_{max}	$v_{\parallel_{max}}$
α	$\tilde{P}_z < 0$	$\pm\sqrt{2}\epsilon L_s\sqrt{\tilde{P}_z + 2(1+\tilde{P}_z^2/4)^{1/2}}$	$-2v_0\sqrt{1+\tilde{P}_z^2/4}$
β	$0 < \tilde{P}_z < 2$	$\pm\sqrt{2}\epsilon L_s\sqrt{2+\tilde{P}_z}$	$-2v_0$
γ	$0 < \tilde{P}_z < 2$	$\pm 2\epsilon L_s\sqrt{\tilde{P}_z}$	$-v_0\tilde{P}_z$
δ	$\tilde{P}_z > 2$	$\pm\sqrt{2}\epsilon L_s\sqrt{2+\tilde{P}_z}$	$-2v_0$
ϵ	$\tilde{P}_z > 2$	$\pm\sqrt{2}\epsilon L_s\sqrt{\tilde{P}_z - 2(\tilde{P}_z^2/4-1)^{1/2}}$	$2v_0\sqrt{\tilde{P}_z^2/4-1}$
κ	$\tilde{P}_z = 2$	$\pm\sqrt{8}\epsilon L_s$	$-2v_0$

Let us first consider the conditions under which two separatrices of type κ are just touching, in the sense discussed above. The parallel velocity at the x-extremum of the separatrix associated with the i^{th} wave is given by $-2\sqrt{e\phi_i/m_e}$. Matching these velocities for both waves requires that $\phi_1 = \phi_2 \equiv \Phi$. The distance between the rational surfaces associated with the two waves is given by θL_s, where θ is the angle between the k-vectors. Therefore, if the quantity

$$S_{\kappa\kappa} \equiv \frac{1}{\theta}\sqrt{\frac{32}{\omega_{ce}L_s}\sqrt{\frac{e\Phi}{m_e}}}$$

is equal to 1, then a particle with initial conditions $\psi_1 = \psi_2 = 0$, $v_\parallel = -2\sqrt{e\Phi/m_e}$, $x = \sqrt{8L_s/\omega_{ce}\sqrt{e\Phi/m_e}}$ would be on one separatrix if $\phi_1 = \Phi$, $\phi_2 = 0$, and would be on the other separatrix if $\phi_2 = \Phi$, $\phi_1 = 0$. We take $S_{\kappa\kappa}$ to be an overlap criterion for the restricted case of this type of separatrix. For $S_{\kappa\kappa} \ll 1$, these two web-like separatrices are well-removed from one another. We emphasize that this overlap criterion makes sense only for the case $\phi_1 = \phi_2$. Since the orbits of type κ, β, and δ all have extremal velocities of $-2\sqrt{e\phi/m_e}$, a similar constraint applies if we seek overlap criteria among pairs of these orbit types.

From Table 6.2, one sees that for the α type separatrices,

$$v_{\parallel_{max}} < -2\sqrt{e\phi/m_e}.$$

For the γ class,

$$v_{\parallel_{max}} > -2\sqrt{e\phi/m_e}.$$

Therefore, if $\phi_2 < \phi_1$, we can find conditions for a type α separatrix associated with the second wave to touch a type γ separatrix associated with the first wave. Let p_1 and p_2 be the particle's value of $\tilde{P}_z$ with respect to the two waves.

Matching the value of $v_{\parallel_{max}}$ one obtains the relation $2\sqrt{\phi_2}\sqrt{1+p_2^2/4} = \sqrt{\phi_1}p_1$, or $p_1 = \sqrt{(4+p_2^2)\phi_2/\phi_1}$. From the allowed ranges of p_1 and p_2, one obtains the condition upon ϕ_2/ϕ_1:

$$0 < \frac{\phi_2}{\phi_1} < \frac{1}{1+p_2^2/4}.$$

From Table 6.2 and the above relation between p_1 and p_2, we find that the α and γ separatrices just touch if

$$S_{\alpha\gamma} \equiv \frac{1}{\theta}\sqrt{\frac{2}{\omega_{ce}L_s}\sqrt{\frac{e\phi_2}{m_e}}}\left\{\sqrt{p_2 + 2(1+p_2^2/4)^{1/2}} + 2(1+p_2^2/4)^{1/4}\right\}$$

equals 1. Here, p_2 is permitted to be in the range $-2\sqrt{\phi_1/\phi_2 - 1} < p_2 < 0$.

Replacing the parameter p_2 by the parameter

$$A \equiv -\frac{p_2}{2\sqrt{\frac{\phi_1}{\phi_2} - 1}},$$

where the allowed range for A is $0 < A < 1$, $S_{\alpha\gamma}$ may be written

$$S_{\alpha\gamma} = \frac{\phi_1^{1/4}}{\theta}\sqrt{\frac{2}{\omega_{ce}L_s}\sqrt{\frac{e}{m_e}}}\quad G\left(\frac{\phi_2}{\phi_1}, A\right),$$

where

$$G(\phi, A) \equiv \sqrt{2\sqrt{\phi(1-A^2)+A^2} - 2A\sqrt{1-\phi}} + 2\left[\phi(1-A^2)+A^2\right]^{1/4}.$$

For a given value of ϕ_2/ϕ_1, one obtains a continuous set of overlap parameters corresponding to the value of A. This reflects the fact that many orbits are of the same class. For each value of ϕ_2/ϕ_1, one may find the maximum value of G with respect to A. Denoting this maximal function by $\bar{G}(\phi_2/\phi_1)$, one finds that $\bar{G}$ varies only between 2 and 3.4 over the domain $0 < \phi_2/\phi_1 < 1$.

Performing a similar calculation, we find that a type δ separatrix associated with wave 1 just touches a type α separatrix associated with wave 2 if

$$S_{\delta\alpha} \equiv \frac{\phi_1^{1/4}}{\theta} v \sqrt{\frac{2}{\omega_{ce} L_s} \sqrt{\frac{e}{m_e}}} \left\{ \sqrt{2+p_1} + \sqrt{2-2\sqrt{1-\frac{\phi_2}{\phi_1}}} \right\}$$

equals 1, where $\phi_2 < \phi_1$. Even for large values of θ, one can make $S_{\delta\alpha} = 1$ by selecting an appropriate value of p_1. This is a reflection of the fact that the δ class of islands are centered about values of x ranging from $\pm\sqrt{L_s v_0/\omega_{ce}}$ to $\pm\infty$. This suggests that for the $\tilde{H} = 1$ torus (on which the δ type orbits occur), the overlap parameter may not be a meaningful quantity. For the $\lambda = 0$ problem, the $\tilde{H} = 1$ torus appears to be a pathological case which is particularly susceptible to the stochastic instability. This issue is discussed further in the next section.

The overlap criteria discussed in this section are somewhat problematic. The expressions diverge as θ approaches 0, which would suggest a large amount of stochasticity for small θ. This is a spurious result, since the equations of motion become integrable as θ goes to 0 and the waves coalesce. However, from the numerical experiments we have performed, a value of S equal to 1 appears to be a sufficient condition for the appearence of global stochasticity.

Figs. 6.2a and 6.3a show Poincaré surfaces of section for cases in which the parameters were chosen in order to yield a value of $S_{\alpha\gamma} = 1$. In both cases, the plots show the branch $u > 0$. For Fig. 6.2a we chose $\theta/\epsilon = 4.06$, $k = 1$, $\tilde{H} = 0$, $\tilde{\mathbf{w}} = 0$, and $\phi = .5$. For these parameters, the separatrix of the corresponding unperturbed problem belongs to the class γ, the figure-eight separatrix of Fig. 5.11. The unperturbed problem thus contains orbits which are qualitatively distinct in character from those occuring in the large $v_{\|}$, pendulum

approximation. For Fig. 6.3a the parameter values were $\theta/\epsilon = 4.828$, $k = 1$, $\tilde{H} = 1$, $\tilde{\mathbf{w}} = 0$, and $\phi = 1$. As Fig. 5.4 indicates, the unperturbed version of this case ($\tilde{H} = 1$ torus) has not one, but a continuous set of infinite-period orbits of types β and δ. This example thus contains a non-universal feature which is typically absent from similar two degree-of-freedom systems investigated in previous works.

Figs. 6.2a and 6.3a both point to the complete destruction of a second isolating integral of the motion, when $S = 1$. In Figs. 6.2b and 6.3b, the same cases were run as in Figs. 6.2a and 6.3a, respectively; except that the perturbation parameter ϕ was reduced to .01. One sees that a high level of stochasticity remains. The persistence of such a large degree of stochasticity at even a one percent perturbation level is quite remarkable. Again, the $\tilde{H} = 1$ torus appears to be highly vulnerable to the stochastic instability.

The appreciable level of stochasticity present at even a one percent perturbation for the small $\tilde{H}$ regime is in sharp contrast with the behavior in the large $\tilde{H}$ regime, where the constant parallel velocity approximation becomes valid. In order to illustrate the qualitative difference between the large $\tilde{H}$ regime and the behavior illustrated in Figs. 6.2b and 6.3b, we present an example of numerically integrated orbits for the $\tilde{H} = 9$ torus. This is well into the regime where the parallel kinetic energy dominates the electrostatic potential energy. In Figs. 6.5a – 6.5f, we plot Poincaré surfaces of section, all with $\phi = 0.01$, $k = 1$, $\tilde{\mathbf{w}} = 0$, and u chosen to have negative sign. In Figs. 6.5a through 6.5f, the value of θ/ϵ is varied through .1, .5, 1.0, 2.0, 3.0, and 6.0, respectively. As one would expect, the level of stochasticity approaches zero as θ/ϵ approaches zero, for the two waves coalesce, becoming one wave. In the opposite limit of

large θ/ϵ, the level of stochasticity likewise becomes negligible, for the resonance trapping regions associated with the two waves become spatially well-separated, and little resonant interaction takes place. At some intermediate value of θ/ϵ, the level of stochasticity reaches an extremum. This occurs roughly when the rational surface associated with the second wave is touching the separatrix associated with the first wave. Even at its maximum, the level of stochasticity is not appreciable: the separatrix broadens into a thin stochastic layer, but nothing remotely approaching global stochasticity occurs.

FIG. 6.5 Poincaré surfaces of section for $\tilde{H} = 9$ torus with $\phi = 0.01$, $k = 1$, $\tilde{\mathbf{w}} = 0$, and u chosen to have negative sign. The value of θ/ϵ is varied through .1, .5, 1.0, 2.0, 3.0, and 6.0 for Figs. (a)–(f), respectively.

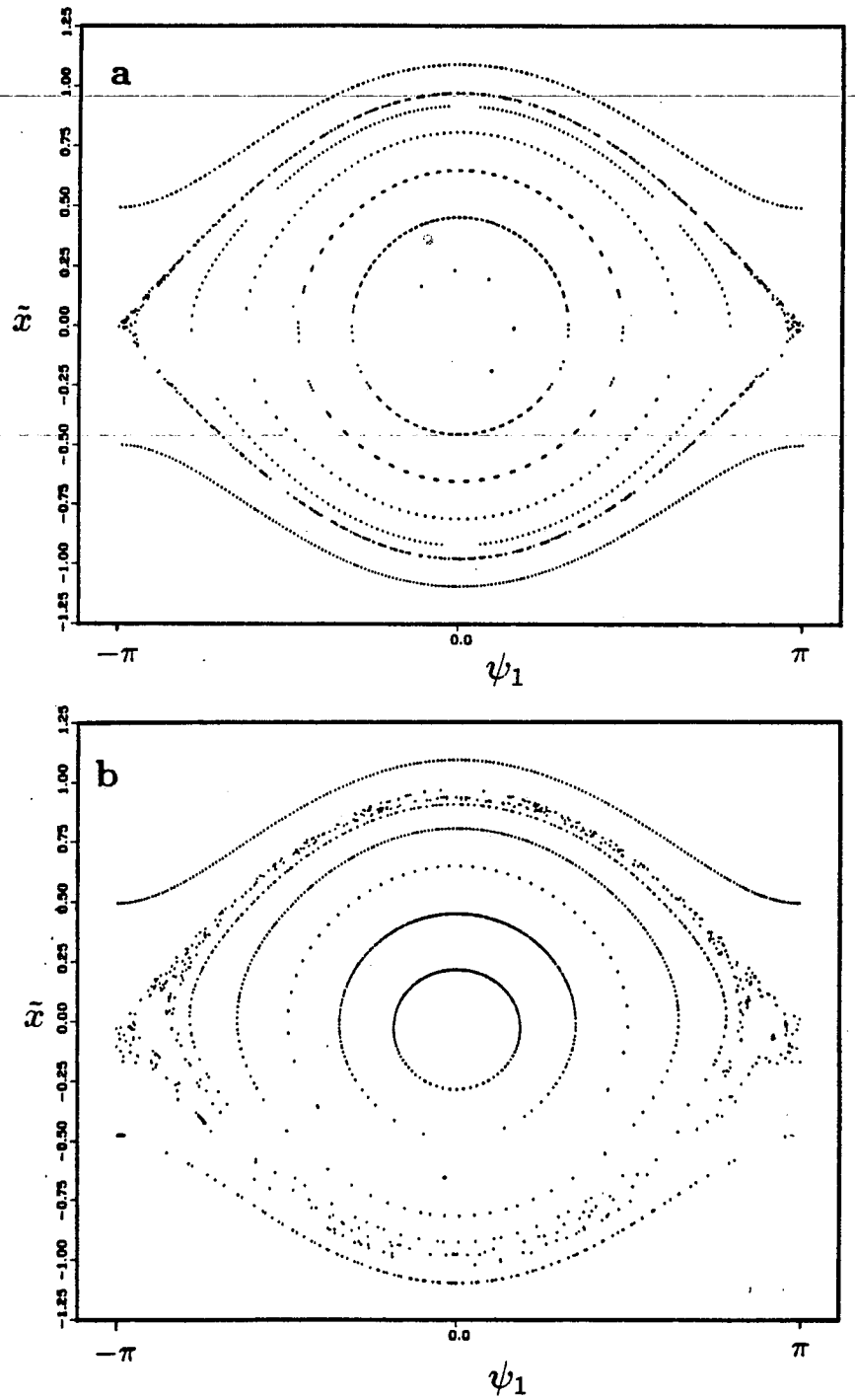

FIG. 6.5 (continued)

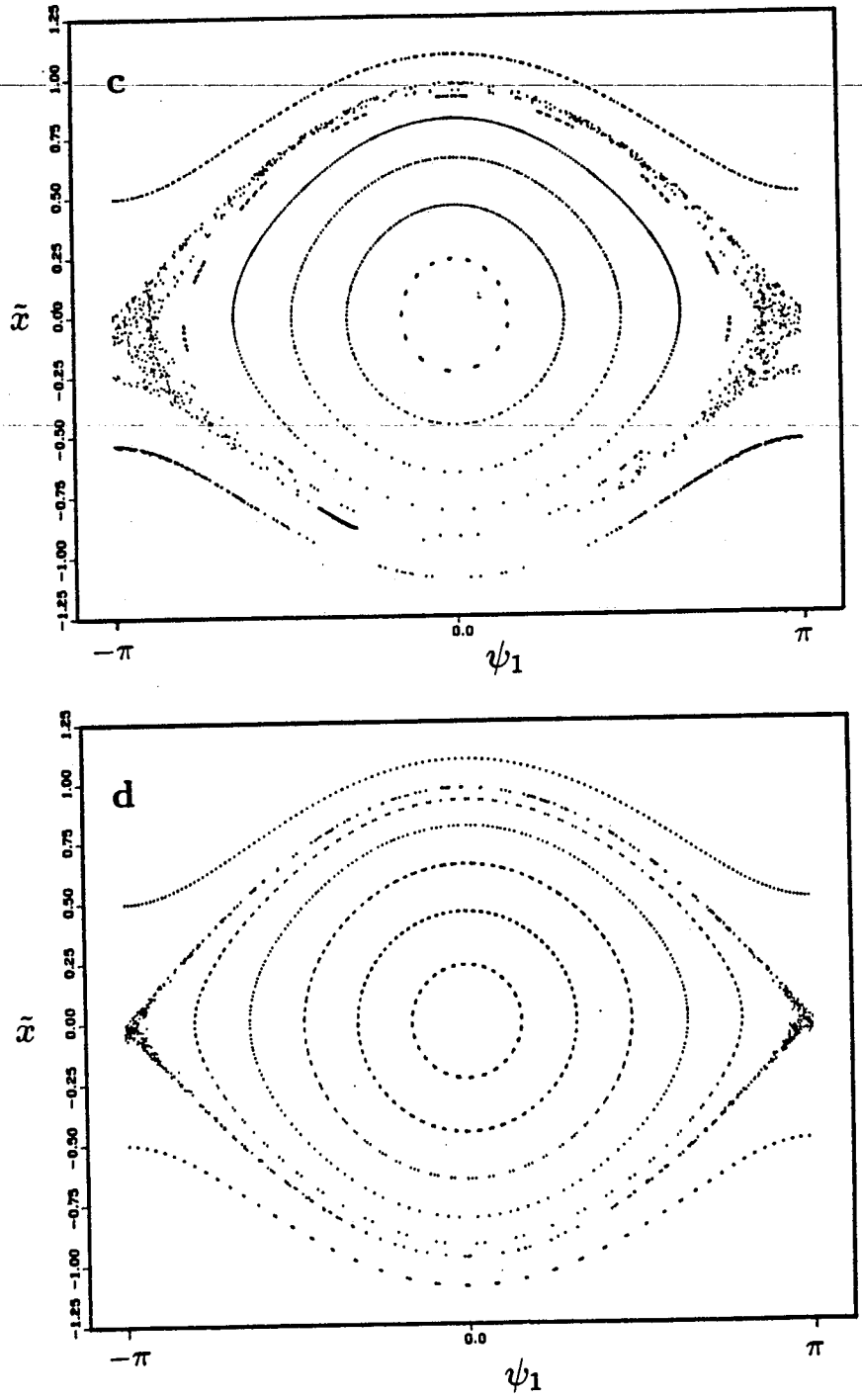

FIG. 6.5 (continued)

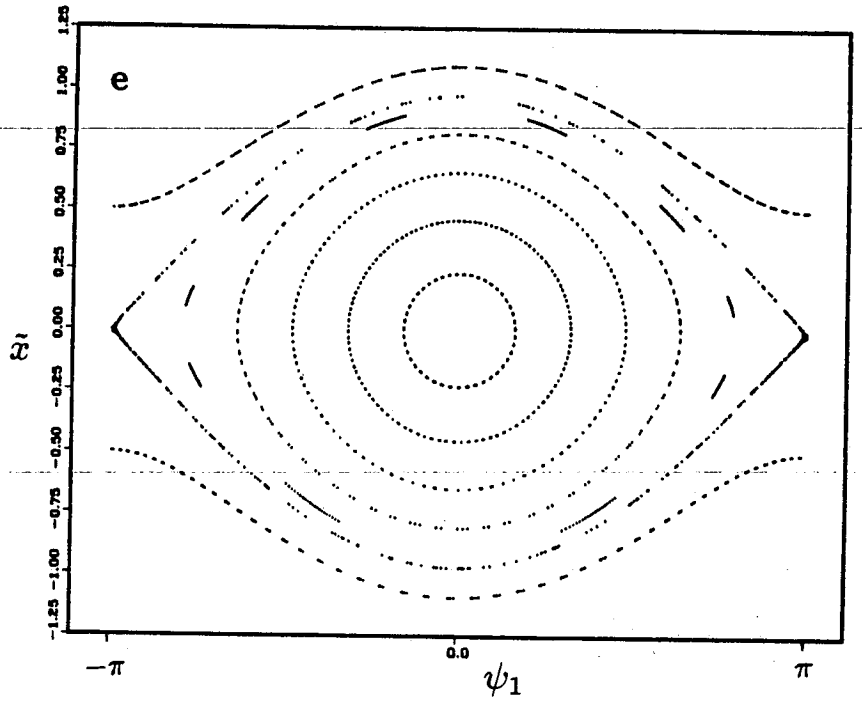

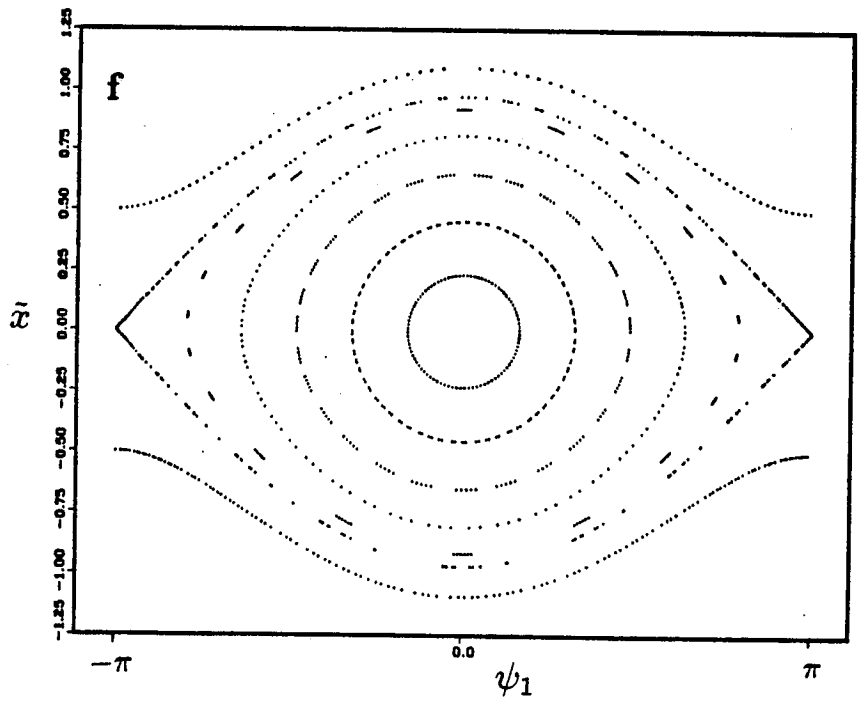

C. The Special Role of the H = 1 Torus

Refering again to Fig. 5.4, consider a particle with initial conditions such that it initially falls on the curve γ in the $(\tilde{P}_z, \tilde{H})$-plane. As mentioned previously, in the absence of the perturbation ($\phi \equiv \phi_2/\phi_1 = 0$), the orbit is represented by a stationary point in this projection. For $\phi \neq 0$, the point is free to move horizontally in the $(\tilde{P}_z, \tilde{H})$-plane, but not vertically. We expect an orbit lying near the locus of separatrices of the unperturbed problem to be subject to the stochastic instability. But in light of the K.A.M. theorem, one expects that, for small enough perturbations, the orbit will remain bounded by nested preserved K.A.M. tori. The horizontal motion in the $(\tilde{P}_z, \tilde{H})$-plane is thus restricted for small perturbations.

If one were to add a third wave to the problem, the added time dependence, not removable through coordinate transformation, would destroy the invariance of the Hamiltonian. The added mobility of the particle in the vertical direction in the $(\tilde{P}_z, \tilde{H})$-plane would enable a particle starting on the γ curve to move along a "corridor" in the vicinity of the locus of separatrices. This is the Arnold diffusion. Even for small perturbations, very large excursions can take place in action space, under these circumstances.

Now consider an orbit starting on one of the curves β or δ. These are exceptional cases, since these curves lie parallel to the $\tilde{P}_z$ axis. Even with only two waves present, the particle apparently has the oportunity to travel along this "corridor" of separatrices, while still strictly conserving the value of $\tilde{H}$. For the $H = 1$ torus, every orbit with a value of $\tilde{P}_z$ between 0 and ∞ is a homoclinic orbit, and is, hence, susceptible to the stochastic instability. We conjecture that, for this special region of phase space, something akin to Arnold diffusion occurs

for the two-wave problem, and that even for small perturbations, a particle could eventually diffuse to large values of $\tilde{P}_z$. We have no *a priori* reason to believe there is anything preventing it from doing so. The growth of $\tilde{P}_z$ to large values does not, however, imply that $v_\parallel$ becomes large. The parallel velocity for the $\mathbf{w} = 0$ problem is restricted by the conservation of the Hamiltonian. The canonical momentum $\tilde{P}_z$ is permitted to attain a large value by virtue of the coordinate $\tilde{x}$ becoming large.

In numerical experiments, we have attempted to confirm the above observations regarding the peculiar nature of the $\tilde{H} = 1$ torus by integrating the orbits for an ensemble of 640 particles. All particles were started with identical initial values of $\tilde{H}$ and $\tilde{P}_z$, but distributed randomly in ψ_1 and ψ_2. In Figs. 6.6a and 6.6b, we have plotted, as a function of time, the root-mean-square deviation in the value of $\tilde{P}_z$, i.e. $[< \tilde{P}_z^2 > - < \tilde{P}_z >^2]^{1/2}$, where the angle brackets denote the ensemble average. For both of the illustrated examples, Eqs. (2.24)–(2.27) were integrated with $\tilde{\mathbf{w}} = 0$, $\phi = .2$, $\theta/\epsilon = .1$, and $k = 1$. For Fig. 6.6a, the initial conditions were $\tilde{H} = 0$, $\tilde{P}_z = \sqrt{2}$. These orbits would, in the absence of the perturbation, thus fall on the curve γ of Fig. 5.4. As time increases, the packet of particles spreads with respect to the value of $\tilde{P}_z$. But, as one would expect, the standard deviation of $\tilde{P}_z$ eventually saturates as the ensemble fills up the stochastic layer in the neighborhood of the unperturbed problem's separatrix. Fig. 6.6b illustrates the case $\tilde{H} = 1$, $\tilde{P}_z = 2$. These initial conditions correspond to the point κ of Fig. 5.4. The qualitative behavior of the ensemble is radically different from that of the former example. We detect no evidence of saturation and the behavior is consistent with our conjecture that a kind of diffusion in $\tilde{P}_z$ takes place.

FIG. 6.6 Standard deviation in $\tilde{P}_z$ as a function of time for ensemble of 640 particles. Parameter values are $\theta/\epsilon = .1$, $\phi = .2$, $k = 1$, $\mathbf{w} = 0$. Particles initially distributed randomly in phase with $\tilde{H} = 0$, $\tilde{P}_z = \sqrt{2}$ (a), and $\tilde{H} = 1$, $\tilde{P}_z = 2$ (b).

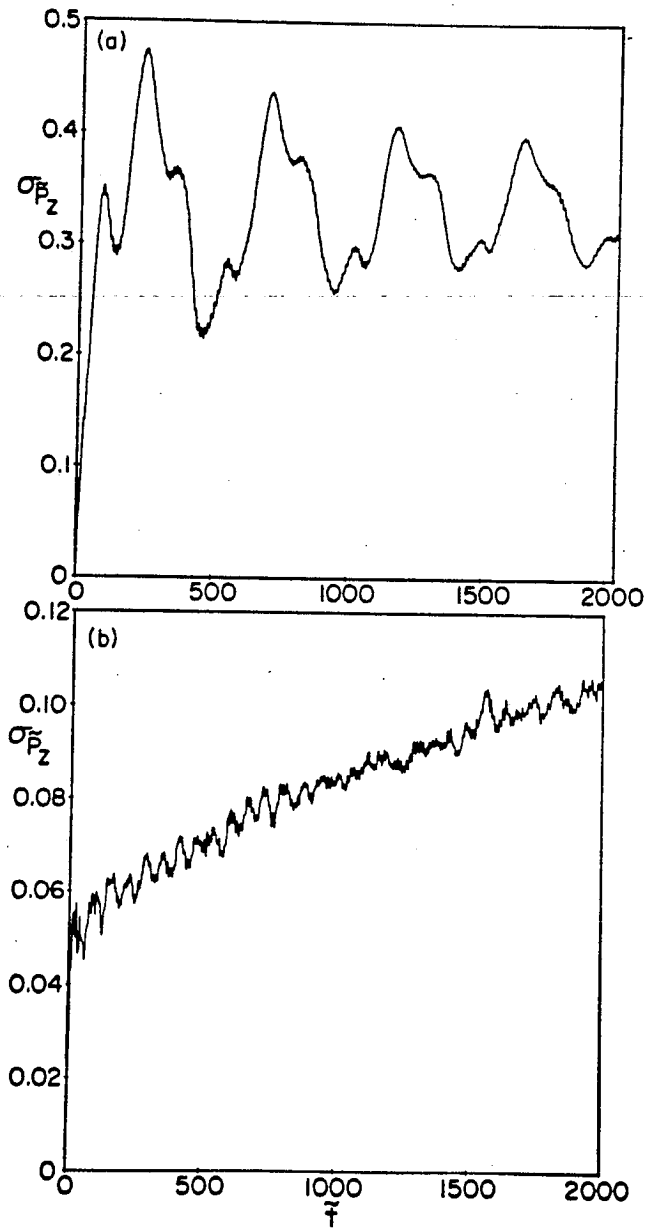

D. The Constraint of the Conserved Energy

Even for highly stochastic regimes of the equations of motion (2.24)–(2.27), the conserved energy

$$\tilde{H} \equiv \frac{u^2}{2} - \cos\psi_1 - \phi\cos\psi_2 + \frac{\tilde{w}_y\tilde{x}}{\epsilon} - \frac{\tilde{w}_z\tilde{x}^2}{2} \tag{6.2}$$

imposes a constraint upon the regions of phase space which a trajectory may visit. For example, for the case $\mathbf{w} = 0$ which we have concentrated on in this work, the invariance of

$$\tilde{H} = \frac{u^2}{2} - \cos\psi_1 - \phi\cos\psi_2$$

may place a restriction upon the allowed values of ψ_1 and ψ_2 . We have thus far largely ignored the details of the behavior of the phase coordinates ψ_1 and ψ_2. For example, in the surfaces of section, ψ_1 is only plotted modulo 2π. This procedure suppresses the information concerning whether the orbit is trapped or untrapped with respect to ψ_1.

In the unperturbed problem ($\phi = 0$), those orbits with $\tilde{H} < 1$ are clearly trapped with respect to the motion of the coordinate ψ_1: motion is restricted to one wave cell. For $\tilde{H} > 1$, the particle may move from wave cell to wave cell.

Now consider the perturbed system with $\phi \equiv \phi_2/\phi_1 = 1$. (This is apparently the case with maximal stochasticity since the waves are of equal amplitude.) For this case, the two-dimensional potential well, $-\cos\psi_1 - \cos\psi_2$, with respect to ψ_1 and ψ_2 has local minima of -2 at $\psi_1 = 2\pi n$ and $\psi_2 = 2\pi m$ and local maxima of $+2$ at $\psi_1 = \pi(2n+1)$ and $\psi_2 = \pi(2m+1)$. The "sea level" contour ($-\cos\psi_1 - \cos\psi_2 = 0$) forms a lattice-work of straight lines interconnecting the points $(\psi_1, \psi_2) = (2\pi n, \pi(2m+1))$ and $(\psi_1, \psi_2) = (\pi(2n+1), 2\pi m)$.

FIG. 6.7 Motion of phase coordinates for $\phi = 1$, $k = 1$, $\mathbf{w} = 0$, $\theta/\epsilon = 4.06$. In (a), particle is trapped in wave cell with $\tilde{H} = -.01$. In (b), particle is untrapped with $\tilde{H} = .005$.

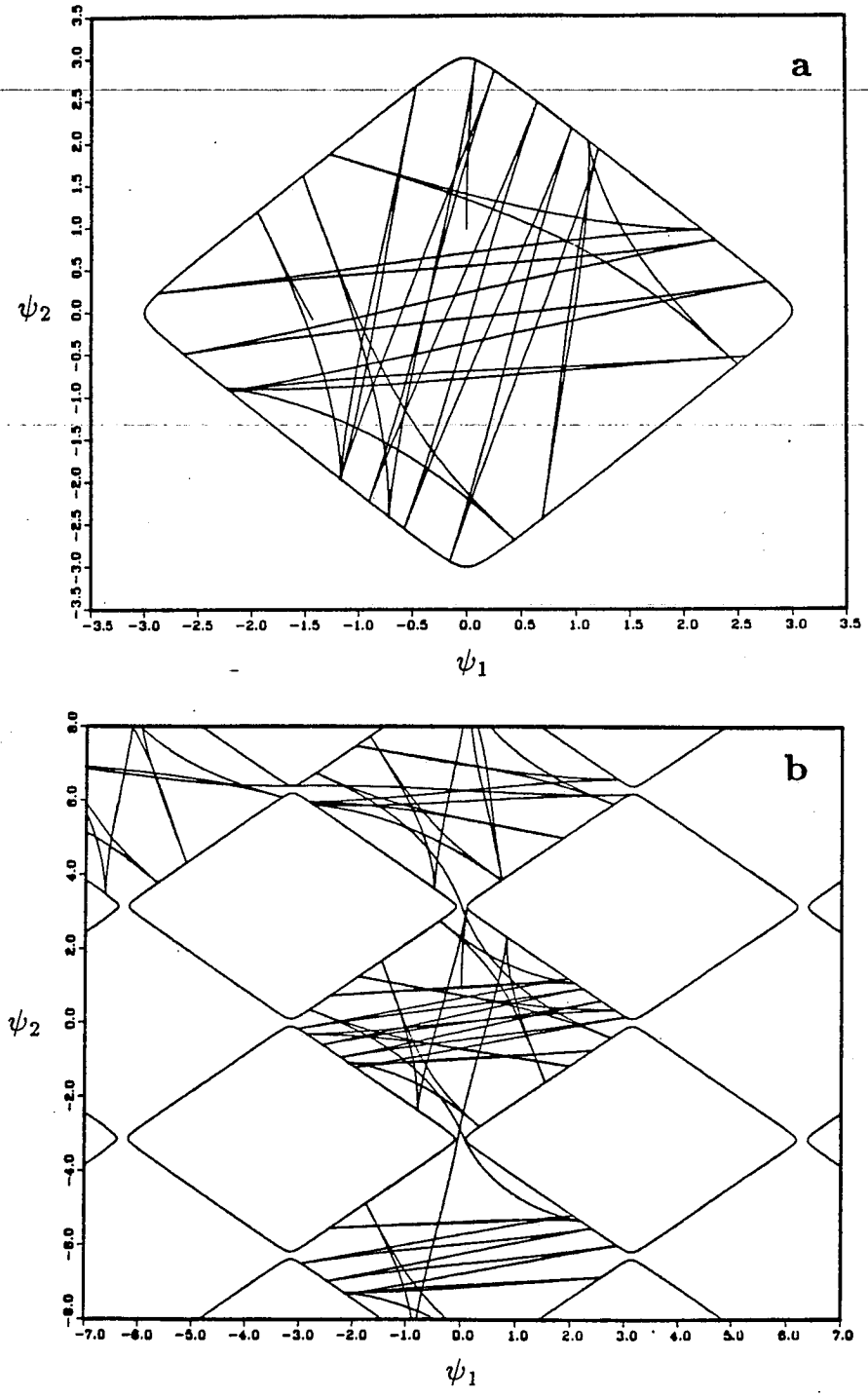

For values of $\tilde{H} < 0$, a particle's motion, for the $\phi = 1$ problem, is constrained to remain within a roughly diamond-shaped region in the (ψ_1, ψ_2)-plane. $\tilde{H} = 0$ is the marginally trapped case. Fig. 6.7a illustrates a plot of the trajectory of a particle in the (ψ_1, ψ_2)-plane for parameter values $\phi = 1$, $k = 1$, $\theta/\epsilon = 4.06$, $\tilde{H} = -.01$. The Poincaré plot for this orbit indicates that it is in the stochastic regime. One can see from Fig. 6.7a that the motion remains confined to a single wave cell. In the figure, we have also plotted the potential barrier

$$\tilde{H} = -.01 = -\cos\psi_1 - \cos\psi_2,$$

where the particle is turned.

For values of the energy slightly above "sea level" ($\tilde{H} > 0$), small "holes" open up between adjacent cells at the corners of the diamond-shaped potential barrier, allowing the particle to escape from cell to cell. The potential barrier is reminiscent of a billiard table with pockets at the corners. For very small positive values of $\tilde{H}$, the particle bounces around in a given cell for a time which becomes longer and longer as $\tilde{H}$ is made closer and closer to 0. The particle eventually hits a pocket and enters an adjacent cell. For very small positive values of $\tilde{H}$, where the probability of hitting a pocket becomes very small, one would expect the successive pockets which the particle exits to become uncorrelated. We conjecture that the result is a two-dimensional random walk from cell to cell. Fig. 6.7b illustrates this type of motion for the case $\tilde{H} = .005$, with the other parameters identical to those of Fig. 6.7a.

The present work has largely concentrated on the case $\mathbf{w} = 0$, as discussed above. For this case, the Hamiltonian is independent of $\tilde{x}$, and thus places no constraint upon the allowed values of $\tilde{x}$. For non-zero values of $\mathbf{w}$, the

Hamiltonian, Eq. (6.2), becomes $\tilde{x}$-dependent. This produces some qualitative changes which we now discuss.

One striking difference between the $\mathbf{w} \neq 0$ and $\mathbf{w} = 0$ problems is the emergence of a broken symmetry in the former case due to the electric current in the z-direction, which is responsible for the shear in the magnetic field. The sign of j_z relative to B_z fixes a "preferred" direction. For $L_s > 0$, j_z and B_z, from Eq. (2.1), are parallel. For $L_s < 0$, they are antiparallel. Throughout, we have implicitly assumed, without loss of generality, that $L_s > 0$ The mobility of the electrons in the x-direction depends upon whether the z-component of the wave-frame's velocity is parallel or anti-parallel to this current. From Eq. (6.2) one finds that the potential energy, as seen in the wave-frame, has an extremum with respect to the x-coordinate at $\tilde{x} = \tilde{w}_y/(\epsilon\tilde{w}_z)$. This extremum is either a maximum or a minimum, depending on whether $\tilde{w}_z$ is positive or negative. The particle thus sees either a potential well or an anti-well in the wave-frame, depending on which direction the wave-frame is moving in.

For $\tilde{w}_z > 0$, the conserved Hamiltonian $H = u^2/2 - \cos\psi_1 - \phi\cos\psi_2 + \tilde{w}_y\tilde{x}/\epsilon - \tilde{w}_z\tilde{x}^2/2$ imposes no constraint upon the value of $\tilde{x}$ which can be achieved. H can be conserved as $\tilde{x}$ grows large by virtue of u^2 becoming large. On the other hand, for $\tilde{w}_z < 0$, the particle sees a potential well with respect to x, and the motion in the x-direction must remain bounded, regardless of the level of stochasticity.

The physical mechanism responsible for this radial trapping phenomenon for $\tilde{w}_z < 0$ is the familiar pinch effect. The y-component of the sheared B-field, being antisymmetric about $\tilde{x} = 0$, produces a Lorentz force directed either inward or outward, depending upon the sign of $\tilde{w}_z$. One may think of the magnetic shear as being due to a current sheet in the z-direction. Our model

has chosen this current to be in the positive z-direction. This corresponds to a current produced by ions traveling in the positive z-direction and electrons traveling in the negative z-direction. For $\tilde{w}_z < 0$, the wave frame moves in the same direction as negative particle flux, and the pinch effect confines the radial excursions of the negatively charged test particle.

This asymmetry of the properties of the electron motion, with respect to the sign of w_z, may be an important unexplored property of nonlinear electron drift waves in a sheared magnetic field. We note that in the linear theory, drift waves propagating with ω/k_z parallel to the electron drift, $v = -j_z/(en_e)$, have slightly larger growth rates than those propagating against the electron flow, $(k_z v/\omega < 0)$.

In the one-wave problem, we also see a phenomenon somewhat analogous to the pinch effect described above. We found in Sec. V that for one wave with zero phase velocity in the lab frame, $(\phi = \tilde{w}_y = 0)$, orbits having canonical momentum $\tilde{P}_z$ less than 0 fall into the class of orbits depicted in Fig. 5.1b. The width of the separatrix labeled α in Fig. 5.1b constricts as $\tilde{P}_z$ is made more and more negative. As one increases $\tilde{P}_z$ to a value larger than 0, the fixed points at $\tilde{x} = 0$ bifurcate into a triplet of fixed points, the outer ones moving apart as $\tilde{P}_z$ is increased. As $\tilde{P}_z$ is increased beyond 2, the outer islands, labeled δ in Fig. 5.1k, move off toward $\pm\infty$. We observe a sort of "focusing" phenomenon for islands corresponding to negative values of $\tilde{P}_z$. For $\tilde{P}_z > 0$, one sees a "defocusing" effect, whereby the islands display a kind of repulsion. $\tilde{P}_z$ parallel to the electron flow results in focusing, and $\tilde{P}_z$ antiparallel to the electron flow results in defocusing. It may be of heuristic value to think of this phenomenon as a pinch effect. In light of the rich variety of features, such as this focusing effect,

which occur even in the one-wave magnetic shear problem, a generalization of the O'Neil problem[2] to the electron orbits given here is suggested as an interesting future problem. However, the lack of closed-form, analytic expressions for the orbits could make the analog of O'Neil's treatment exceedingly difficult.

VII. Guiding-Center Motion in Toroidal Geometry

The extension of the problem of drift motion in a slab geometry with shear to the more realistic toroidal geometry of the tokamak is a logical next step to take. A detailed analysis of the analogous toroidal problem goes beyond the scope of the present work. The model of a slab with shear is already very rich with new features and complications in comparison with some previously considered idealized multiple-wave systems. We do, however, wish to touch upon some aspects of the toroidal electrostatic wave problem.

For the toroidal problem, the Lagrangian formulation of guiding-center motion greatly facilitates the analysis. For example, transforming to the wave frame is accomplished by a simple change of variables in the Lagrangian. In the toroidal problem, this is much easier than the approach we took in the slab geometry. There, we made a Galilean transformation to an inertial frame moving with the waves. This was the simplest approach for that case, since the fundamental equations of physics are the same in all inertial frames. In contrast, for a single electrostatic wave in a tokamak, the wave-frame is a non-inertial, rotating frame. Using the Lagrangian approach, the fictitious forces associated with the non-inertial frame automatically emerge from the Lagrangian when the change of variables is made. Using the Lagrangian approach, there seems to be less likelihood of omitting some important physics.

In Sec. VIIA, we briefly discuss the variational formulation of the guiding-center motion and derive the energy equation from the Lagrangian for arbitrary time-dependent fields. In Sec. VIIB, we present the equations of motion for the problem of electrostatic waves in the toroidal geometry. We have not explored an analytic or numerical analysis of these equations of motion to any degree,

outside of running a few numerical simulations to confirm that a perturbing wave produces a transition to stochastic motion.

We do however consider a problem of guiding-center motion in the tokamak in the presence of a somewhat simpler perturbation. We look at the effect which an adiabatic perturbation has upon the orbits. In particular, we do an analytic treatment, in Sec. VIIC, of tokamak orbits in the presence of a slowly varying radial electric field $E_r(t)$, and a slowly varying toroidal component of the vector potential, $A_\varphi(t)$. The time-dependent A_φ produces the inductive toroidal electric field $E_\varphi = -\frac{1}{c}\frac{\partial A_\varphi}{\partial t}$, responsible for driving the plasma current of the tokamak. The time-dependent radial electric field can arise if there are departures from quasi-neutrality. These could be due to such phenomena as runaway electrons or the greater penetration of fast-ions into the plasma than electrons upon the ionization of an injected neutral beam.

The field E_φ produces the familiar Ware pinch effect, whereby trapped particle orbits drift toward the magnetic axis of the device. The time-varying radial field $E_r(t)$ produces an orbital drift, called the neoclassical polarization drift,[20] similar to the Ware effect. The direction of the drift, inward or outward, depends upon the sign of $\dot{E}_r$ and the sign of the particle's charge.

The fields $A_\varphi(t)$ and $E_r(t)$ are taken to vary slowly on the time-scale of the "unperturbed" drift orbits. The resulting non-stochastic, adiabatic drifts can be treated analytically.

The present derivation of the drifts from the guiding-center equations of motion extends the results of the Ware pinch in two ways. First, the time-dependent $E_r(t)$ is shown to produce an effect similar to that produced by the toroidal electric field E_φ: The Ware pinch velocity $\bar{v}_r = -cE_\varphi/B_\theta$ is simply

modified to become $\bar{v}_r = -c[E_\varphi - \dot{E}_r/\Omega_\theta]/B_\theta$, where Ω_θ is the Larmor frequency calculated with the θ-component of the magnetic field. Secondly, the present derivation extends the results for the Ware pinch and the neoclassical polarization drift to the untrapped orbit regime. Our result for the average drift velocity is continuous across the trapping boundary.

A. Variational Formulation of Drift Motion

In Sec. II, the equations of motion for drift orbits in a slab geometry were derived from a guiding-center Lagrangian. For that model, the magnitude of the magnetic field was spatially and temporally invariant. For the toroidal problem, the strength of the magnetic field is non-uniform, varying principally as the inverse of the major radius coordinate. The guiding-center Lagrangian of Eqs. (2.10) and (2.13) must be modified by adding the perpendicular kinetic energy term, $\mu B = \frac{1}{2}mv_\perp^2$, to the Hamiltonian:

$$H \equiv \frac{1}{2}mv_\parallel^2 + \mu B - q\Phi. \tag{7.1}$$

Here, μ is taken to be an adiabatic invariant.

Littlejohn has provided a method of deriving the guiding-center equations to arbitrary order in the small expansion parameter ϵ which gives the ratio of the Larmor radius to the gradient scale length. He starts with the phase space Lagrangian

$$L(\mathbf{x},\mathbf{v},\dot{\mathbf{x}},\dot{\mathbf{v}},t) = \dot{\mathbf{x}}\cdot\left[m\mathbf{v} + \frac{q}{c}\mathbf{A}\right] - \frac{1}{2}m|\mathbf{v}|^2 - q\Phi, \tag{7.2}$$

whose Euler-Lagrange equations

$$\dot{\mathbf{x}} = \mathbf{v} \tag{7.3}$$

$$m\dot{\mathbf{v}} = -q\left[\nabla\Phi + \frac{1}{c}\frac{\partial\mathbf{A}}{\partial t}\right] + \frac{q}{c}\dot{\mathbf{x}}\times(\nabla\times\mathbf{A}) \tag{7.4}$$

are equivalent to the exact Newton-Lorentz equations

$$m\frac{d^2\mathbf{x}}{dt^2} = q\mathbf{E} + \frac{q}{c}\dot{\mathbf{x}}\times\mathbf{B}.$$

By applying a series of coordinate and gauge transformations to this Lagrangian and carefully ordering terms in the smallness parameter ϵ, Littlejohn obtains a

variational principle for the guiding-center equations. We use his results to first order in ϵ. The equations of motion for the guiding-center position $\mathbf{x}$ and parallel velocity $v_\parallel$, to lowest order in the gyro-radius, follow from the Lagrangian

$$L(v_\parallel, \mathbf{x}, \dot{\mathbf{x}}) = \left[m v_\parallel \hat{\mathbf{b}} + \frac{q}{c} \mathbf{A} \right] \cdot \dot{\mathbf{x}} - H, \tag{7.5}$$

where H is given in Eq. (7.1).

We now derive an expression for the time-derivative of the kinetic energy, for arbitrarily varying fields. The Lagrangian (7.5) is of the form

$$L(\mathbf{q}, \dot{\mathbf{q}}, t) = \gamma_i(\mathbf{q}, t) \dot{q}^i - H(\mathbf{q}, t) \tag{7.6}$$

The Euler-Lagrange equation

$$\frac{d}{dt} \frac{\partial L}{\partial \dot{q}^i} = \frac{\partial L}{\partial q^i} \tag{7.7}$$

implies that

$$\frac{\partial \gamma_i}{\partial t} + \frac{\partial H}{\partial q^i} = \omega_{ij} \dot{q}^j, \tag{7.8}$$

where

$$\omega_{ij} \equiv \frac{\partial \gamma_j}{\partial q^i} - \frac{\partial \gamma_i}{\partial q^j}. \tag{7.9}$$

With $\mathbf{J} \equiv \omega^{-1}$, one has

$$\dot{q}^i = J^{ij} \left[\frac{\partial \gamma_j}{\partial t} + \frac{\partial H}{\partial q^j} \right]. \tag{7.10}$$

The total time-derivative of an arbitrary function of the coordinates and time is given by

$$\frac{d}{dt} f(\mathbf{q}, t) = \frac{\partial f}{\partial t} + \frac{\partial f}{\partial q^i} J^{ij} \left[\frac{\partial \gamma_j}{\partial t} + \frac{\partial H}{\partial q^j} \right] \tag{7.11}$$

In particular, for f equal to the Hamiltonian,

$$\frac{dH}{dt} = \frac{\partial H}{\partial t} + \frac{\partial H}{\partial q^i} J^{ij} \frac{\partial \gamma_j}{\partial t}, \tag{7.12}$$

due to the antisymmetry of $\mathbf{J}$. From Eq. (7.10) and again using the antisymmetry of $\mathbf{J}$, one finds

$$\dot{q}^j = -\left[\frac{\partial \gamma_i}{\partial t} + \frac{\partial H}{\partial q^i}\right] J^{ij}.$$

Substituting this into Eq. (7.12), one finds

$$\frac{dH}{dt} = \frac{\partial H}{\partial t} - \dot{q}^j \frac{\partial \gamma_j}{\partial t}. \tag{7.13}$$

Using this result for the guiding-center Lagrangian, one finds the following expression for the rate of change of the kinetic energy:

$$\frac{d}{dt}\left[\frac{1}{2}mv_\parallel^2 + \mu B\right] = \mu\frac{\partial B}{\partial t} + \dot{\mathbf{x}} \cdot \left[q\mathbf{E} - mv_\parallel \frac{\partial \hat{\mathbf{b}}}{\partial t}\right]. \tag{7.14}$$

This result is similar to that obtained by Northrop[18]

$$\frac{d}{dt}\left[\frac{1}{2}mv_\parallel^2 + \mu B + \frac{1}{2}mu_E^2\right] = \mu\frac{\partial B}{\partial t} + q\dot{\mathbf{x}} \cdot \mathbf{E},$$

except for two differneces. Northrop includes the average cross-field drift velocity, $\mathbf{u}_E = c\mathbf{E} \times \mathbf{B}/B^2$, in the expression for the kinetic energy on the left-hand side. Furthermore, the expression (7.14) contains an additional force term $-mv_\parallel \partial\hat{\mathbf{b}}/\partial t$, which apparently represents a reactive force due to the change in the direction of the B-field.

B. Multiple Electrostatic Waves in Toroidal Geometry

In toroidal coordinates, the Lagrangian (7.2) is transformed to

$$L(v_\parallel, r, \theta, \varphi, \dot{r}, \dot{\theta}, \dot{\varphi}, t) = P_r\dot{r} + P_\theta\dot{\theta} + P_\varphi\dot{\varphi} - H$$

where

$$P_r \equiv mv_\parallel b_r + \frac{q}{c}A_r$$

$$P_\theta \equiv r[mv_\parallel b_\theta + \frac{q}{c}A_\theta]$$

$$P_\varphi \equiv (R_0 + r\cos\theta)[mv_\parallel b_\varphi + \frac{q}{c}A_\varphi]$$

and

$$H \equiv \frac{1}{2}mv_\parallel^2 + \mu B + q\Phi.$$

We assume an electrostatic potential of the form

$$\Phi = \sum_i \phi_i(r)\cos(m_i\theta + n_i\varphi - \omega_i t).$$

Assuming a toroidally symmetric tokamak, the toroidal magnetic field is taken to be

$$B_\varphi = \frac{B_0 R_0}{R_0 + r\cos\theta}.$$

One may transform to the wave frame of the first wave by introducing the phase coordinate

$$\psi \equiv n_1\varphi - \omega_1 t.$$

We wish to describe the problem from the vantage point of a frame moving in the toroidal direction at the correct velocity required to remain in phase with the first wave. Replacing the cordinate φ with ψ, the Lagrangian becomes

$$L(v_\parallel, r, \theta, \psi, \dot{r}, \dot{\theta}, \dot{\psi}, t) = P_r\dot{r} + P_\theta\dot{\theta} + P_\varphi\frac{\dot{\psi}}{n_1} - H',$$

where

$$H' = \frac{1}{2}mv_{\|}^2 + \mu B + q\phi_1(r)\cos(m_1\theta + \psi) - \frac{\omega_1}{n_1}P_\varphi$$

$$+q\sum_{i=2,3,\ldots}\phi_i(r)\cos\left(m_i\theta + \frac{n_i}{n_1}\psi + (\omega_1 n_i/n_1 - \omega_i)t\right)$$

The only explicit time-dependence appears in the potential terms for waves 2,3,..., and in the term $A_\varphi(t)$ responsible for the inductive electric field. For the time being, we ignore the time-dependence of A_φ. Then, if only one wave is present, the equations of motion comprise a two degree of freedom, autonomous system. With more than one wave present, the system becomes non-autonomous. It is generally impossible to find a time-independent wave frame with 2 or more waves present. This is because of the θ-dependence of B_φ. If one transformed to a frame of reference moving with a component of velocity in the θ-direction, then the background magnetic field would become modulated in time. We thus find that in the toroidal geometry, the one-wave problem is somewhat analogous to the two-wave problem we have studied in slab geometry, insofar as we have ignored the inductive electric field E_φ. The magnetic potential well of the toroidal magnetic field acts, in effect, like a stationary wave. With two waves present, the problem is intrinsically non-autonomous (i.e. a $2\frac{1}{2}$ degree of freedom system). The two-wave problem in toroidal geometry is thus similar to the three-wave problem in slab geometry.

For an axially symmetric tokamak, ψ appears only in the wave potential terms. In the absence of the perturbing waves, the Lagrangian is cyclic in ψ and the canonical momentum P_φ is conserved. With two conserved integrals H and P_φ, the unperturbed motion may, in principle, be reduced to quadrature.

With P_φ a constant specified by initial conditions, one may eliminate $v_{\|}$

from the Lagrangian, and the motion in the (r,θ)-plane for the unperturbed problem is derived from the Lagrangian

$$L(r,\theta,\dot{r},\dot{\theta};P_\varphi) = P_r(r,\theta;P_\varphi)\dot{r} + P_\theta(r,\theta;P_\varphi)\dot{\theta} - H_0,$$

where

$$H_0 = \frac{1}{2mb_\varphi^2}\left[\frac{P_\varphi}{R_0 + r\cos\frac{x}{L_s}\theta} - \frac{q}{c}A_\varphi\right]^2 + \mu B.$$

The Euler-Lagrange equations for the unperturbed problem are then given by

$$\dot{\theta}\left[\frac{\partial P_\theta}{\partial r} - \frac{\partial P_r}{\partial \theta}\right] = \frac{\partial H_0}{\partial r}$$
$$\dot{r}\left[\frac{\partial P_\theta}{\partial r} - \frac{\partial P_r}{\partial \theta}\right] = -\frac{\partial H_0}{\partial \theta}$$

Without any further approximations, these equations are quite complicated. We note, however, that the term $[\partial P_\theta/\partial r - \partial P_r/\partial\theta]$ has no effect upon the shape of the orbits in the (r,θ)-plane. One could define a reparametrized time

$$\tau(r,\theta,t) \equiv \frac{t}{\frac{\partial P_\theta}{\partial r} - \frac{\partial P_r}{\partial \theta}}$$

which absorbs this factor into the independent variable. Then the canonical system

$$\frac{d\theta}{d\tau} = \frac{\partial H_0}{\partial r}$$
$$\frac{dr}{d\tau} = -\frac{\partial H_0}{\partial \theta},$$

with H_0 defined above, gives the correct (r,θ) coontours for the unperturbed problem.

Adding a single wave breaks the toroidal symmetry and destroys the invariance of P_φ. One expects this to lead to the appearence of the stochastic instability in some regions of phase space. Adding a second wave destroys the invariance of the Hamiltonian. One expects the extra half degree of freedom to open up the possibility of Arnold diffusion in the two-wave system.

C. Neoclassical Polarization Drift

We now look at the simpler problem of adiabatic perturbations acting upon the unperturbed orbits in toroidal geometry. We derive the average radial drift velocity for both trapped and passing regimes from the guiding-center equations of motion. We include the effects of both a time-dependent radial electric field $\dot{E}_r$ and a time-independent, uniform toroidal electric field E_φ . The former field results in the neoclassical polarization drift[20], and the latter field produces the Ware pinch[21].

The present analysis is performed in the limit of small inverse aspect ratio, $a << R_0$, where a is the minor radius and R_0 is the major radius of the tokamak's magnetic center. We also make the so-called small banana width approximation, assuming that over one complete period of the unperturbed motion, both the trapped and untrapped orbits depart only slightly from a given (circular) flux surface ($\delta r << a$). We consider the time-dependent radial field $E_r(t)$ and the time-dependent potential $A_\varphi(t)$ (responsible for the toroidal inductive field) to be adiabatic perturbations.

The guiding-center equations, to lowest order in the gyro-radius, follow from the Lagrangian

$$L(v_\parallel, \mathbf{x}, \dot{\mathbf{x}}) = \left[m v_\parallel \hat{\mathbf{b}} + \frac{q}{c}\mathbf{A} \right] \cdot \dot{\mathbf{x}} - H, \tag{7.15}$$

where

$$\hat{\mathbf{b}} \equiv \mathbf{B}/B, \tag{7.16}$$

$$H \equiv \frac{1}{2} m v_\parallel^2 + \mu B + q\Phi, \tag{7.17}$$

and μ is the particle's constant magnetic moment.

Transforming to toroidal coordinates, the Lagrangian becomes

$$L(v_\parallel, r, \theta, \varphi, \dot{r}, \dot{\theta}, \dot{\varphi}, t) = P_r \dot{r} + P_\theta \dot{\theta} + P_\varphi \dot{\varphi} - H, \tag{7.18}$$

where

$$P_r \equiv m v_\parallel b_r + \frac{q}{c} A_r \tag{7.19}$$

$$P_\theta \equiv r \left[m v_\parallel b_\theta + \frac{q}{c} A_\theta \right] \tag{7.20}$$

$$P_\varphi \equiv R \left[m v_\parallel b_\varphi + \frac{q}{c} A_\varphi \right]. \tag{7.21}$$

Here, $R \equiv R_0 + r\cos\theta$ is the major radius. We approximate the φ-component of the magnetic field $B_\varphi = B_0 R_0 / R$ with the first 2 terms in the Taylor expansion:

$$B_\varphi = B_0 \left[1 - \frac{r}{R_0} \cos\theta \right]. \tag{7.22}$$

We ignore the major-radial dependence of the induced electric field, taking $E_\varphi(t)$ to depend only upon t. We also ignore the θ-dependence of $B_\theta(r)$, consistent with our assumption of a small inverse aspect ratio tokamak of circular cross-section. We make no specific assumptions as to the detailed form of $E_\varphi(t)$ and $B_\theta(r)$, except that changes in E_φ are adiabatic on the time scale of a drift period and that changes in B_θ over a drift period are small. With these assumptions, we may expand E_φ and B_θ about given values of time and minor radius, respectively.

A vector potential of the form

$$A_r = 0 \tag{7.23}$$

$$A_\theta = \frac{B_0 r}{2} \tag{7.24}$$

$$A_\varphi = -c \int^t dt' E_\varphi(t') - \int^r dr' B_\theta(r') \tag{7.25}$$

reproduces the desired fields. Here, terms of order a/R_0 have been left out. The time-dependent radial electric field is derived from a scaler potential $\Phi(r,t)$.

With our choice of electromagnetic gauge in which $A_r = 0$, and the assumption that B_r/B is negligible, we take the radial canonical momentum, P_r, to be 0. Furthermore, one may assume that the term $mv_\parallel b_\theta$ in P_θ is negligible compared with qA_θ/c. The ratio of the former term to the latter is

$$\frac{2mcv_\parallel b_\theta}{qB_0 r} = \frac{2v_\parallel b_\theta}{\Omega_c r}.$$

But $v_\parallel b_\theta$ is the projection of the parallel velocity in the θ-direction. The above term therefore represents roughly the ratio between the instantaneous angular frequency of the guiding-center motion with respect to the θ-direction and the gyro-frequency. One must assume this ratio to be small in order for the guiding-center description to be valid in the first place. We therefore drop the term $rmv_\parallel b_\theta$ in the Lagrangian.

The Lagrangian is now written

$$L(r,\theta,v_\parallel,\dot{\theta},\dot{\varphi},t) = \frac{q}{c}B_0\frac{r^2}{2}\dot{\theta} + P_\varphi\dot{\varphi} - H \tag{7.26}$$

In the following analysis, we use the fact that a Lagrangian is gauge-invariant under the addition of constants, functions which explicitly involve only the time, and functions which are the perfect time-derivatives. In other words, such gauge terms do not affect the resulting dynamics. We shall freely throw such terms away without re-labeling the Lagrangian.

We take the tokamak to be axisymmetric, and the Lagrangian is cyclic in the φ coordinate. Therefore $dP_\varphi/dt = 0$ and P_φ is a constant of the motion. Note that the conservation of P_φ does not reduce the dimensionality of the manifold

which a given orbit is constrained to lie on, unlike conserved integrals we have discussed previously. This is because A_φ, and hence P_φ, contains explicit time-dependence, and so the conservation of P_φ does not specify a time-independent equation of constraint among the spatial coordinates.

Taking $B_\varphi >> B_\theta$, we approximate b_φ with 1. Inverting the expression for P_φ, the parallel velocity is given by

$$v_{\|} = \frac{1}{m}\left[\frac{P_\varphi}{R} - \frac{q}{c}A_\varphi\right] \tag{7.27}$$

In the Hamiltonian, we approximate μB with μB_φ. Replacing the generalized coordinate $v_{\|}$ with P_φ, the Lagrangian becomes

$$L(r,\theta,P_\varphi,\dot{\theta},\dot{\varphi},t) = \frac{q}{c}\frac{B_0 r^2}{2}\dot{\theta} + P_\varphi\dot{\varphi} - q\Phi - \frac{1}{2m}\left[\frac{P_\varphi}{R} - \frac{q}{c}A_\varphi\right]^2 + \frac{\mu B_0 r}{R_0}\cos\theta. \tag{7.28}$$

The Euler-Lagrange equation for P_φ is given by

$$0 = \frac{\partial L}{\partial P_\varphi} = \dot{\varphi} - \frac{1}{mR}\left[\frac{P_\varphi}{R} - \frac{q}{c}A_\varphi\right]. \tag{7.29}$$

Assuming that one has solved the equations of motion for r and θ as functions of t, the solution for φ may be obtained from this equation by quadrature.

To first order in r/R_0, the last two terms in the Lagrangian (7.28) are approximately equal to

$$-\frac{1}{2m}\left[\frac{P_\varphi}{R_0} - \frac{q}{c}A_\varphi\right]^2 + \frac{r\,\cos\theta}{R_0}\left[\mu B_0 + \frac{P_\varphi}{mR_0}\left(\frac{P_\varphi}{R_0} - \frac{q}{c}A_\varphi\right)\right].$$

The term proportional to $r\cos\theta/R_0$ contains both grad-B and curvature drift terms. The time and space dependence of A_φ greatly increases the difficulty of dealing with the curvature effects analytically compared with the grad-B term.

We shall ignore the curvature terms in the following in order to simplify the analytic treatment, retaining $\mu B_0 \frac{r\cos\frac{x}{L_s}\theta}{R_0}$ as the only θ-dependent term in the Lagrangian. Thus, for high parallel velocity particles, in which the curvature drift dominates, the present treatment is inadequate. This is probably the most serious defect of the present analysis. In our first attack on the present system, we sidestepped the issue of the curvature drift by looking at a straight cylinder (infinite aspect ratio tokamak), with an externally applied uniform horizontal electric field $\Phi = -E_x r\cos\theta$, $E_x = -\mu B_0/(R_0 q)$, mocking up the effect of the magnetic well.

The term $P_\varphi \dot{\varphi}$ may be dropped in the Lagrangian by gauge-invariance and the motion in the (r,θ)-plane is then obtained from

$$L(r,\theta,\dot{\theta},t;P_\varphi) = \frac{qB_0}{2c} r^2\dot{\theta} - H(r,\theta,t;P_\varphi), \tag{7.30}$$

where

$$H(r,\theta,t;P_\varphi) \equiv \frac{1}{2m}\left[\frac{P_\varphi}{R_0} - \frac{q}{c}A_\varphi\right]^2 - \frac{\mu B_0}{R_0} r\cos\theta + q\Phi(r,t), \tag{7.31}$$

with P_φ fixed by initial conditions. If one makes the substitution

$$r = \sqrt{2cP_\theta/(qB_0)},$$

then motion for the canonical coordinate θ and canonical momentum P_θ is given by Hamilton's equations $\dot{P}_\theta = -\partial H/\partial\theta$ and $\dot{\theta} = \partial H/\partial P_\theta$. Except for the specific perturbations which we are considering here, this is equivalent to Hamiltonian formulations of drift motion in large aspect ratio tokamaks considered previously by other authors.[19]

Rather than using the coordinates θ and P_θ, we expand the radial motion about a given magnetic surface of minor radius r_0, defining

$$r \equiv r_0 + \delta r,$$

and look at the behavior of θ and δr. To lowest order in $\delta r/r_0$, the Lagrangian becomes

$$L(\delta r, \theta, \dot{\theta}, t; P_\varphi) =$$

$$\frac{qB_0 r_0}{c}\delta r\dot{\theta} - \frac{1}{2m}\left[P' + q\int_0^t dt' E_\varphi(t') + \frac{q}{c}B_\theta(r_0)\delta r\right]^2 + \frac{\mu B_0 r_0}{R_0}\cos\theta + qE_r(r_0)\delta r. \tag{7.32}$$

Again, gauge terms have been dropped, and P_φ/R_0 has been denoted by P'. At this stage, one clearly sees that the system is equivalent to the Hamiltonian system

$$H'(\theta, \delta r, t) \equiv$$

$$\frac{c}{qB_0 r_0}\left\{\frac{1}{2m}\left[P' + q\int_0^t dt' E_\varphi(t') + \frac{q}{c}B_\theta(r_0)\delta r\right]^2 - \frac{\mu B_0 r_0}{R_0}\cos\theta - qE_r(r_0)\delta r\right\}, \tag{7.33}$$

with θ and δr serving as the canonical coordinate and momentun, respectively.

The equations of motion for δr and θ are then given by

$$\delta\dot{r} = -\frac{\mu c}{qR_0}\sin\theta \tag{7.34}$$

$$\dot{\theta} = \frac{c}{B_0 r_0}\left\{\frac{B_\theta(r_0)}{mc}\left[P' + \frac{qB_\theta(r_0)}{c}\delta r\right] + \Omega_\theta\int_0^t dt' E_\varphi(t') - E_r\right\}, \tag{7.35}$$

where

$$\Omega_\theta \equiv \frac{qB_\theta(r_0)}{mc}. \tag{7.36}$$

These may be combined to give

$$\frac{d^2\theta}{dt^2} = \frac{c}{B_0 r_0}\left\{-\frac{\Omega_\theta B_\theta \mu}{qR_0}\sin\theta + \Omega_\theta E_\varphi - \dot{E}_r\right\}. \tag{7.37}$$

FIG. 7.1 Effective potential function for motion in toroidal angle for tokamak orbits including the poloidal electric field and an adiabatically changing radial electric field.

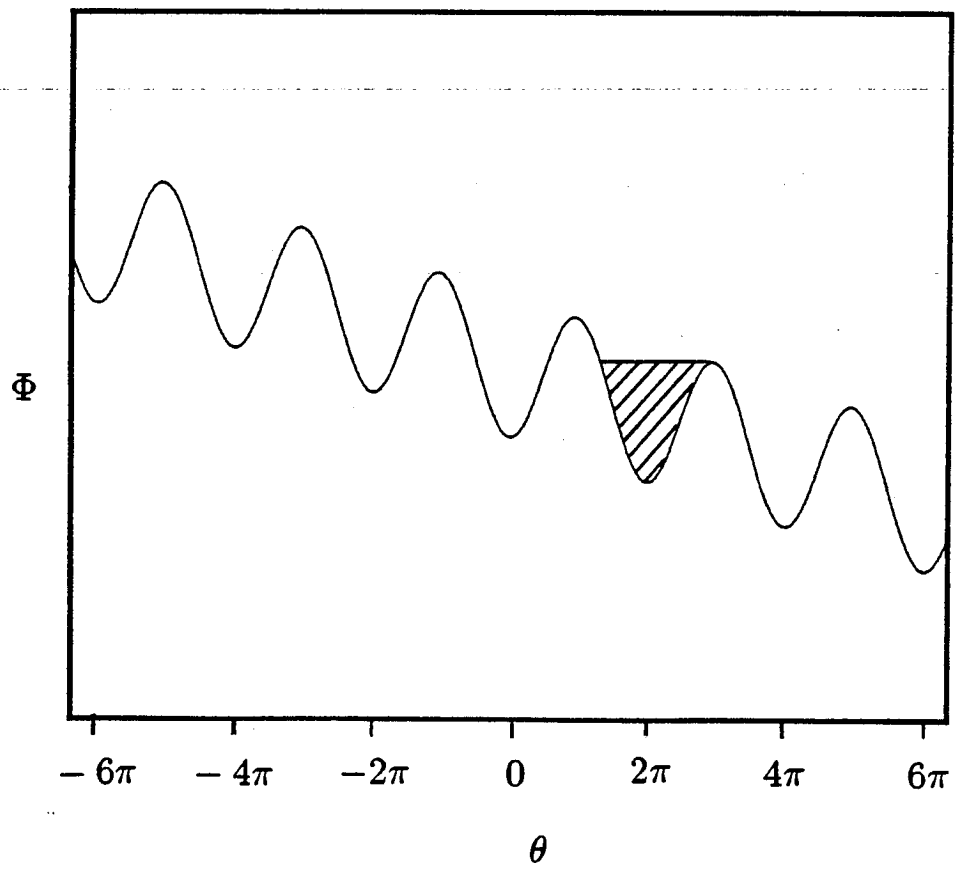

FIG. 7.2 Phase portrait of toroidal angle and toroidal angular velocity of tokamak orbits. Dotted curve indicates fate of typical passing orbit whose parallel velocity eventually changes sign.

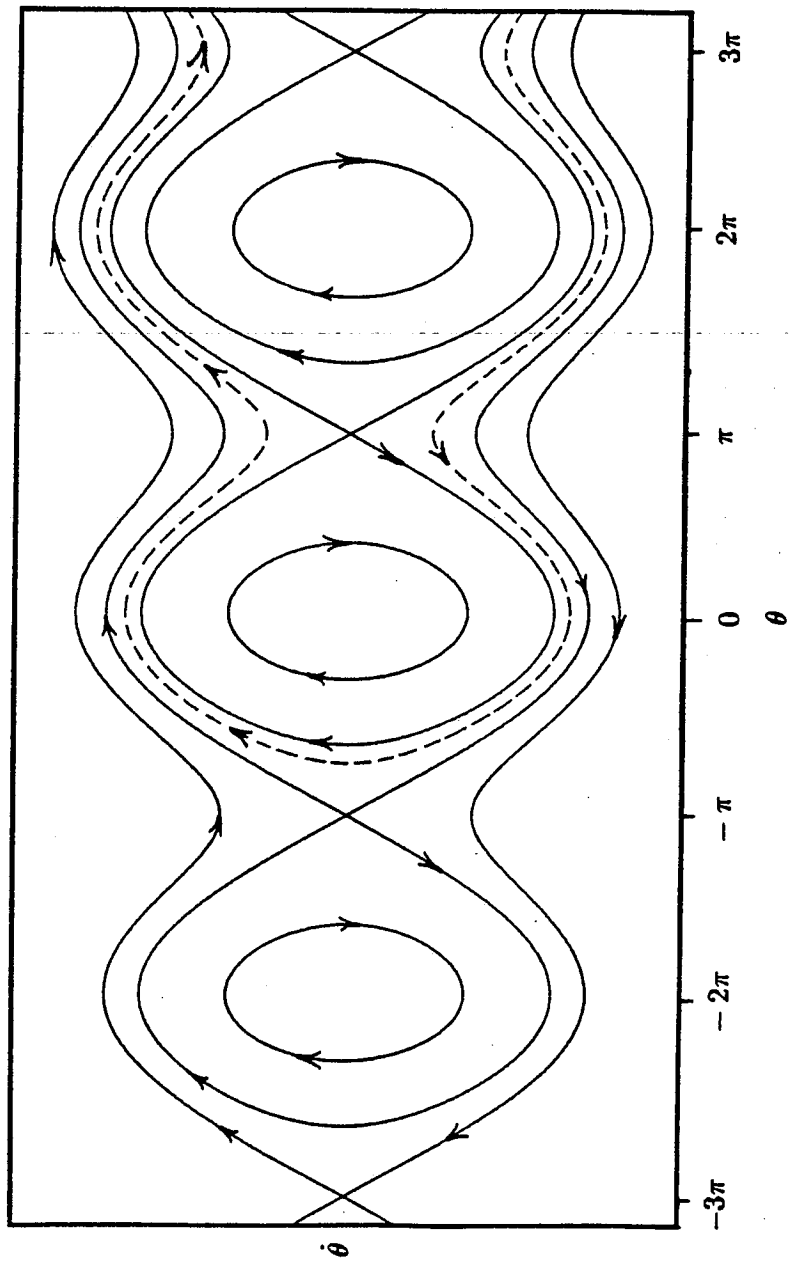

With the definitions

$$\alpha \equiv \frac{c\Omega_\theta B_\theta \mu}{B_0 r_0 q R_0} \tag{7.38}$$

$$\epsilon \equiv \frac{c}{B_0 r_0}\left[\Omega_\theta E_\varphi - \dot{E}_r\right], \tag{7.39}$$

we have

$$\frac{d^2\theta}{dt^2} = -\alpha \sin\theta + \epsilon. \tag{7.40}$$

This describes a pendulum subjected to a constant torque of magnitude ϵ. The θ motion corresponds to a particle moving in a potential well of the form illustrated in Fig. 7.1. The phase portrait of the motion in the $(\theta, \dot{\theta})$-plane is shown in Fig. 7.2. Orbits in the shaded region of Fig. 7.1. correspond to trapped, radially drifting banana orbits. The dashed line of Fig. 7.2 illustrates the fate of the typical counter-going passing particle: it eventually slows down and is turned to become a co-going particle.

One easily obtains a first integral of Eq. (7.40):

$$\dot{\theta} = \pm\sqrt{2[\epsilon\theta + \alpha(2k-1) + \alpha\cos\theta]}\,, \tag{7.41}$$

where k is an integration constant. With an appropriate choice of initial conditions, we have

$$k = \frac{m u_0^2 R_0}{4\mu B_0 r_0}$$

where u_0 is the initial parallel velocity.

One can, in principle, integrate Eq. (7.41) to find θ as a function of t. Then $\delta r(t)$ is found by solving Eq. (7.35) for δr, and combining the result with Eq. (7.41):

$$\delta r = -\frac{cP'}{qB_\theta(r_0)}$$

$$+\frac{c}{\Omega_\theta B_\theta(r_0)}\left\{\pm\frac{B_0 r_0}{c}\sqrt{2[\epsilon\theta+\alpha(2k-1)+\alpha\cos\theta]}-\Omega_\theta\int_0^t dt' E_\varphi(t')+E_r\right\} \tag{7.42}$$

Note that for the unperturbed problem, a value of $k = 1$ corresponds to the separatrix, i.e., the infinite period banana orbit whose turning points occur at $\theta = \pm\pi$, as illustrated in Fig. 7.3. The width of this orbit at $\theta = 0$, which represents the maximal radial excursion for the unperturbed problem, is then found from Eq. (7.42) to be

$$\Delta r = \frac{4}{\Omega_\theta}\sqrt{\frac{\mu B_0 r_0}{m R_0}}.$$

We demand that this be small compared with r_0 in order that the small banana-width approximation be valid.

After obtaining explicit solutions for $\theta(t)$ and $\delta r(t)$, Eq. (7.29) may be integrated to give $\varphi(t)$ and Eq. (7.27) yields $v_\parallel(t)$, which completes the solution of the equations of motion.

For the present purpose, it is not necessary to explicitly carry out this prescription. In order to determine the average radial velocity, $\bar{v}_r$, we evaluate Eq. (7.42) at t_0 and $t_0 + \Delta T$, where the orbit is assumed to be at $\theta = 0$ at $t = t_0$ and is assumed to return to $\theta = 0 \bmod 2\pi$ after a period ΔT. We adopt the approximation

$$E_r(t_0+\Delta T) - E_r(t_0) = \dot{E}_r \Delta T.$$

This ignores the change in E_r due to the particle's change in radius r over the course of one period.

First, let us consider the trapped orbits. After a period ΔT, the values of θ and $\dot{\theta}$ return to their original values. One finds

$$\delta r(t_0+\Delta T) - \delta r(t_0) = \frac{c}{\Omega_\theta B_\theta(r_0)}\left[\dot{E}_r - \Omega_\theta E_\varphi(t_0)\right]\Delta T.$$

FIG. 7.3 The separatrix between trapped banana orbits and untrapped passing orbits for tokamak, ignoring electric fields.

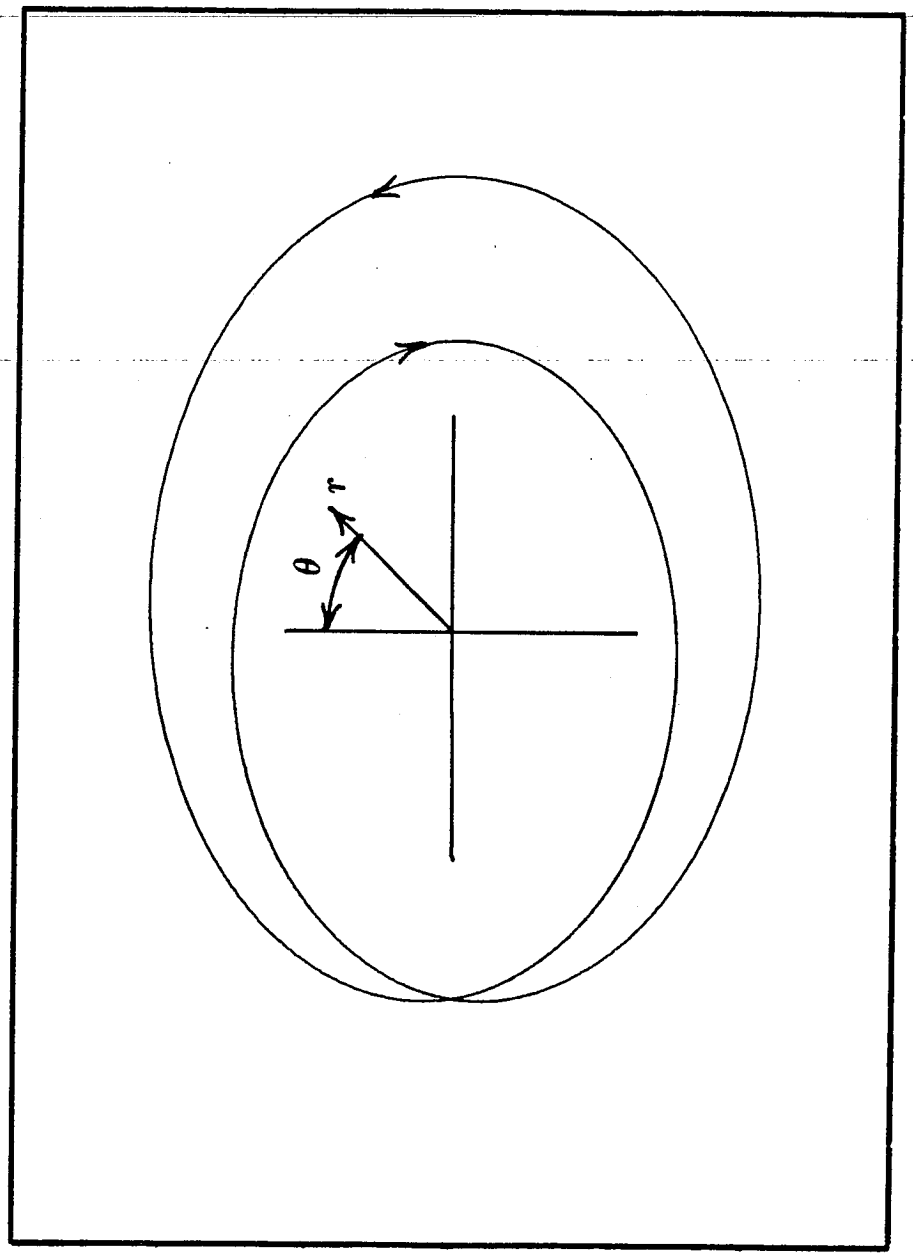

The average radial drift velocity is then

$$\bar{v}_r = \frac{\delta r(t_0 + \Delta T) - \delta r(t_0)}{\Delta T} = \frac{c}{\Omega_\theta B_\theta(r_0)} \dot{E}_r - \frac{c}{B_\theta(r_0)} E_\varphi.$$

In the absence of $\dot{E}_r$, we recover the usual expression for the Ware pinch velocity. We find that the addition of a time-dependent radial field simply modifies the Ware pinch by replacing E_φ with $E_\varphi - \dot{E}_r/\Omega_\theta$. Note that while the Ware pinch velocity is always directed radially inward, for any particle species, the direction of the neoclassical polarization drift depends upon the particle's charge.

We repeat the above argument for the circulating particles. After a period ΔT, the value of θ increases or decreases by 2π, depending on whether the particle is co-going or counter-going. Let σ be the sign of $\dot{\theta}$. Then

$$\delta r(t_0 + \Delta T) - \delta r(t_0) =$$

$$\frac{c}{\Omega_\theta B_\theta} \left\{ \sigma \frac{2B_0 r_0}{c} \left[\sqrt{\sigma\pi\epsilon + k\alpha} - \sqrt{k\alpha} \right] + \Delta T(\dot{E}_r - \Omega_\theta E_\varphi) \right\}$$

Assuming $|\sigma\pi\epsilon| << k\alpha$, we expand the square root to obtain the approximation

$$\delta r(t_0 + \Delta T) - \delta r(t_0) = \frac{c}{\Omega_\theta B_\theta} \left\{ \frac{B_0 r_0 \pi\epsilon}{c\sqrt{k\alpha}} + \Delta T(\dot{E}_r - \Omega_\theta E_\varphi) \right\}.$$

Using the definition of ϵ, the average radial drift velocity at $\theta = 0$ is therefore

$$\begin{aligned} \bar{v}_r &= \frac{\delta r(t_0 + \Delta T) - \delta r(t_0)}{\Delta T} \\ &= \frac{c}{\Omega_\theta B_\theta} \left[1 - \frac{\pi}{\Delta T \sqrt{k\alpha}} \right] \left[\dot{E}_r - \Omega_\theta E_\varphi \right]. \end{aligned}$$

The period ΔT can be approximated with the period of the unperturbed pendulum

$$\Delta T = \frac{2}{\sqrt{k\alpha}} K(k^{-1/2}),$$

where K is the complete elliptic integral of the first kind. We then obtain

$$\bar{v}_r = \frac{c}{\Omega_\theta B_\theta}\left[1 - \frac{\pi}{2K\left(k^{-1/2}\right)}\right]\left[\dot{E}_r - \Omega_\theta E_\varphi\right].$$

In the limit of barely untrapped particles, $k = 1$, the period becomes infinite, and this expression for $\bar{v}_r$ becomes identical to that derived for the trapped orbits. $\bar{v}_r$ is therefore continuous across the trapping boundary. For $k >> 1$, (highly untrapped particles), the radial drift velocity takes on the assymptotic form

$$\bar{v}_r = \frac{c}{\Omega_\theta B_\theta}\left[\dot{E}_r - \Omega_\theta E_\varphi\right]\frac{1}{4k}$$

In Fig. 7.4, the complete form of $\bar{v}_r$, in units of $c(\dot{E}_r - \Omega_\theta E_\varphi)/(\Omega_\theta B_\theta)$, is plotted as a function of the trapping parameter k. The dashed curve shows the assymptotic form for large k. One sees that as k is increased beyond the trapping boundary, the radial velocity rapidly falls to a small fraction of its value for trapped particles.

If instead of examining δr at $\theta = 0$ and $\theta = \pm 2\pi$, one examines δr at $\theta = \pi$ and $\theta = \pi \pm 2\pi$, one finds that the average radial drift velocity for untrapped particles at $\theta = \pi$ is given by

$$\bar{v}_r = \frac{c}{\Omega_\theta B_\theta}\left[1 - \frac{\pi}{2K\left(k^{-1/2}\right)}\sqrt{\frac{k}{k-1}}\right]\left[\dot{E}_r - \Omega_\theta E_\varphi\right].$$

This has the assymptotic of

$$\bar{v}_r = -\frac{c}{\Omega_\theta B_\theta}\left[\dot{E}_r - \Omega_\theta E_\varphi\right]\frac{1}{4k},$$

the negative of the result obtained at $\theta = 0$. We thus find that the drift of the untrapped particles is not so much a pinch (or anti-pinch) as an inward (or outward) drift in the major radial direction.

FIG. 7.4 The average radial drift velocity for the Ware pinch effect or the neoclassical polarization drift as a function of the trapping parameter k. $k = 1$ corresponds to the marginally trapped case. Dashed line gives assymptotic formula.

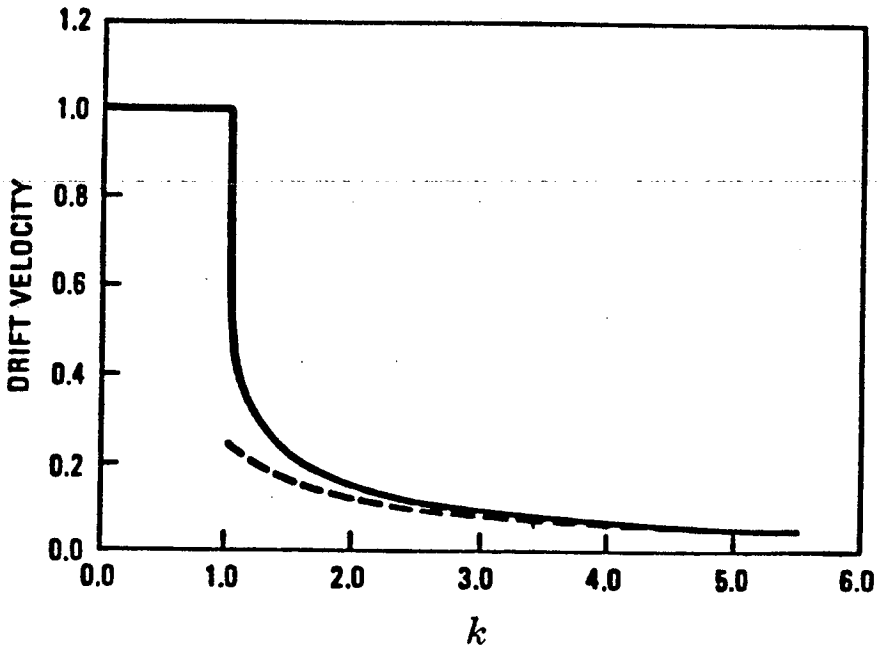

The above analytic results for the radial drift velocity overlook an important feature of the untrapped regime. We observed the radial displacement of the particle at $\theta = 0$ and after θ had increased or decreased by 2π. This is valid for passing particles which are able to get the whole way around in the θ-direction. However, all counter-going untrapped particles slow down and are eventually turned to become co-going. One sees this from the energy diagram of Fig. 7.1. An untrapped particle coming in from the right eventually hits the potential barrier and is turned. The sign of $\dot{\theta}$ changes, and the particle begins circulating in the opposite direction with respect to θ. When this reversal occurs, the untrapped particles take a step in the radial direction

One can see from the potential-well diagram of Fig. 7.1 that for small values of ϵ (i.e. the sinusoidal potential is very gradually "ramped"), the counter-going orbit is turned at a value of θ close to π. Therefore, for small ϵ, the banana width of the separatrix illustrated in Fig. 7.3 provides a good approximation for the radial step which the particle takes as its velocity is turned. A careful analysis of the above equations indicates that the radial step taken by the untrapped particles as they reverse their direction of circulation is always in the opposite direction as the the drift of the trapped particles. Hence, for the Ware pinch, the trapped particles pinch inward in radius, whereas the untrapped particles take a step outward in radius as they are turned.

Figs. 7.5 and 7.6 show the results of numerical integration of Eqs. (7.34) and (7.35). The signs were chosen to correspond to the Ware pinch. Fig. 7.5 shows the trapped orbits cascading inward. In Fig. 7.6, the particle starts out counter-going, and can be seen to be drifting in the major radial direction toward the axis of the tokamak. It is turned, takes a step outward, then resumes its

inward drift at an assymptotically decreasing rate.

FIG. 7.5 Neoclassical polarization drift in (r, θ)-plane for banana regime.

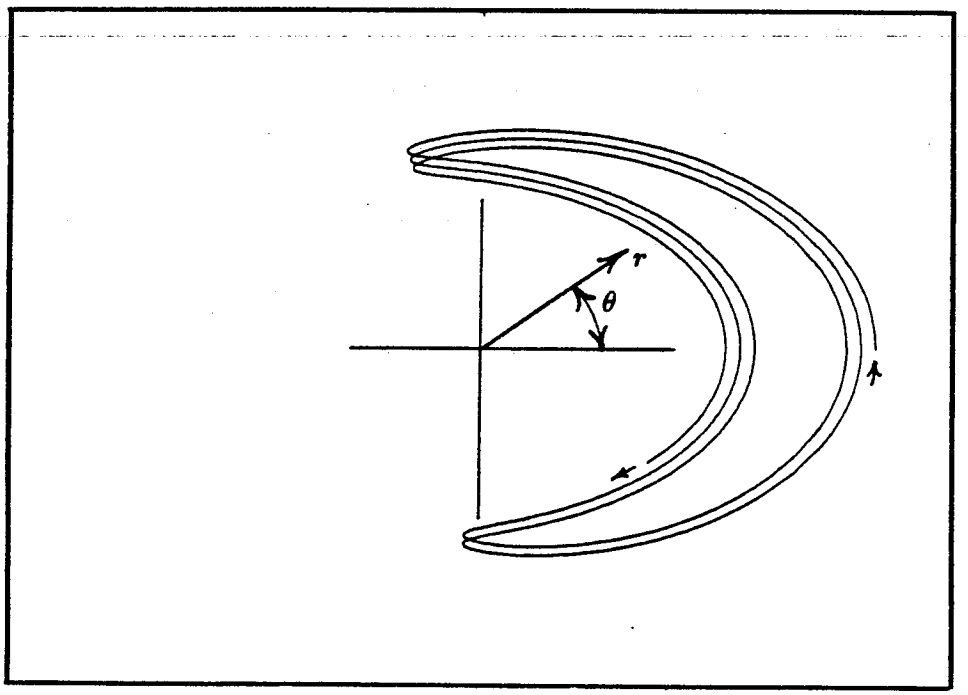

FIG. 7.6 Neoclassical polarization drift in (r, θ)-plane for untrapped regime.

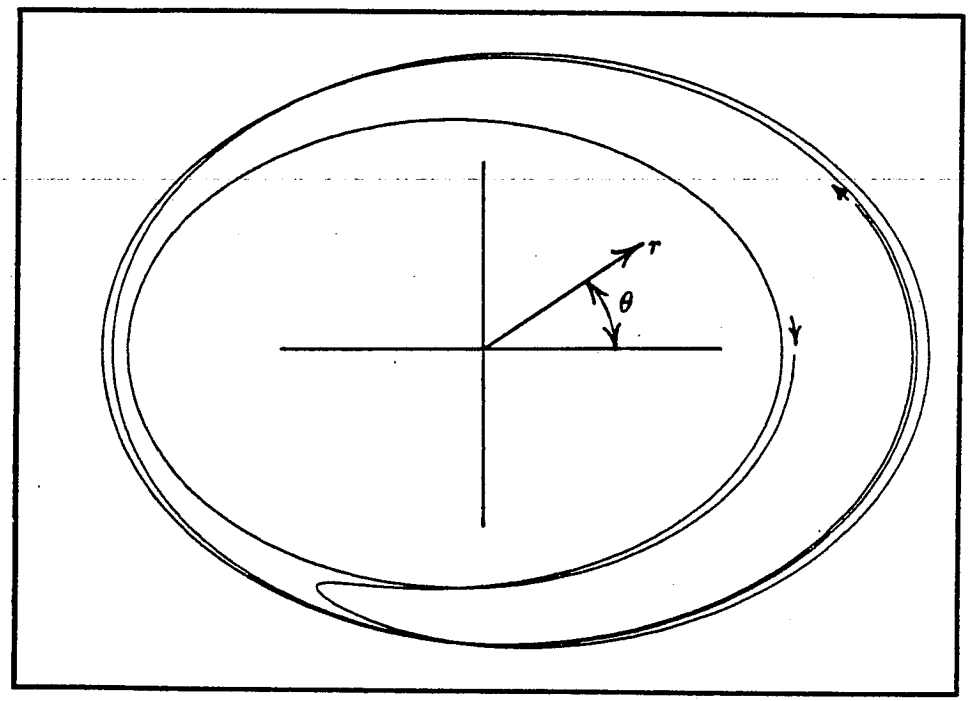

VIII. Conclusions

This work examines the motion of electrons in two electrostatic plane waves in a slab magnetic field geometry with shear. We show that the drift orbits are described by a two degree-of-freedom, autonomous Hamiltonian system. A conserved energy confines each orbit to a three-dimensional manifold in phase space. Each energy surface is topologically equivalent to a toroidal volume. Our dynamical system is thus quite similar to the field-line problem in toroidal confinement devices, except that here we have one complete toroidal system for each value of the conserved energy.

With only one wave present, the existence of a symmetry direction leads to a conserved canonical momentum P_z, and the motion can be reduced to quadrature. The motion on homoclinic trajectories may be expressed in terms of elliptic integrals, but the general one-wave orbits do not appear to admit analytic solutions in terms of well-known functions.

In the limit of large parallel kinetic energy, we show that the two-wave system becomes equivalent to the pendulum subjected to a time-dependent perturbation, a system which has been exhaustively studied by others. In this work, we have focused our attention upon the regime in which the electron's parallel kinetic energy and potential energy are comparable and the pendulum approximation ceases to be valid.

In this low parallel velocity regime, the separatrices have characteristic widths which are on the order of $\sqrt{L_s v_0/\omega_{ce}}$, where v_0 is the trapping velocity. This width scales as the fourth root of the wave potential as contrasted with the pendulum separatrix widths which scale as the square root of the potential. This difference in scaling suggests that for small wave amplitude, the low en-

ergy electrons, when subjected to the second perturbing wave, may display an early onset of stochasticity in comparison with those electrons in the pendulum regime.

In addition to this quantitative difference in scaling, the low kinetic energy regime displays qualitatively different behavior. A much richer variety of unperturbed orbit classes occur in the small energy regime. We have provided a comprehensive catalogue of all possible orbit classes, for any combination of parameter values. In our analysis of the unperturbed motion, we have found that for a given value of the conserved canonical momentum, chains of elliptic and hyperbolic fixed points are located at values of the radial coordinate satisfying a cubic equation. For canonical momenta less than $3/2m_e(\omega/k_y)^{2/3}v_0^{1/3}$, one chain of X and O points exists. For P_z greater than this value, the chain bifurcates into three chains of fixed points. Depending upon the parameter ranges and value of P_z, these fixed points may be tied together in a variety of topologically distinct ways, including a web-like homoclinic trajectory connecting all three chains.

For values of canonical momentum exceeding a certain positive value, which depends upon the wave's phase velocity, three disjoint chains of pendulum-like islands occur. (Here, the direction of positive P_z is the direction of the current j_z.) The central chain is located close to the rational surface and for large P_z, may be identified with the positive $v_{||}$ pendulum separatrix occuring in the ususal constant $v_{||}$ approximation. The other two island chains, located on either side of the rational surface, are a new feature of the low energy regime, being entirely absent in the constant $v_{||}$ approximation. As P_z is made large, the distance of these two island chains from the rational surface increases without bound. In

the opposite limit of large negative canonical momentum (P_z antiparallel to j_z), there appears only the usual single chain of islands near the rational surface.

In light of these features of the low energy regime, one expects far greater resonant interaction of the two waves than the usual constant $v_{||}$ approximation would permit. In the constant $v_{||}$ approximation, all regions of resonant trapping are spatially localized near the rational surface. If the rational surfaces of the two waves are well-separated, resonant interaction simply doesn't take place. In contrast, for the low energy regime, resonance trapping occurs at arbitrary radial distance from the rational surface (insofar as we have ignored the radial structure of the modes) and spatial coincidence of trapping regions associated with the two waves takes place regardless of the separation of the rational surfaces. Again, this leads to an enhanced level of stochasticity for low energy electrons. Numerical integration of the equations of motion and examination of Poincaré surfaces of section has confirmed our expectations that the low parallel velocity regime is especially fragile to the onset of chaos.

We have undertaken an examination of diffusion rates by numerically integrating the evolution of an ensemble of several hundred particles. In Sec. VIC, we compared the temporal behavior of the spread in the canonical momentum for two different values of energy. Our investigations of radial diffusion rates are too preliminary to be included here. We can, however, make some statements concerning the scaling of the diffusion rates. Assuming that under conditions of global stochasticity the radial motion can be characterized as a diffusive process, one should be able to calculate a dimensionless radial diffusion coefficient $\tilde{D}_x$ as a function of the ensemble distribution and the dimensionless parameters $\{\tilde{w}_y/\epsilon, \phi, k, \theta/\epsilon, \tilde{w}_z\}$. From the definitions of the dimensionless quantities $\tilde{x}$

and $\tilde{t}$, we then know that the diffusion coefficient D_x in real units must scale as $[(L_s^2 k_{1y}^4 c^6 \phi_1^5 m_e)/(eB_0^6)]^{1/4}$ or $\left(\frac{m_e}{m_i}\right)^{1/4} \frac{cT_e}{eB_0} k_{1y}\rho_s \left(\frac{L_s}{\rho_s}\right)^{1/2} \left(\frac{e\phi_1}{T_e}\right)^{5/4}$ times the dimensionless number $\tilde{D}_x$. In future work we will investigate the validity of the diffusion approximation and the parametric dependence of $\tilde{D}_x$ on the dimensionless parameters of the two-wave Hamiltonian system.

Appendix: Nambu Mechanics

We have found that the guiding-center equations of motion, Eqs. (2.4)–(2.5), while being non-Hamiltonian, may be described by a generalized Hamiltonian mechanics investigated by Y. Nambu.[22] This is a generalization of Hamiltonian mechanics which is distinct from the more familiar Hamiltonian systems in non-canonical coordinates. In this appendix, we demonstrate how the drift equations may be represented as a Nambu system. We also discuss some of the features of Nambu's formalism and show its relation to ordinary Hamiltonian mechanics and the Clebsch representation of magnetic fields. With Nambu mechanics, one is able to construct exactly integrable systems of non-linear ordinary differential equations, even for many degree-of-freedom systems. The integrable Nambu systems are, in a sense, the antithesis of many degree-of-freedom physical systems where all but a few integral invariants are generally expected to be destroyed (the ergodic hypothesis). We discuss how this ability to construct integrable systems may be exploited to find solutions to non-linear algebraic equations.

The equations of motion (2.4)–(2.5), or the dimensionless version Eqs. (2.20)–(2.23), are non-Hamiltonian. As discussed above, the factor β of Sec. IIA, which comes out of Littlejohn's guiding-center formalism, is required for the equations to have the Hamiltonian structure. Eqs. (2.20)–(2.23) may be written in the form

$$\dot{z}^i = J^{ij}\frac{\partial H}{\partial z^j}, \tag{A.1}$$

where $(z^1, z^2, z^3, z^4) \equiv (u, \tilde{x}, \psi_1, \psi_2)$,

$$H \equiv \frac{u^2}{2} - \cos\psi_1 - \phi\cos\psi_2 + \frac{1}{\epsilon^2}\left[\tilde{w}_y \sin\epsilon\tilde{x} + \tilde{w}_z \cos\epsilon\tilde{x}\right], \tag{A.2}$$

$$\mathbf{J} \equiv \begin{pmatrix} 0 & \mathbf{M} \\ -\mathbf{M}^T & 0 \end{pmatrix}, \tag{A.3}$$

and

$$\mathbf{M} \equiv \begin{pmatrix} -\frac{\sin\epsilon\tilde{x}}{\epsilon} & -\frac{k}{\epsilon}\sin(\epsilon\tilde{x}+\theta) \\ \cos\epsilon\tilde{x} & k\cos(\epsilon\tilde{x}+\theta) \end{pmatrix}. \qquad (A.4)$$

However, the Jacobi tensor calculated from this $\mathbf{J}$, whose contravariant components are given by

$$S^{ijk} \equiv J^{il}\frac{\partial J^{jk}}{\partial z^l} + J^{jl}\frac{\partial J^{ki}}{\partial z^l} + J^{kl}\frac{\partial J^{ij}}{\partial z^l},$$

has non-vanishing components. This precludes the possibility of finding a coordinate transformation which brings the equations of motion into canonical form.

Despite the fact that these equations of motion are non-Hamiltonian, they belong to a generalization of Hamiltonian mechanics investigated by Y. Nambu. Consider the coordinate transformation from u to w where

$$w \equiv e^{-\epsilon^2 u}. \qquad (A.5)$$

The equations of motion (2.20)–(2.23) are transformed to

$$\dot{w} = \epsilon w[\sin(\epsilon\tilde{x})\,\sin\psi_1 + \phi k\,\sin(\epsilon\tilde{x}+\theta)\,\sin\psi_2] \qquad (A.6)$$

$$\dot{\tilde{x}} = \cos(\epsilon\tilde{x})\,\sin\psi_1 + \phi k\,\cos(\epsilon\tilde{x}+\theta)\sin\psi_2 \qquad (A.7)$$

$$\dot{\psi}_1 = \frac{1}{\epsilon}\left\{-\frac{\ln(w)}{\epsilon^2}\sin(\epsilon\tilde{x}) - [\tilde{w}_y\cos(\epsilon\tilde{x}) - \tilde{w}_z\sin(\epsilon\tilde{x})]\cos(\epsilon\tilde{x})\right\} \qquad (A.8)$$

$$\dot{\psi}_2 = \frac{k}{\epsilon}\left\{-\frac{\ln(w)}{\epsilon^2}\sin(\epsilon\tilde{x}+\theta) - [\tilde{w}_y\cos(\epsilon\tilde{x}) - \tilde{w}_z\sin(\epsilon\tilde{x})]\cos(\epsilon\tilde{x}+\theta)\right\} \qquad (A.9).$$

In these coordinates, the flow in phase-space is volume-preserving and the Liouville theorem holds, since

$$\frac{\partial\dot{w}}{\partial w} + \frac{\partial\dot{\tilde{x}}}{\partial\tilde{x}} + \frac{\partial\dot{\psi}_1}{\partial\psi_1} + \frac{\partial\dot{\psi}_2}{\partial\psi_2} = 0. \qquad (A.10)$$

Rewriting H in terms of w,

$$H = \frac{1}{2\epsilon^4}\ln^2 w - \cos\psi_1 - \phi\cos\psi_2 + \frac{1}{\epsilon^2}\left[\tilde{w}_y \sin\epsilon\tilde{x} + \tilde{w}_z \cos\epsilon\tilde{x}\right]$$

is a constant of the motion. Furthermore, in the limit $\phi \longrightarrow 0$,

$$F \equiv w\ \cos\epsilon\tilde{x}$$

is also a constant of the motion. On the other hand, in the limit $\phi \longrightarrow \infty$,

$$G \equiv k\ w\ \cos(\epsilon\tilde{x} + \theta)$$

is a constant of the motion. The complete set of equations (A.6)–(A.9) may be written concisely as

$$\frac{d}{d\tilde{t}} f(w, \tilde{x}, \psi_1, \psi_2) = \frac{\partial(f, H, F)}{\partial(w, \tilde{x}, \psi_1)} + \frac{\partial(f, H, G)}{\partial(w, \tilde{x}, \psi_2)}. \qquad (A.11)$$

Here, f denotes an arbitrary function of the phase-space coordinates, and the expressions on the right hand side are Jacobian deteminants. In particular, setting f equal to each of the coordinates w, $\tilde{x}$, ψ_1 and ψ_2 yields the 4 equations of motion (A.6)–(A.9), respectively.

Using elementary properties of determinants, Eq. (A.11) may be written in a form which is more symmetrical over the four phase-space coordinates:

$$\dot{f} = \frac{\partial(f, H, F, \psi_2)}{\partial(w, \tilde{x}, \psi_1, \psi_2)} + \frac{\partial(f, H, \psi_1, G)}{\partial(w, \tilde{x}, \psi_1, \psi_2)}. \qquad (A.12)$$

This dynamical structure falls into a class of systems studied by Nambu.

A. Elementary Properties of Nambu Systems

Nambu desired to investigate a more general class of dynamical systems which, like canonical Hamiltonian systems, obey a Liouville theorem. He considered the motion in an $N \times M$-dimensional phase-space produced by the system

$$\dot{f}(\mathbf{z}) = \sum_{i=1}^{M} \frac{\partial(f, H_1, H_2, ..., H_{N-1})}{\partial(z_i^1, z_i^2, z_i^3, ..., z_i^N)}. \qquad (A.13)$$

The M sets of coordinates $(z_i^1, z_i^2, ..., z_i^N)$, $i = 1, ..., M$, are each considered to be a canonical N-tuple, in analogy with the canonical pairs of Hamiltonian mechanics. The motion is "generated" by a set of "Hamiltonians" $H_1, ..., H_{N-1}$. One can see that Eq. (A.13) is a straightforward generalization of the Poisson bracket description of Hamiltonian systems:

$$\dot{f}(\mathbf{z}) = \{f, H\}_{P.b.} = \sum_{i=1}^{M} \frac{\partial(f, H)}{\partial(q_i, p_i)}$$

Nambu dynamics for the case $N = 2$ degenerates to ordinary Hamiltonian mechanics.

We consider the simplest case of a Nambu dynamical system where there is only a single canonical N-tuple, in order to make the notation less cumbersome. This case is analogous to the one degree of freedom Hamiltonian system with a single q and a single p. Eq. (A.13) may be written in terms of the Levi-Civita tensor as

$$\begin{aligned} \dot{f} &= \frac{\partial(f, H_1, H_2, ..., H_{N-1})}{\partial(z^1, z^2, z^3, ..., z^N)} \\ &= \frac{\partial f}{\partial z^i} \frac{\partial H_1}{\partial z^j} \frac{\partial H_2}{\partial z^k} \frac{\partial H_3}{\partial z^l} \cdots \frac{\partial H_{N-1}}{\partial z^m} \epsilon^{ijkl...m} \end{aligned} \qquad (A.14)$$

The divergence of the flow velocity is

$$\begin{aligned} \frac{\partial \dot{z}^i}{\partial z^i} &= \frac{\partial}{\partial z^i} \frac{\partial H_1}{\partial z^j} \frac{\partial H_2}{\partial z^k} \frac{\partial H_3}{\partial z^l} \cdots \frac{\partial H_{N-1}}{\partial z^m} \epsilon^{ijkl...m} \\ &= \left\{ \frac{\partial^2 H_1}{\partial z^i \partial z^j} \frac{\partial H_2}{\partial z^k} \cdots \frac{\partial H_{N-1}}{\partial z^m} + \frac{\partial H_1}{\partial z^j} \frac{\partial^2 H_2}{\partial z^i \partial z^k} \frac{\partial H_3}{\partial z^l} \cdots \frac{\partial H_{N-1}}{\partial z^m} + ... \right\} \epsilon^{ijkl...m} \end{aligned}$$

Due to the symmetry of $\frac{\partial^2 H_1}{\partial z^i \partial z^j}$ and the antisymmetry of $\epsilon^{ijkl\ldots m}$ under interchange of i and j, the terms cancel pairwise, and

$$\frac{\partial \dot{z}^i}{\partial z^i} = 0,$$

demonstrating the volume-preserving property of the phase-space flow.

Since the determinant of a matrix with two identical rows or columns vanishes, one can see that setting f equal to any one of the H_i in Eq. (A.13) causes the Jacobian to vanish. All of the H_i are therefore integrals of the motion. One can view the constraints $H_i = \text{const.}$ from a geometrical standpoint as follows: Each relation $H_i = \text{const.}$ constrains the orbit to lie on an $(N-1)$-dimensional surface. The intersection of M such surfaces produces an $(N-M)$-dimensional surface. Intersecting all $(N-1)$ of these surfaces thus yields a one-dimensional surface. With the existence of $N-1$ integrals of the motion for an N-dimensional phase-space, the resulting motion is therefore restricted to a one-dimensional manifold, (i.e. a curve). In the above form, Nambu mechanics thus always produces completely integrable motion.

Nambu provides, as an example of an integrable system in a three dimensional phase-space, the Euler equations for the motion of a rigid body. Taking the 3 components of the angular momentum, L_x, L_y, L_z, as phase-space coordinates, the Euler equations (in the absence of externally applied torques) are expressed concisely as

$$\dot{f}(L_x, L_y, L_z) = \frac{\partial(f, L^2/2, E)}{\partial(L_x, L_y, L_z)},$$

where

$$E \equiv \frac{1}{2}\left[\frac{L_x^2}{I_x} + \frac{L_y^2}{I_y} + \frac{L_z^2}{I_z}\right]$$

is the total energy and

$$L^2 \equiv \left[L_x^2 + L_y^2 + L_z^2\right]$$

is the square of the total angular momentum.

As a further generalization, Nambu suggests the use of several Jacobians, each containing a different set of "Hamiltonians," to produce systems which are not necessarily integrable. Eq. (A.14) is replaced with

$$\dot{f} = \sum_k \frac{\partial(f, H_1^k, H_2^k, ..., H_{N-1}^k)}{\partial(z^1, z^2, ..., z^N)}. \qquad (A.15)$$

One can easily show that the system is still volume-preserving. Our guiding-center system, given by Eq. (A.12), falls into this category. For this type of system, only those "Hamiltonian" functions which appear in all Jacobians are guaranteed to be invariants of the motion.

In the Nambu formulation of the equations of motion (A.6)–(A.9), the integral invariants are at the forefront of the representation. The invariance of H is manifest in Eq. (A.12). Furthermore, if $\phi = 0$, then F, H, ψ_1, and G are all independent of ψ_2. Thus, it is apparent from Eq. (A.12) that $\dot{F}$ also vanishes if $\phi = 0$.

B. Relation to Clebsch Representation

As we mentioned above, in a two-dimensional phase-space, the Nambu formalism reduces to ordinary Hamiltonian mechanics. In 3 dimensions, the Nambu formalism is essentially equivalent to the Clebsch representation of the magnetic field. Recall that in the Clebsch representation, a magnetic field is written in terms of two functions $\psi(x,y,z)$ and $\eta(x,y,z)$ as

$$\mathbf{B}(\mathbf{z}) = (\nabla\psi(\mathbf{z})) \times (\nabla\eta(\mathbf{z}))\,.$$

Using vector identities, one can easily show that the divergence of the above-defined $\mathbf{B}$ is 0 for arbitrary ψ and η. As an example, the field of a dipole oriented along the z-axis may be written as

$$\mathbf{B} = \nabla\alpha \times \nabla\varphi,$$

where

$$\alpha \equiv \frac{m(x^2+y^2)}{(x^2+y^2+z^2)^{3/2}}$$

and

$$\varphi \equiv \arctan\frac{y}{x}.$$

This yields the correct dipole fields

$$B_x = \frac{3mxz}{|\mathbf{z}|^5},$$
$$B_y = \frac{3myz}{|\mathbf{z}|^5},$$
$$B_z = \frac{m(2z^2-x^2-y^2)}{|\mathbf{z}|^5}.$$

The magnetic field lines are, in general, defined by the differential relations

$$\frac{dx}{B_x} = \frac{dy}{B_y} = \frac{dz}{B_z}.$$

One can trace the field lines by solving the initial value problem

$$\frac{d\mathbf{z}}{ds} = \mathbf{B}(\mathbf{z}).$$

The field lines are viewed as the orbits of a fictitious dynamical system. With the Clebsch representation of $\mathbf{B}$, one has

$$\frac{dz^i}{ds} = B^i = (\nabla\psi \times \nabla\eta)^i = \frac{\partial\psi}{\partial z^j}\frac{\partial\eta}{\partial z^k}\epsilon^{ijk},$$

which is equivalent to Eq. (A.14) for $N = 3$. Nambu mechanics thus subsumes both ordinary Hamiltonian mechanics and the magnetic field line problem.

C. Further Extensions of Nambu Formalism

If one modifies Eq. (A.15) by multiplying the entire right-hand side by a function of the coordinates, $g(\mathbf{z})$,

$$\dot{f} = g(\mathbf{z}) \sum_k \frac{\partial(f, H_1^k, H_2^k, ..., H_{N-1}^k)}{\partial(z^1, z^2, ..., z^N)}, \qquad (A.16)$$

then the system is not volume preserving. However, one can show that the divergence of the flow velocity is given by

$$\frac{\partial \dot{z}^i}{\partial z^i} = \frac{d}{dt} (\ln g(\mathbf{z})),$$

the perfect time derivative of a function of the coordinates. So, from Eq. (4.10), one finds that the volume δV of an infinitesimal phase element multiplied by $g(\mathbf{z})$ remains invariant. Eq. (A.16) thus is a measure-preserving system. However, if each of the Jacobians in the sum in Eq. (A.16) is multiplied by a different, independent function $g^k(\mathbf{z})$,

$$\dot{f} = \sum_k g^k(\mathbf{z}) \frac{\partial(f, H_1^k, H_2^k, ..., H_{N-1}^k)}{\partial(z^1, z^2, ..., z^N)}, \qquad (A.17)$$

then the divergence of the flow velocity is evidently not the perfect time derivative of a function of the coordinates. With Eq. (A.17), one can thus generate non-conservative systems.

It is perhaps questionable whether the various dynamical formalisms discussed in this appendix are very useful from the standpoint of theoretical physics. Nambu's attempts at quantizing this type of system and his investigation of a possible role for this formalism in subatomic physics yielded dissappointing results. The Clebsch representation of the magnetic field is likewise problematic. Finding the functions which generate the B-field is rather *ad hoc*; there is no

straightforward, elementary procedure for calculating them from the currents. Similarly, the representation of the guiding-center equations given by Eq. (A.12) was arrived at by a process of guessing, rather than by some guiding physical principle. It is unclear whether the Nambu formalism has a fundamental role in physics. I find it curious, nevertheless, that the equations of motion (2.4)–(2.5) and (2.17), which differ by a numerically small factor, should belong to two distinct generalizations of Hamiltonian mechanics: namely Nambu mechanics and Hamiltonian mechanics in non-canonical coordinates.

Regardless of their physical interest, the dynamical formalisms discussed in this section may be of interest from an academic standpoint in the general study of systems of ordinary differential equations. With Eq. (A.17), one can custom-tailor a system in an N-dimensional phase-space to have any desired number of integral invariants. One can make the system measure preserving or introduce any degree of departure from the measure-preserving property that one wishes. For example, the system

$$\dot{f} = h(\mathbf{z}) \frac{\partial(f, G, H, F, I)}{\partial(v, w, x, y, z)} + (h(\mathbf{z}) + \varepsilon\, g(\mathbf{z})) \frac{\partial(f, J, H, F, K)}{\partial(v, w, x, y, z)}$$

inhabits a 5-dimensional phase-space, possesses two exact integral invariants, H and F, is measure-preserving if ε is set to 0, and loses the measure-preserving property for $\varepsilon \neq 0$.

D. Applications to Finding Roots to Non-Linear Algebraic Equations

The capability of constructing a system of differential equations, using the Nambu formalism, which exactly conserves a given set of functions may be exploited for numerically solving non-linear algebraic equations. We outline an algorithm, based on Nambu dynamics, for locating roots to algebraic equations.

Consider the problem of solving the system of N algebraic equations

$$f_1(\mathbf{z}) = f_2(\mathbf{z}) = ... = f_N(\mathbf{z}) = 0$$

for the N unknowns $\mathbf{z} = (z_1, z_2, ..., z_N)$. The f_i are given functions of N variables. From a geometrical standpoint, each of the equations $f_i(\mathbf{z}) = 0$ defines an $(N-1)$-dimensional surface, which we denote by the set S_i. The set of roots is the zero-dimensional set P defined as the intersection of all of the surfaces S_i:

$$P \equiv \bigcap_{i=1}^{N} S_i.$$

The intersection of $(N-1)$ of the surfaces S_i is a one-dimensional curve which passes through all of the roots. Let us define the curve L_j as the intersection of all the surfaces S_i *except* S_j.

$$L_j \equiv \bigcap_{i \neq j} S_i, \quad j = 1, ..., N.$$

At every root to the system, N different curves L_j intersect. One may think of the roots as cities and the curves L_j as highways interconnecting the cities.

Suppose that one has located one of the roots by some means such as Newton's method. One can then follow each of the curves L_j passing through this root in order to locate additional roots. As the curve L_j is followed, one monitors the value of $f_j(\mathbf{z})$. A new root is uncovered when the value of f_j

passes through 0. Each time a new root is found, $(2N-1)$ additional avenues for exploration are opened up. The search for roots is exhausted when all avenues have been explored. (Some curves L_j may diverge to infinity without passing through a root. An implementation of the algorithm which we are sketching must have some criterion for abandoning the exploration of a path which appears to be diverging.)

The curves L_j may be followed with a Nambu dynamical system which uses the functions $f_i(\mathbf{z})$ as "Hamiltonians." One numerically integrates the system of equations

$$\dot{z}_i = \frac{\partial(z_i, f_1, f_2, ..., f_{j-1}, f_{j+1}, ..., f_{N-1}, f_N)}{\partial(z_1, z_2, z_3, ..., z_N)}, \quad i = 1, ..., N,$$

in order to follow the curve L_j. Note that all of the f_i appear in the Jacobian *except* f_j.

As a numerical example, consider the non-linear system of 3 algebraic equations in 3 unknowns given by

$$f_1(z_1, z_2, z_3) = 3(z_1^2 + z_2^2) - z_3 - 2 = 0$$

$$f_2(z_1, z_2, z_3) = z_1^2 + z_2^2 + z_3^2 - 1 = 0$$

$$f_3(z_1, z_2, z_3) = 8z_1^3 - 3z_1 - z_3 = 0$$

One can verify analytically that exactly 10 real solutions exist. We begin with the root $P_1 = (-0.644842, 0.628967, 0.434259)$ which was obtained using Newton's method. Using this root as an initial condition, we used a Runge-Kutta solver to integrate the 3 systems

$$\dot{f}(\mathbf{z}) = \frac{\partial(f, f_1, f_2)}{\partial(z_1, z_2, z_3)},$$

$$\dot{f}(\mathbf{z}) = \frac{\partial(f, f_2, f_3)}{\partial(z_1, z_2, z_3)},$$

$$\dot{f}(\mathbf{z}) = \frac{\partial(f, f_3, f_1)}{\partial(z_1, z_2, z_3)}$$

both forward and backward in time; a total of 6 different paths emanating from the first root. As each new root is found, it is numerically refined to high precision using Newton's method, and 5 additional paths are added to those remaining to be explored. In this manner, we are able to uncover all 10 of the roots:

$$\begin{aligned} P_1 &= (-.644842, .628967, .434259), & P_2 &= (-.644842, -.628967, .434259), \\ P_3 &= (-.111324, .893883, .434259), & P_4 &= (-.111324, -.893883, .434259), \\ P_5 &= (.210572, .605361, -.767592), & P_6 &= (.210572, -.605361, -.767592), \\ P_7 &= (.577901, .277187, -.767592), & P_8 &= (.577901, -.277187, -.767592), \\ P_9 &= (.756166, .489524, .434259), & P_{10} &= (.756166, -.489524, .434259). \end{aligned}$$

The structure of the network of roots and paths interconnecting the roots, for this example, is illustrated schematically in Fig. A.1. The arrows on the arcs represent the direction of motion when the differential equations are integrated forward in time.

FIG. A.1 Schematic representation of orbits interconnecting roots to non-linear algebraic equations.

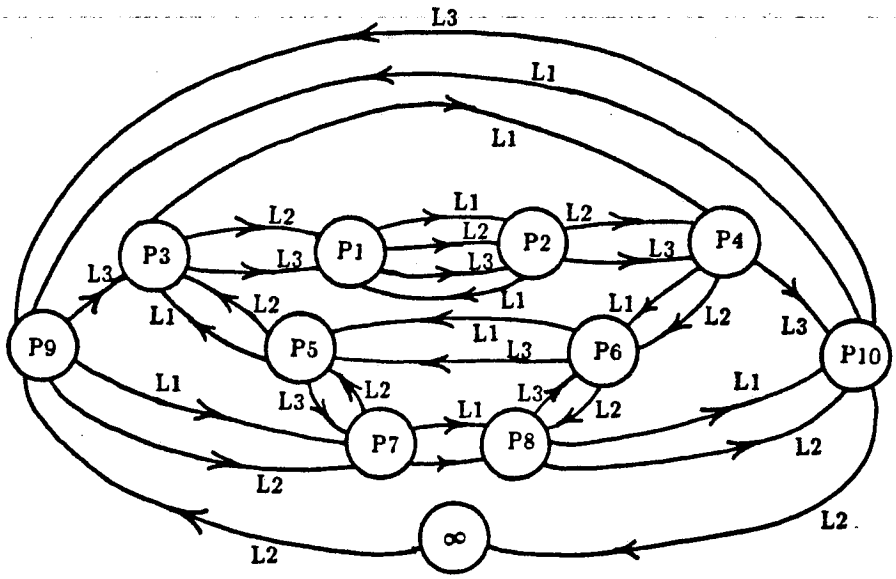

The solution of non-linear algebraic equations is one of the fundamental unsolved problems of mathematics. No comprehensive, universally applicable algorithm exists for solving an arbitrary non-linear system. Iterative, contracting maps, such as Newton's method, provide extremely efficient means for numerically refining a solution. However, this merely reduces the problem of searching for roots to the problem of searching for the iterative map's domains of attraction. The procedure outlined above provides a method for traveling from one domain of attraction to another.

The present approach, using Nambu dynamics, unfortunately does not provide a universal solution to the problem of solving algebraic equations. This is owing to the fact that, in general, each of the surfaces defined by $f_i(\mathbf{z}) = 0$ may be composed of several disjoint branches. As a result, the network of roots and curves interconnecting the roots may be composed of several disjoint circuits with no means of getting from one circuit to another. Our algorithm may yield additional roots starting from a known root; but does not guarantee all roots, unless every surface S_i is known to be simply connected. Note, however, that the real unknowns z_j may be replaced by the complex unknowns $(x_j + iy_j)$, where the x_j and y_j are real. Separating the functions $f_i(\mathbf{z})$ into real and imaginary parts, $f_j(\mathbf{z}) = g_j(\mathbf{x},\mathbf{y}) + ih_j(\mathbf{x},\mathbf{y}) = 0$, the original system of N simultaneous equations in N unknowns is replaced by $2N$ equations in $2N$ real unknowns. It is quite possible that a network composed of disjoint circuits may become linked into a single network when the unknowns are extended, in this way, to the complex domain.

References

1. W. Horton, *Handbook of Plasma Physics, vol. II*, ed. A.A. Galeev and R.N. Sudan, (North-Holland, Amsterdam, 1984), pp. 383–449.
2. T.M. O'Neil, Phys. Fluids **8**, 2255 (1965).
3. T.H. Dupree, Phys. Fluids **10**, 1049 (1967).
4. S.D. Hirshman and K. Molvig, Phys. Rev. Lett. **42**, 648 (1979).
5. R.G. Kleva and J.F. Drake, Phys. Fluids **27**, 1686 (1984).
6. W. Horton, Plasma Physics **27**, 937 (1985).
7. B.V. Chirikov, Phys. Reports **52**, 263 (1979).
8. D.F. Escande, Phys. Reports **121**, 165 (1985).
9. J.M. Greene, J. Math. Phys. **20**, 1183 (1979).
10. P. Terry and W. Horton, Phys. Fluids **26**, 106 (1983).
11. B.V. Chirikov, Phys. Reports **52**, 347 (1979).
12. V.I. Arnold, *Mathemetical Methods of Classical Mechanics*, (Springer Verlag, New York, 1978), p. 407.
13. W.M. Nevins, J. Harte, and Y. Gell, Phys. Fluids **22**, 2108 (1979).
14. R.G. Littlejohn, J. Plasma Phys. **29**, 111 (1983).
15. V.I. Arnold, *Mathemetical Methods of Classical Mechanics*, (Springer Verlag, New York, 1978), pp. 243–244.
16. A.B. Rechester and T.H. Stix, Phys. Rev A **19**, 1656 (1979).
17. D.I. Choi and W. Horton, Phys. Fluids **20**, 628 (1977).
18. T.G. Northrop, *The Adiabatic Motion of Charged Particles* (Interscience, New York, 1963), p. 11.
19. A.N. Kaufman, Phys. Fluids **15**, 1063 (1972).
20. F.L. Hinton and J.A. Robertson, Phys. Fluids **27**, 1243 (1984).

21. A.A. Ware, Phys. Rev. Lett. **25**, 916 (1970).

22. Y. Nambu, Phys. Rev. D **7**, 2405 (1973).

23. E.T. Whittaker and G.N. Watson, *A Course of Modern Analysis.* (Cambridge University Press, London, 1973), Sec. 22.7.

24. E.N. Lorenz, J. Atmos. Sci. **20**, 130 (1963).

25. D. Bohm, *The Characteristics of Electrical Discharges in Magnetic Fields*, ed. A. Guthrie and R.K. Walkerling (McGraw-Hill, New York, 1949), Chap. 2, Sec. 5.

26. H. Okuda, W.W. Lee and A.T. Lin, Phys. Fluids **22**, 1899 (1979).

27. G.R. Smith and A.N. Kaufmann, Phys. Fluids **21**, 2230 (1978).

VITA

James Alexander Robertson was born in Pittsburgh, Pennsylvania, on April 17, 1955, the son of Margaret Gasaway Robertson and James A. Robertson, Jr. After completing his work at Riverview High School, Oakmont, Pennsylvania, in 1973, he entered Yale College in New Haven, Connecticut. He received the degree of Bachelor of Science from Yale College in May, 1977. During the following two years, he was employed at Yale University in the Engineering and Applied Science Department and the Beinecke Rare Book and Manuscript Library, and was enrolled at Yale University as a Special Student. In September, 1979, he entered The Graduate School of The University of Texas. From March, 1982 to February, 1985, he worked as a research scientist associate at G.A. Technologies, Inc. in San Diego, California.

Permanent address: 500 Tenth Street

Oakmont, Pennsylvania